# The Emergence of Chaos in Continuously Monitored Open Quantum Systems

**Jessica K. Eastman**

**A thesis submitted for the degree of**
**Doctor of Philosophy**
**at The Australian National University**

**November, 2019**

# The emergence of chaos in continuously monitored open quantum systems

**Jessica K. Eastman**
Department of Quantum Science,
Research School of Physics and Engineering,
The Australian National University, Canberra, Australia.

*Supervisory committee:* Dr André R. R. Carvalho
Prof. Joseph J. Hope
Dr Stuart S. Szigeti
Prof. Matthew James

## Abstract

This thesis makes a unique contribution to the field of quantum chaos by theoretically demonstrating the effect that measurement has on the emergence of chaos from the quantum world and demonstrating a means to control the onset of chaos in the quantum system using adaptive measurements. Here we investigate how the choice of the continuous measurement strategy for an open quantum system affects the emergence of chaos in the transition from the quantum limit to the classical limit when the system is dissipative. We consider two models in our research. The Duffing oscillator is classically chaotic and also dissipative (ie. an open quantum system), whereas the driven top is classically a closed system; adding dissipation via continuous measurement therefore changes the behaviour in the classical limit.

The first half of this thesis presents the investigation of a dissipative system whose classical limit is chaotic. We explore the emergence of chaos from the open quantum system that is continuously monitored and investigate the dependence on the choice of monitoring by changing a single parameter in a homodyne measurement scheme, effectively changing the information gained by the measurement. We show that the emergence of chaos in the regime where quantum effects are still present can be determined solely by changing the measurement parameter. This is a result of the interplay between the quantum interference effects induced by the nonlinear dynamics and the localisation and decoherence that occurs due to the measurement. We also investigate the case where the classical limit is regular for the Duffing oscillator, and demonstrate the semiclassical effect of chaos induced by the measurement back-action. A certain choice of measurement leads to a noise which drives the system to large spread in the dimensionless position enabling a non-classical transition mechanism that is classically forbidden, inducing chaos in the

system. These results are verified by the numerical calculation of the maximal Lyapunov exponent in the quantum regime.

The second part of this thesis investigates the possibility of controlling the degree of chaos with quantum control. We design an effective control scheme to control the degree of chaos using the measurement dependency of the state. We propose an adaptive measurement scheme which changes the homodyne measurement angle in real time depending on the direction of the state's interference fringes in phase space. This is done using the knowledge gained by the measurement signal. We show that this control scheme can enhance or suppress chaos. By enhancing the degree of chaos we are also able to push the onset of chaos further into the quantum regime than was possible before. By suppressing chaos we generate highly non-classical states and regular motion. The feasibility of experimentally realising this control technique is discussed in detail.

The final section of this thesis considers a chaotic system that is not dissipative in the classical limit: the driven top. We investigate the effect that opening the quantum system to decoherence has on the degree of chaos when we continuously measure the system. We demonstrate that the presence of decoherence suppresses the chaos and alters the dynamics of the quantum system. This is seen to worsen as the strength of the measurement is increased unless a particular measurement is chosen that perfectly cancels out the decoherence resulting in the Hamiltonian evolution in addition to noise from the measurement. These results are verified by the separation time between classical and quantum dynamics.

# Declaration

Except where acknowledged in the customary manner, the material presented in this thesis is, to the best of my knowledge, original and has not been submitted in whole or part for a degree in any university. Where work has been performed in collaboration with others, I have acknowledged the contributions of all authors.

Jessica K. Eastman
November, 2019

# Acknowledgements

They say that it takes a village to raise a child. The same could be said for a PhD student. This is not a solo effort. The process to get to this point has been a minefield of emotional trauma (I feel like I'm waking up from a very strange dream and everything is suddenly so much clearer). I could not have made it this far without the people that have raised me. All of the people who have supported me in some way or another over the years. To everyone that had to put up with me and my selfish self centred behaviour as I hid away from in my PhD hole, avoiding adult life; I'm sorry, thank you for waiting, I'm done now, I can be a human and interact with you again. Theres a lot of people that got me to this point, so many in fact that I don't want to forget anyone so I'm not naming names. But here's to my colleagues at DQS that made my work days into coffee time and burger time and beer time and fun times all round. DQS feels like my home, with all the wonderful and unique people that passed through that tearoom. Thanks for sharing the adventure with me. Here's to my friends that I spent countless Friday nights with at the OCI. You guys are the best and I cherish your friendship. You got me through it. It was a crazy time made less crazy with you guys. Here's to the friends that I barely saw over the PhD years because you weren't in my department. The divide between DQS and RSPE is real, you were just too far away (a 20 minute walk is just too far I'm sorry). Here's to the friends that got me into rock climbing and pushed me up cliffs literally and metaphorically. We had some really awesome adventures, and I look forward to many more sick sends in the future. Let's do Yosemite! Here's to the atomoptics (and the rest of the department actually) indoor soccer group that sadly died out. We had some wild times and soo many injuries, it was great. Here's to all the friends I have made here in London when I left my life to go half way across the world. I would literally go insane if I didn't have all of you to keep me social.

Special thanks to my parents, mum, dad, and Suzy. You have shaped me into the person I am today and I like who I am because of you. You have supported me the whole way through and made it possible for me to achieve things. Words cannot express how grateful I am. To the rest of my family that I feel like I have neglected over these years, again my self centred behaviour. Thank you for being there and being patient.

Here's to my supervisors most of all. Thank you Andre, you are the reason I am here. I have enjoyed research because of you. You are so enthusiastic and passionate about what you do and I always aspire to be as passionate as you are. You leaving ANU was devastating but you taught me to be an independent researcher. Thank you for the time and support you have given me. I am grateful that you have shared your stories with me, you are an amazing story teller.

Thank you Joe. I'm not very good at expressing this in person, but I'm so glad to have had you as a supervisor. You are an extraordinary academic and your dedication to your teaching is always so inspiring, I hope to be like you. In fact you are an amazing role model as far as academics go. To see your ability to teach and improve education for young people and continue to research and write fiction all at the same time is inspiring

to me as someone who wants to be good at all of those things as well. Joe you are always trying to give advice and words of wisdom and guiding me towards being a healthier and happier version of myself. Your attempts to check in and make sure I am doing alright will always be appreciated. You're like the academic father figure for all of us in the group and I always aspire to seek your approval. I appreciate your efforts to keep the group fit and strong as well.

Thank you Stuart. You didn't have to come in as a supervisor but you did when I needed you and I am always grateful for all the support you provide, you go above and beyond anything asked of you and you are an amazingly kind person. And I am so glad that you and Tegan share my joy for board games and halloween costume parties.

I would like to say thank you as well to Eva-Maria Graefe and the mathematical physics group at Imperial College London. Starting a post doc position with an incomplete PhD thesis was perhaps not the best move on my part but I am so thankful to belong to such a great group while tackling my own mad decisions. You have been so patient with me while I get through this and I am so grateful to have found such a wonderful group of people to work with.

And finally I would like to say a thank you to all the lovely women out there that have acted as my informal mentors, pushing me along the path of being a successful researcher. Without your voices guiding me along and helping me believe it was possible I would not be here. I look up to all of you.

*I saw my life branching out before me like the green fig tree in the story.*
*From the tip of every branch, like a fat purple fig, a wonderful future beckoned and winked.*
*One fig was a husband and a happy home and children...*
*...and another fig was a famous poet...*
*...and another fig was Ee Gee, the amazing editor...*
*...and another fig was a brilliant professor...*
*...and another fig was Europe...*
*...and Africa and South America...*
*...and another fig was Constantin and Socrates and Attila and a pack of other loves with queer names and offbeat professions.*
*And another fig was an Olympic lady crew champion.*
*And beyond and above these figs were many more figs I couldn't quite make out.*
*I saw myself sitting in the crotch of this fig tree,*
*starving to death, just. because I couldn't make up my mind which of the figs I would choose.*
*I wanted each and every one of them, but choosing one meant losing all the rest.*
*And as I sat there, unable to decide...*
*...the figs began to wrinkle and go black...*
*...and one by one...*
*...they plopped to the ground at my feet.*

Sylvia Plath
*The Bell Jar*

# Publications

## Publications Featured in this Thesis

The main results of our work were published in:

- *'Tuning quantum measurements to control chaos'*, J. K. Eastman, J. J. Hope, A. R. R. Carvalho, Scientific Reports, **7**, 44684 (2018).
- *'Controlling chaos in the quantum regime using adaptive measurements'*, J. K. Eastman, S. S. Szigeti, J. J. Hope, A. R. R. Carvalho, Phys. Rev. A. **99**, 012111 (2019).

## Other Publications

- *The effects of amplification of fluctuation energy scale by quantum measurement choice on quantum chaotic systems: Semiclassical analysis*, S. Greenfield, Y. Shi, J. K. Eastman, A. R. R. Carvalho, A. K. Pattanayak, Proceedings of the 5th International Conference on Applications in Nonlinear Dynamics, Springer, Cham, 72-83 (2019).

# Contents

# 1 Introduction

Hyperion tumbles chaotically through the vacuum of space as she orbits the planet Saturn. She is a moon of Saturn, and her orbit is unlike the other moons. It is chaotic. Any small perturbation, any small error in our calculations and we completely misjudge her evolution. She is extremely sensitive to these small perturbations and yet her evolution can be explained deterministically. That is, if we knew exactly her initial condition and the parameters that govern her dynamics, we could know exactly where she would be at any given time. This is the beauty of chaos.

Chaos can arise when a system's evolution is governed by nonlinear equations of motion and leads to an extreme sensitivity to initial conditions. It is the reason we cannot predict the weather over long time scales. Even the tiniest perturbation can result in completely different dynamical behaviour. A butterfly flaps its wings in Brazil and creates a tornado in Texas or so the saying goes. This leads to interesting and wonderfully complicated behaviour that on first glance looks entirely random. However, just because the evolution looks complicated does not mean it is inexplicable. The underlying theoretical models that describe the weather (eg. atmospheric convection and its coupling to oceans, land surface, and sea ice) are well established, and the accuracy and timescale of weather predictions increase in proportion with computational power [84]. The cardiac signal of a human heart is another well-known example where chaos is known to be present and well understood [20]. In this case the presence of chaos is unwanted and efforts are made to control the system towards non-chaotic behaviour [40]. There are myriad examples from physics [134, 142], chemistry [122], biology [129], of systems that appear to behave randomly and unpredictably but can be deterministically described by chaos. The study of chaos in classical systems is incredibly interesting and useful in its own right, but how does it arise from the underlying microscopic principles of quantum mechanics?

From the time of the ancient Greeks, we have theorised about objects smaller than what we observe, that this table that I write my thesis on is made up of even smaller objects, atoms. When we finally developed the technology to observe the world of small things, we were also interested in how they evolved. How does the evolution of sub-atomic particles govern the motion of atoms? And how does the motion of these particles link to what we see in everyday life? The connection between quantum mechanics and classical mechanics

is something that we are constantly striving to understand. The correspondence principle tells us that if we take a quantum object and make it bigger or put more energy into it, then at some point the dynamics will start to look like what we see in the classical world. And for the most part, physics has confirmed this. But there are still open questions as to how we arrive at the classical world, particularly for the fields of quantum gravity and quantum chaos. This thesis will focus on the emergence of chaos in quantum systems.

## 1.1 Emergence of Chaos from the quantum world

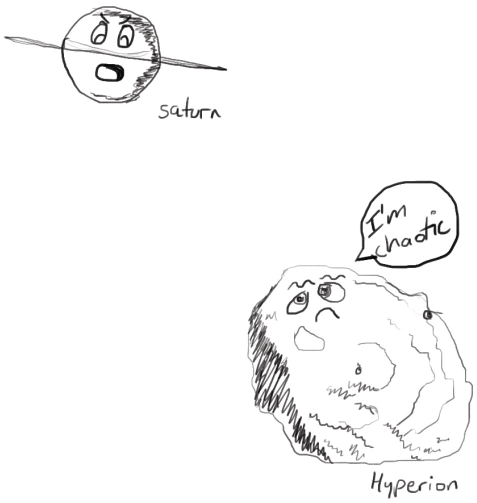


**Figure 1.1:** Saturn's moon Hyperion has a chaotic orbit, the presence of decoherence leads to the emergence of chaos.

Now consider again the moon Hyperion as she tumbles chaotically through the vacuum of space, her motion governed by a set of nonlinear equations. She is made of many orders of magnitude of atoms which are bound together to form a solid object. These atoms are made of even smaller particles, protons and neutrons and electrons. The protons and neutrons are split into smaller still fundamental particles which are called quarks. The study of physics has shown us that the fundamental behaviour of nature is governed by quantum mechanics so the evolution of the individual particles that make up Hyperion is linear and therefore non-chaotic. More precisely, the wavefunction of a quantum system is governed by the Schrödinger equation, which is a linear equation of motion. So how do we get the chaotic dynamics of the entire moon from the quantum evolution of the individual particles?

The first step towards solving this apparent paradox is to note that whilst the wavefunction evolution is linear, the quantum-mechanical observables can evolve according to nonlinear equations of motion. Specifically, the Heisenberg equations of motion for the observables are nonlinear. According to the correspondence principle, in the limit as the system goes towards the classical, the dynamics will match the corresponding chaotic classical system.

### 1.1.1 Quantum chaos for closed systems

Quantum chaos is the study of quantum systems whose classical counterpart is chaotic. There are different branches in the study of quantum chaos. The more traditional treatment of quantum chaos is the consideration of the spectral characteristics of a chaotic Hamiltonian. This has been done for systems such as the Bose-Hubbard model [73], chaotic billiards [2], and the kicked top [53]. Each of these systems has a classical counterpart that is chaotic. The more traditional treatment involves comparing the level spacing statistics of the quantum system with random matrix theory [53]. In these studies, the signatures of chaos are found in the eigenvalues of the Hamiltonian rather than the dynamics of the quantum system. The eigenvalues for the quantum system with a classically regular counterpart follow Poissonian statistics [5]. However, when the classical limit is chaotic, the statistics are described by the statistics of random matrices [9, 53, 73] ie. the Wigner Dyson statistics [152, 32]. However, this treatment does not investigate what happens to the dynamics of a quantum system as it transitions to a chaotic limit. For this we must fairly compare the classical dynamics with the quantum dynamics via the phase space methods utilised in the study of classical chaos.

### 1.1.2 Ehrenfest time and the breakdown of the correspondence principle

The time it takes for the dynamics of a closed quantum system and the particle dynamics of the corresponding classical system to look different is known as the Ehrenfest time. In principle, the position and momentum of a classical particle can be known exactly. In constrast, a quantum system is described by a wavefunction that in general is delocalised in space, and we cannot know the exact position and momentum of a quantum particle simultaneously due to Heisenberg's uncertainty principle. Consequently, for closed system dynamics, the wavefunction over time spreads out with more uncertainty in position and momentum. As this happens, the dynamics starts to look very different from the classical dynamics of a point particle.

How do we reconcile the classical behaviour with the fundamental quantum behaviour that the particles in the universe obey? We can take the quantum system to the classical limit by increasing the number of particles in the model, or by increasing the energy of the system. For a closed quantum system, the natural classical counterpart is the isolated classical system and the closed quantum system will asymptotically approach this limit, resulting in the proportionate growth of the Ehrenfest time. There will not, however, be any agreement between the closed quantum system and a classically dissipative limit.

### 1.1.3 Dissipation and interaction with an environment

Many works have focused on trying to solve the puzzling question of correspondence breakdown between the classical and quantum for chaotic systems [166, 55]. The major problem that we encounter with the classically chaotic system is the time before the quantum dynamics departs from the classical. This is the problem pondered by Zurek and Paz in the 1990s [168]. In a thought experiment posed by Zurek and Paz, they considered the moon Hyperion. Hyperion tumbles chaotically through the vacuum of space. The fundamental nature of the constituent particles that form Hyperion is quantum in nature. But we see a classical evolution governed by chaos. What is the estimated breakdown time when we start to see the quantum dynamics diverge from the classical dynamics? In their argument, Zurek and Paz estimate the time to be about 20 years! Since Hyperion's

age is much older than this, we would expect Hyperion to be in a quantum superposition. But the evolution appears classical, why? The answer is decoherence.

In reality, a system is never truly isolated, there is some interaction with the surrounding environment. This coupling to an environment leads to a loss of coherence in the system when information is transferred to the environment that cannot be followed by the observer, this is decoherence. The decoherence destroys interference and superpositions, leading to localisation of states and this provides a crucial step in the smooth transition from the quantum system to the classical [100, 28, 166, 55, 103, 18]. The study of dissipative chaotic systems naturally requires the introduction of a coupling to an environment, and an ever expanding part of the field of quantum chaos is the study of chaos for open quantum systems.

## 1.2 The approaches of open quantum systems to quantum chaos

### 1.2.1 Unconditional dynamics: Master equation

There have been two schools of thought in chaos in open quantum systems. The first takes the approach of the ensemble average behaviour of the system, given by the master equation. Historically, the ensemble average was believed to be the only way of observing quantum mechanics with the seminal work done by Feynman and Vernon [41] and built upon by Caldeira and Leggett [14]. Using this approach, the phase-space distribution of the classical system is compared with the quasi-probability distribution of the ensemble of quantum states, given by the Wigner function [55]. This does not allow a self-consistant quantification of chaos suitable for both the classical and quantum system. Classically, chaos can be determined by classical trajectories of motion and looking at the exponential divergence of initially infinitesimally close trajectories in phase space. However, there is no clear way to measure the divergence in phase space for the ensemble average of a quantum system. The ensemble will usually approach a steady state, meaning the sensitivity to initial conditions cannot be seen [18].

### 1.2.2 Conditional dynamics: Measurement

The other approach is to adopt a continuous monitoring of the quantum system. In this case, the monitoring is said to produce an "unraveling" of the master equation in terms of individual stochastic quantum trajectories that evolve conditioned on the measurement record. Using this approach, it has been shown that the Poincaré section of a single quantum trajectory reproduces the corresponding strange attractor in the macroscopic limit [131, 13], even when considering a few different monitoring strategies [117]. It also allows for a quantitative comparison between the classical and quantum Lyapunov exponents as the system is varied [6, 99, 54, 68].

In general, when the classical motion is large compared to the quantum noise induced by the stochastic nature of the trajectories, the quantum Lyapunov exponent approaches the classical value [6], while there is a crossover to the quantum regime where noise predominates and chaos is suppressed [99]. Interestingly, positive Lyapunov exponents have been found away from the classical limit [54] but perhaps even more surprising is that they have also been reported for parameters where the corresponding classical system is regular [68, 107]. These results show not only that the onset of chaos at the quantum level

is possible, but also that it has a rich behaviour due to the interplay between the strength of the nonlinear dynamics and the amount of noise introduced by the measurement back-action. But quantum mechanics allows us to go beyond that and explore more complex scenarios where, even when the form and strength of the system-environment interaction are kept unchanged, different choices of measurement schemes can have a drastic affect on the dynamics of the system. A fundamental question that I will ask as part of this thesis is: How does the measurement strategy affect the Lyapunov exponent of the system?

The conditional dynamics of a quantum system has been used as a tool to explore the emergence of chaos from the quantum in a quantitative way. With single quantum trajectories we are able to calculate the divergence in phase space of two trajectories and calculate the Lyapunov exponent just as we did with the classical system. But we are not limited in our choice of measurement. There is an infinite number of ways of unraveling the master equation in order to get conditional dynamics. The quantum nature of the measurement means that the choice of measurement itself can play a role in how the system behaves. When we measure a classical system, the system will behave the same way no matter which way we decide to measure the system. This is not the case for quantum systems! The very act of measurement will disturb the state of the quantum system, leading to different outcomes depending on how we choose to measure the system [74]. And this fact has been used to the advantage of controlling quantum systems in the past. So it begs the question: Does the choice of measurement also change the degree of chaos present in a quantum system? If we can change the behaviour of a quantum system simply by changing how we measure it, will we see this change in the Lyapunov exponent for the system as we transition to the classical system where chaos is present? This question is also explored in this thesis.

Moreover, if we do see a change in the quantum Lyapunov exponent just by changing how we measure the system, can we use this as a control so that we may control the degree of chaos in a quantum system by using our measurement device?

## 1.3 Controlling Chaos

Hyperion tumbles chaotically through the vacuum of space, but what if we could control the dynamics, making her motion regular? The idea of dynamical control is nothing new.

### 1.3.1 Control of classical chaos

In classical systems, controls that suppress chaos have applications to regularising the behaviour of cardiac rhythms [40] and to improving energy harvesting from cantilever devices [38, 75]. The presence of chaos in experimental set-ups may or may not be desirable and controlling these systems can be vitally important. Controlling dynamical systems is itself an incredibly diverse field, with applications to everyday technology such as the practical and necessary control of car braking or the ability to control an unstable inverse pendulum. Control is an important aspect of stable dynamical systems. And understanding how to control systems in the presence of chaos is incredibly important. The control of chaotic systems has been studied extensively for classical systems. In most experimental systems, the presence of chaos is common, however it is generally unwanted and troublesome when trying to achieve a stable system performance. Ott, Grebogi and Yorke (OGY) came up with a control algorithm to control chaos in 1990 that is based on the fact that the chaotic strange attractor has an infinite number of unstable periodic orbits (UPOs)

embedded in it [101, 120]. Their method uses discrete time-dependent perturbations of some system parameter to stabilise a chosen UPO that gives improved system performance and kick the system into a periodic orbit. This algorithm has been implemented in the past on classically chaotic systems such as the Henon map, the double rotor map and the Duffing oscillator, using only the time series data that can be measured experimentally to find the desired UPO. While OGY control focuses on the control of a discrete system. Pyragas *et al* have proposed a control algorithm for continuous systems, taking a more "always on" type of control where the system is continuously pushed towards a stable periodic orbit [109]. These control techniques have been proven to work well for classical chaos, and have been shown to control irregular heartbeats in the cardiac rhythm of a human heart [40]. For the quantum system however, we do not know the precise state of the system, which makes it harder to control the system with these techniques. Fortunately, the field of quantum control is also a rich field with experimentally viable techniques [158]. Techniques can be borrowed from this area in order to control chaos in quantum systems.

### 1.3.2 Quantum control

Quantum control comes in two flavours, open loop control and closed loop control or otherwise known as non-feedback and feedback control respectively. In open loop control, all controls are put in place in the beginning and no corrections are made based on the dynamics of the system of interest. In contrast, closed loop control uses feedback in order to alter the control based on the dynamics of the system. In this thesis we are only interested in the use of closed loop control, which we will discuss below. To date, some of the main applications of quantum control are quantum computing and metrology [4, 114] as well as the feedback cooling of Bose Einstein condensates [64, 138, 137]. Experiments have been done using quantum control techniques to stabilise quantum states and improve phase estimation in metrology experiments [143, 22, 61, 104]. The control technique used in these instances relies on a real time feedback control where the dynamics of the quantum system is monitored over time and corrections are applied to the system dependent on the dynamics.

### 1.3.3 Quantum control with adaptive measurements

There has been a lot of work done in the theoretical and practical implementation of quantum control in the field of quantum optics. The main motivation for quantum control in quantum optics may be for the purpose of quantum computing and quantum communication, but the same techniques can be applied to chaotic systems as well. Take for instance the adaptive measurement control scheme developed by Wiseman [153, 4] in order to improve phase estimation. This control scheme involves making changes to the measurement scheme as information about the state of the quantum system is gained so that the measurement can be as efficient in the measurement of the phase as possible. This is possible because of how the measurement gathers information about the state of the system. Adaptive measurement techniques have been implemented previously in experiments [114, 61, 104].

## 1.4 Observing quantum chaos experimentally

Chaos has been explored in quantum systems experimentally for decades. Experimental set-ups with cold atoms have been a good testbed for the realisation of quantum chaos due

to their extremely good controllability. Ultra-cold bosonic atoms in a trap also have the remarkable physical phenomenon that when they are cooled down to a critical temperature, the bosons condense into the ground state of the trap, forming a macroscopic wavefunction. This phenomenon is known as Bose-Einstein condensation [10, 36] and we mention it here because it can be useful for the simulation of quantum systems that are chaotic. The tunability of the Feschbach resonance allows for tunability of the scattering length [21] which means the interaction strength between the atoms can be easily tuned. This set up can look at the single particle behaviour by turning off interactions, or it can look at the different dynamics established by turning interactions on. The diverse range of systems that could be simulated by tuning the experiment means the platform provides many opportunities to explore different chaotic dynamics in the same quantum system. Quantum chaos has been realised experimentally in the past [112, 72, 144, 94, 19]. The most common and easily investigated systems being the kicked rotor [112] and the kicked/driven top [19, 144, 94]. Recently, the kicked top has been proposed in the nuclear spin of a single atom [90]. But none so far have considered the continuous measurement of the quantum system.

There has been a recent resurgence of experimental interest in exploring quantum chaos due in part to the recent links that quantum chaos has to other areas of physics. Many-body quantum chaos may be connected to areas such as information scrambling and holographic duality [85, 127, 135, 88]. It may also be linked to nonequilibrium thermodynamics [94] and the thermalisation of closed quantum systems. The ability to describe quantum chaos using techniques of random matrices almost certainly leads to connections to random unitaries [37]. The potential advantage to precision measurement and quantum sensing that has recently been explored in the presence of chaos [42] hints at advantages to considering quantum chaos.

To experimentally verify the work we do in quantum chaos, we need a method of quantifying the chaos. How we do this in numerical simulations is to calculate the Lyapunov exponent. For this we require a long time average and two trajectories initially infinitesimally close to each other. We cannot do this in experiments, it is infeasible. So we need to consider how we can measure chaos in an experiment. One potential is looking at the breakdown time between the classical and quantum dynamics. This has been well explored theoretically in the past [66, 18].

A more recent potential candidate is the use of out-of-time-order correlators (OTOCs), which has been experimentally explored by several experimental groups [44, 79] and the theoretical study of OTOCs has also been recently investigated [123, 43, 161, 162, 115, 78]. This topic has exploded in recent years with suggestion that the OTOCs could act as a probe to explore chaos as well as the link to information scrambling in black holes [127, 85]. The idea of the OTOCs uses the sensitivity of the chaotic dynamics to the system parameters. However, the drawback of this probe relies on the fact that you must be able to perform a perfect time reversal of the Hamiltonian, which is not possible for systems where dissipation is present. For dissipative chaos, we need other techniques.

## 1.5 Research Questions Addressed in this Thesis

### 1.5.1 How does measurement affect chaos?

Environment-induced decoherence has long been recognised as being of crucial importance in the study of chaos in quantum systems. In particular, the exact form and strength of the

system-environment interaction play a major role in the quantum-to-classical transition of chaotic systems. In this work we focus on the effect of varying monitoring strategies, i.e. for a given decoherence model and a fixed environmental coupling, there is still freedom on how to monitor a quantum system. We show here that there is a region between the deep quantum regime and the classical limit where the choice of the monitoring parameter allows one to control the complex behaviour of the system, leading to either the emergence or suppression of chaos. Our work shows that this is a result from the interplay between quantum interference effects induced by the nonlinear dynamics and the effectiveness of the decoherence for different measurement schemes. This thesis also compares the effect of measurement when the classical system is in both a chaotic and a regular regime by investigating different sets of parameters for the system. We not only show that the measurement plays an important role in determining how the emergence of chaos occurs from the quantum dynamics, but how the noise from the measurement can also induce chaos when the classical limit is regular. The results discussed in this thesis make a valuable contribution to understanding how chaos emerges from the quantum system when it is continuously monitored, which could have serious consequences for experiments where chaos can be present whether it is desired or not. The very act of measuring a quantum system can induce chaos in these systems and we need to be aware of this.

### 1.5.2 Can we use adaptive measurement to control chaos?

The continuous monitoring of a quantum system strongly influences the emergence of chaotic dynamics near the transition from the quantum regime to the classical regime. Here we present a feedback control scheme that uses adaptive measurement techniques to control the degree of chaos in the driven-damped quantum Duffing oscillator. This control relies purely on the measurement backaction on the system, making it a uniquely quantum control, and is only possible due to the sensitivity of chaos to measurement. We quantify the effectiveness of our control by numerically computing the quantum Lyapunov exponent over a wide range of parameters. We demonstrate that adaptive measurement techniques can control the onset of chaos in the system, pushing the quantum-classical boundary further into the quantum regime.

### 1.5.3 General effect or system-dependent?

In this thesis, the effect that measurement can have on the emergence of chaos in dissipative quantum systems is investigated, but is this a general effect that can be seen in multiple systems or is it system dependent? Two completely different systems are investigated in this thesis. The Duffing oscillator, a system that can be described by the motion of a single atom in a double well potential, and the driven top, a system that can be described by two modes within a double well potential or by the angular momentum of a single atom of large spin or by a collection of two level atoms. The Duffing oscillator is effectively just a simple harmonic oscillator (SHO) with the lowest order perturbation that a system can have (quartic potential). In the small oscillation limit, the SHO can be found in a multitude of systems, that in itself makes the behaviour of the Duffing oscillator a general behaviour for many nonlinear systems. The Driven top could be thought of as an extension of the Duffing oscillator to include many body effects. By investigating both systems, we gain some understanding of what the general effect of measurement is on the emergence of chaos.

### 1.5.4 Consequence of opening an isolated quantum system to the environment

The first system that we investigate in this thesis is the quantum Duffing oscillator that is continuously used as a model for investigating the emergence of chaos for dissipative systems. As is said above, it is well understood that in order to see a smooth transition to the classical regime for these systems, we must consider an open quantum system that interacts with its environment. In contrast, the quantum driven top is the classical limit of a closed system that undergoes Hamiltonian evolution. This is very different to the first system that we look at which has a dissipative and therefore open evolution in the classical limit. The driven top is quite often studied as a closed quantum system, but experimentally there is often some kind of loss to the environment, which motivates the investigation of what happens when this system interacts with an environment. What happens as it transitions to the classical regime? This thesis will also aim to answer this question, studying what happens when we open the quantum driven top, specifically when we continuously monitor the quantum driven top as an open system. Previous work has of course considered the effect of decoherence on the quantum driven top and shown the presence of chaos to still exist for small amounts of loss [46], we will aim to contribute to this research by adding the measurement as another parameter we can play with. Not only has this system been experimentally realised in cold atom experiments [144] but it is intriguing because the classical limit is isolated from the environment. As we said earlier, no system is ever really isolated from the environment. Experiments in cold atoms try to eliminate as much noise as physically possible but still there will always be some coupling to the environment and by looking at the effect of opening the quantum driven top, we can determine how this coupling will effect the emergence of chaos in these experiments. The recent interest in this area of open quantum systems and the emergence of chaos demonstrates how relevant this current work is. This is still a generally new area of an old field and there are many open questions. This thesis addresses some of the questions related to the role that continuous measurement has to play.

## 1.6 Outline of thesis

The first two chapters will act as an introduction to the background needed. This thesis is investigating the emergence of chaos from a continuously monitored quantum system, and some tools are required in order to describe this. **Chapter 2** will firstly give a background on what we define as chaos and then it will provide a general background for the "quantum tools" we require to describe the system of interest and compare the quantum system with the classical counterpart. **Chapter 3** will provide the background for the evolution of quantum systems, where we will mainly be interested in the evolution of open quantum systems under continuous measurement. This thesis will be comprised of three main results chapters. The first part (**chapter 4**) will deal with the continuous measurement of an open quantum system that is chaotic in the classical limit, focusing on the driven and damped Duffing oscillator that exhibits chaos for certain choices of the system parameters. In this section, we will discuss the results of the paper on "Tuning quantum measurements to control chaos", where the Lyapunov exponent is calculated for the quantum Duffing oscillator for different choices of continuous measurement to show the dependence of chaos on measurement. This chapter will also look at the interesting result that comes from the driven and damped Duffing oscillator when it is regular in the classical regime with a

different set of parameters. In this case we again study the effect that measurement has on the emergence of the classical limit. This case is interesting because we show that the measurement induces chaos in the quantum regime even when the classical system is not chaotic. In **chapter 5**, we will follow on with the work of the first section, focusing on the classically chaotic set of parameters and looking at the implementation of an adaptive measurement technique to control the chaos. The development of the control algorithm and the numerical simulations to model it are given in this chapter as well as the discussion of experimentally realising this in different experimental set ups. This chapter will discuss the underlying mechanisms that result in dynamical sensitivity to measurement. Again, this will be done with the model of the quantum Duffing oscillator. In **chapter 6** the measurement dependence and the effect of opening the quantum driven top to the environment coupling will be investigated with relevance to experimental realisations of a different toy model, the driven top. We make suggestions for how the quantum Lyapunov exponent could be calculated for this system and we explore possible methods to quantify chaos in an experimentally feasible way for this system by looking at the breaking time between the classical and quantum dynamics. **Chapter 7** will give a conclusion, summarising the work done in this thesis and an outlook on the questions left to be answered in the future.

# 2

# Background I: Chaos and Quantum Mechanics

Let us now introduce the background concepts and techniques needed for the investigation into the emergence of chaos in continuously monitored dissipative systems. In the history of quantum mechanics, the correspondence between classical mechanics and quantum mechanics has been a key area of research. How do we link what we see in the classical world with how the fundamental particles that make us up behave? At some point, the behaviour of the quantum system should look like the behaviour of the classical world as we make the system more energetic or larger. The motion of the quantum harmonic oscillator should in the classical limit behave just as the classical harmonic oscillator. To investigate the emergence of chaos in continuously monitored dissipative systems, we will require a few key areas of knowledge that will be introduced in the next two chapters. Firstly, the concept of classical chaos and the usual methods to study it shall be introduced. Secondly, we will require an introduction to quantum mechanics and the methods by which we can compare the classical and quantum evolution using phase space methods.

In this thesis we will focus on two different quantum systems of interest, the quantum Duffing oscillator (Ch. 4& 5) and the quantum driven top (Ch. 6). For each of these systems, we require a different algebra to describe the quantum state in the appropriate basis and phase-space geometry. For the Duffing oscillator we require the eigenstates of the harmonic oscillator, ie. the energy basis states or number states for a single bosonic mode. For the driven top we require the pseudo-angular momentum basis given by the Dicke states for two bosonic modes. Both toy models can be realised in trapped bosonic systems. A Duffing oscillator can be engineered by confining bosons in a single site of a double well potential. In the case of the driven top, this system can be realised with two bosonic modes corresponding to two sites of a double well lattice potential, with the ability to interact and tunnel between the sites. In this chapter we will discuss the physics that describes the quantum states of such systems.

In this thesis it is necessary to compare the dynamics of our quantum system with a classical counterpart. The multidimensional Hilbert space of our quantum system has an embedded classical phase space. The classical phase space for the Duffing oscillator is a 2D plane, while for the driven top it is the surface of a sphere, which in the classical limit also looks like the 2D plane. This background chapter presents these phase-space mappings and

the corresponding "semi-classical" quantum states that occupy these embedded classical phase spaces. We also discuss the semiclassical approximations we can make for our quantum systems that will enable easy numerical simulations. We will also introduce the phase space methods by which we can visualise the quantum state, making comparison with the classical state easier.

The goal of this chapter will be to introduce enough background to the two worlds of classical and quantum so that we can move on to the goal of the thesis which is to investigate the evolution of the quantum system with dissipation present and when the system is continuously monitored. The evolution of an open quantum system will be introduced in the next chapter.

## 2.1 Phase space dynamics

As we briefly mentioned above, it is necessary to compare the evolution of classical systems and quantum systems. The correspondence principle tells us that we should expect to recover the classical evolution that we see in nature when we take quantum theory to the limit of large quantum numbers. The space of quantum states is described by a high dimensional Hilbert space but in order to make a comparison between the classical and quantum theory, we compare the observable quantities, such as the position and momentum of a particle. To do this, it is convenient to describe the dynamics of the particle in a phase space that is given by the position and momentum. This is the usual space that we will deal with when modelling the dynamics of a classical particle. For a useful reference on the nonlinear dynamics of classical systems, with description of phase space dynamics, see [133]. The classical particle will take a trajectory in the phase space with the position and momentum $(x, p)$ evolving over time as the particle moves. The motion is described by the equations of motion for the system.

To generalise to higher dimensions, a point in the phase space flowing along the vector field given by the point $\mathbf{x}$ and the velocities $\dot{\mathbf{x}}$ in the phase space will trace out a solution $\mathbf{x}(\mathbf{t})$ to the equations of motion $\dot{\mathbf{x}} = \mathbf{f}(\mathbf{x})$, this corresponds to a trajectory winding through the phase space. A fixed point in the phase space satisfies $\mathbf{f}(\mathbf{x}^*) = \mathbf{0}$, this is a steady state. Closed orbits correspond to periodic solutions for which $\mathbf{x}(t + T) = \mathbf{x}(t)$. In the phase space, we can easily visualise the trajectory of the system for a given initial condition. But it can be hard to determine the behaviour of the system just from the trajectory. For this we can move to looking at the Poincaré section.

### 2.1.1 Poincaré section

Let us consider an $n$-dimensional system whose dynamics is governed by the equations of motion $\dot{\mathbf{x}} = \mathbf{f}(\mathbf{x})$. Let $S$ be an $(n-1)$-dimensional surface of section that is transverse to the flow. The Poincaré section is a mapping from $S$ to itself obtained by following trajectories from one intersection with $S$ to the next. The map is defined as $\mathbf{x_{k+1}} = P(\mathbf{x_k})$. This is shown in Fig. 2.1. Now consider a closed orbit in the phase space as we describe above. The trajectory starting at the point $\mathbf{x}$ will return to the same point after time $T$. The corresponding Poincaré mapping will be a fixed point $P(\mathbf{x}^*) = \mathbf{x}^*$. We can see that the problems of closed orbits will be converted into the problems of fixed points in this mapping. This is in theory easier to interpret than the orbits in the phase space. However this is not always the case in practice and it is usually not possible to analytically determine the expression for the mapping. For periodic solutions, the mapping can be made easily.

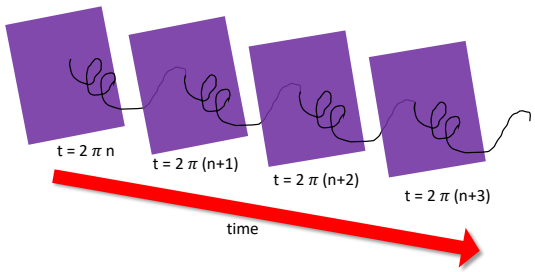


**Figure 2.1**: Poincaré section

### 2.1.2 Periodic orbits in phase space

The regular dynamics of a classical system is described by a periodic orbit in phase space. If we take the Poincaré section of a periodic orbit, we see that the classical trajectory will return to the same point in the section. A period-1 orbit is defined as an orbit that will return once every period to the same place in phase space, and the Poincaré section will be a single point for all time sections. A period-2 orbit will return once every two periods to the same point and the Poincaré section will be two points in phase space, and so on. A chaotic orbit will look very different to this.

## 2.2 Classical chaos

As we discussed briefly in the introduction, the emergence of chaos comes about from the nonlinear equations that govern the evolution of a system. What exactly is chaos? It is dynamical behaviour that appears seemingly complex and random but is actually a result of fully deterministic evolution that we can understand and model very accurately. See [133] for more detail.

The presence of chaos is defined by a few characteristic features:

- Sensitivity to initial conditions: The tiniest perturbation of the initial condition leads to completely different evolution. This is quantified by an exponential rate of divergence of trajectories in phase space. The rate is given by the Lyapunov exponent which is positive for chaotic systems.
- Aperiodic motion: A chaotic system is characterised by the behaviour that it will never come back to the same place. The orbit will always visit a different place in the phase space of the system. This makes it aperiodic. The Poincaré section allows us to visualise this, for chaotic dynamics, the section looks like a sea of chaos, ie. many points covering the phase space.
- Bounded in phase space.

### 2.2.1 Poincaré Section for Dissipative chaos

Systems that are dissipative and chaotic are a bit stranger than Hamiltonian chaotic systems. This is because of the emergence of a strange attractor in the Poincaré section. Before we define a strange attractor, let us consider an attractor in general [133]. An attractor ($A$) is a closed invariant set. Any trajectory that starts in the set will remain for

all time. An open set $U$ of initial conditions that contains $A$ as a subset will be attracted. The distance of any trajectory in $U$ to $A$ will approach zero as $t \to \infty$. The largest possible $U$ is called the basin of attraction of $A$. There is no proper subset of $A$ that satisfies these conditions ($A$ in minimal).

A strange attractor is then defined to be an attractor that has a sensitive dependence on initial conditions. The strange attractor for the Duffing oscillator is shown as an example in Fig. 2.2. Any starting condition for this set of parameters will fall onto the strange attractor, leading to chaos. For Hamiltonian dynamics that preserve area, it is impossible to have an attractor of any kind.

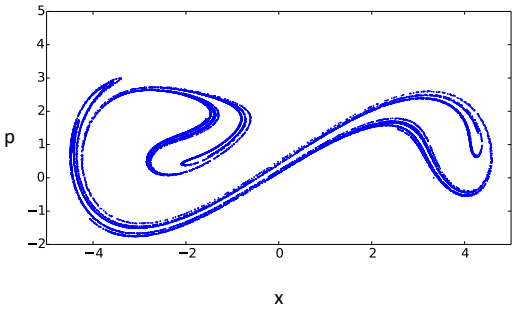


**Figure 2.2**: Strange attractor for the Duffing oscillator.

### 2.2.2 Lyapunov exponent

The sensitivity to initial conditions can be quantified by the Lyapunov exponent which gives the rate of divergence of trajectories in phase space [98]. This is defined as:

$$\lambda = \lim_{t\to\infty} \lim_{d_0\to 0} \frac{\ln\left(d_t/d_0\right)}{t}, \tag{2.1}$$

where $d_t$ is the distance between the two trajectories in phase space at time $t$ and $d_0$ is the initial distance. A system is chaotic when the rate of divergence is positive ie. when $\lambda > 0$ and regular when $\lambda \leq 0$. A negative Lyapunov exponent is a consequence of a regular dissipative system. A system will generally have a spectrum of Lyapunov exponents. We define the presence of chaos by a positive maximal Lyapunov exponent. The sum of Lyapunov exponents must be negative for a dissipative system and one must zero in a dynamical system that has flow along a trajectory. For a Hamiltonian system, the sum of Lyapunov exponents is zero.

## 2.3 Quantum mechanics in phase space

For the comparison of the classical and quantum phase spaces, we require "semiclassical" states that will survive for long times. Recall from the introduction that the process of decoherence is key to a smooth transition from quantum mechanics to dissipative chaos. This means that states that are robust to decoherence will survive, making them "semi-classical" in a sense and the natural choice for comparison between classical and quantum mechanics. These states lie on a classical phase space that is embedded within the quantum Hilbert space. In the following section, we will use standard definitions from a few references ([**Walls:1994**, 111, 77]).

### 2.3.1 Harmonic oscillator

The harmonic oscillator is given by a single particle within a harmonic trap or by a single mode of light [26]. And it is often the first system to be considered when we discuss the connections between classical and quantum mechanics because the physics of the two are the same. In the quantum case we have quantised energy levels of the particle. The state of the particle sitting in the harmonic trap can be described by the occupation number of the energy levels:

$$|\psi\rangle = \sum_n c_n |n\rangle, \tag{2.2}$$

where the coefficients $c_n$ are complex and satisfy $\sum_n |c_n|^2 = 1$.

### 2.3.2 Creation and Annihilation operators

The operators that we can act on the Hilbert space will change the number $n$ of quanta of energy in the harmonic mode. We can create or destroy a quantum from the mode. Now we define these operators:

$$\begin{aligned} \hat{a}|n\rangle &= \sqrt{n}|n-1\rangle \\ \hat{a}^\dagger|n\rangle &= \sqrt{n+1}|n+1\rangle, \end{aligned} \tag{2.3}$$

These are called the creation $\hat{a}^\dagger$ and annihilation $\hat{a}$ operators and they do not commute, ie. $[\hat{a}, \hat{a}^\dagger] = 1$. These operators act on particle to raise and lower the quantised energy level. The annihilation operator cannot annihilate a quantum from the vacuum state. The number operator in terms of the creation and annihilation operators is defined as $\hat{n} = \hat{a}^\dagger\hat{a}$, and the Hamiltonian is given by

$$\hat{H} = \sum \hbar\omega \left(\hat{a}^\dagger\hat{a} + \frac{1}{2}\right). \tag{2.4}$$

We can define the Fock state in terms of the creation operators acting on the vacuum state $|0, ...0\rangle \equiv |0\rangle$:

$$|n\rangle = \frac{(\hat{a}^\dagger)^n}{\sqrt{n!}}|0\rangle. \tag{2.5}$$

The energy of the system is given by the occupation number:

$$E = \hbar\omega(n + \frac{1}{2}), \tag{2.6}$$

and the vacuum energy (when there is no quanta) or zero point energy is $E_0 = \hbar\omega/2$ is not zero.

### 2.3.3 Glauber Coherent States

Glauber proposed coherent states in 1963 [50], motivated by the need to understand the quantum/ classical correspondence for optics and the wave/ particle duality of the electromagnetic (EM) field. Coherent states of the field offer a convenient basis with which the distinction and similarity of the quantum and classical theory can be made, as we will discuss below. The classical EM field is a harmonic oscillator made up of many bosonic modes which are each quantum harmonic oscillators. The coherent states $|\beta\rangle$ of

the EM field must be the eigenstate of the annilhilation operators for each mode $k$.

$$\hat{a}_k|\beta\rangle = \alpha_k|\beta\rangle, \tag{2.7}$$

so the coherent state for each mode $|\alpha_k\rangle$ of the field must be the eigenstate of the annihilation operator $\hat{a}_k$ for that mode

$$\hat{a}_k|\alpha_k\rangle = \alpha_k|\alpha_k\rangle. \tag{2.8}$$

The coherent states of the field are then the product state of the individual states

$$|\beta\rangle = \prod_k |\alpha_k\rangle. \tag{2.9}$$

To find the state $|\alpha\rangle$ for a single bosonic mode which satisfies Eq. 2.8, we begin by taking the scalar product of each side with the number state $\langle n|$:

$$\langle n|\hat{a}|\alpha\rangle = \langle n|\alpha|\alpha\rangle, \tag{2.10}$$

which gives us the recursion relation

$$(n+1)^{1/2}\langle n+1|\alpha\rangle = \alpha\langle n|\alpha\rangle. \tag{2.11}$$

Solving the recursion relation gives

$$\langle n|\alpha\rangle = \frac{\alpha^n}{\sqrt{n!}}\langle 0|\alpha\rangle. \tag{2.12}$$

Using the completeness of the number basis $\sum_u |n\rangle\langle n| = \hat{1}$ we have

$$\begin{aligned} |\alpha\rangle &= \sum_u |n\rangle\langle n|\alpha\rangle \\ &= \langle 0|\alpha\rangle \sum_n \frac{\alpha^n}{\sqrt{n!}}|n\rangle, \end{aligned} \tag{2.13}$$

and if we have a normalised coherent state $\langle\alpha|\alpha\rangle = 1$ then we can find

$$\langle 0|\alpha\rangle = e^{-|\alpha|^2/2}, \tag{2.14}$$

so that the coherent states are given by

$$|\alpha\rangle = e^{-|\alpha|^2/2} \sum_n \frac{\alpha^n}{\sqrt{n!}}|n\rangle. \tag{2.15}$$

The coherent state is a coherent sum of number states. And $\alpha = |\alpha|\exp(i\theta)$ is a complex number which describes the location of the centre of the coherent state in phase space.

### 2.3.4 Displacement operator as a definition of a coherent state

We can also define the coherent states as a displacement of the ground state of the system. If we start with a vacuum state of the electromagnetic field, a displacement of the state

by a complex amplitude $\alpha$ will give a coherent state.

$$|\alpha\rangle = \hat{\mathcal{D}}(\alpha)|0\rangle, \tag{2.16}$$

where $\mathcal{D}(\alpha) = \exp(\alpha\hat{a}^\dagger - \alpha^*\hat{a})$. We express this in a form that easily acts upon the ket $|0\rangle$ by using the Baker Campbell Hausdorff (BCH) theorem. For two operators $\hat{A}$ and $\hat{B}$ that do not commute but do commute with the commutator (ie. $[\hat{A},[\hat{A},\hat{B}]] = [\hat{B},[\hat{A},\hat{B}]] = 0$), then the reordering theorem can be expressed as [111]

$$e^{\theta(\hat{A}+\hat{B})} = e^{p(\theta)\hat{A}}e^{q(\theta)\hat{B}}e^{r(\theta)[\hat{A},\hat{B}]}, \tag{2.17}$$

where $p(\theta) = q(\theta) = \theta$ and $r(\theta) = -\theta/2$. So the displacement operator acting on the vacuum state is simply given by

$$\begin{aligned}
\mathcal{D}(\alpha)|0\rangle &= e^{[\alpha\hat{a}^\dagger - \alpha^*\hat{a}]}|0\rangle \\
&= e^{(-|\alpha|^2/2)}e^{\alpha\hat{a}^\dagger}e^{-\alpha^*\hat{a}}|0\rangle \\
&= e^{(-|\alpha|^2/2)}e^{\alpha\hat{a}^\dagger}|0\rangle \\
&= e^{(\frac{-|\alpha|^2}{2})}\sum_{n=0}^{\infty}\frac{\alpha^n}{\sqrt{n!}}|n\rangle,
\end{aligned} \tag{2.18}$$

which agrees with the definition based on the eigenstates of the annihilation operator.

### 2.3.5 Connection to the classical phase space

Since coherent states are the eigenstates of the annihilation operator, they are robust to quantum loss processes such as decoherence. Intuitively, we therefore expect coherent states to behave semiclassically. We can confirm this intuition by expressing the wavefunction of a coherent state within the classical phase space given by the position and momentum co-ordinate. We first introduce the canonical conjugate pair $\hat{q},\hat{p}$ which obeys the commutation relation $[\hat{q},\hat{p}] = i\hbar$, so that the annihilation and creation operators in terms of the quadratures are

$$\begin{aligned}
\hat{a} &= \frac{1}{\sqrt{2\hbar}}(\hat{q} + i\hat{p}) \\
\hat{a}^\dagger &= \frac{1}{\sqrt{2\hbar}}(\hat{q}^\dagger - i\hat{p}).
\end{aligned} \tag{2.19}$$

The conjugate pair represent the dimensionless position and momentum operators and are referred to as the quadrature operators. The expectation values for the conjugate pair $\langle\hat{q}\rangle = q$ and $\langle\hat{p}\rangle = p$ give the real and imaginary parts of the coherent field respectively:

$$\langle\alpha|\hat{q}|\alpha\rangle = \sqrt{\hbar}\langle\alpha|\frac{1}{\sqrt{2}}(\hat{a}+\hat{a}^\dagger)|\alpha\rangle = \sqrt{\hbar}\frac{1}{\sqrt{2}}(\alpha+\alpha^*) = \sqrt{2\hbar}\mathrm{Re}(\alpha), \tag{2.20}$$

$$\langle\alpha|\hat{p}|\alpha\rangle = \sqrt{\hbar}\langle\alpha|\frac{i}{\sqrt{2}}(\hat{a}-i\hat{a}^\dagger)|\alpha\rangle = \sqrt{\hbar}\frac{i}{\sqrt{2}}(\alpha-\alpha^*) = -\sqrt{2\hbar}\mathrm{Im}(\alpha), \tag{2.21}$$

and

$$\alpha = \sqrt{\frac{\hbar}{2}}\,(q + ip)\,. \tag{2.22}$$

If we look at the uncertainty of $\hat{q}$ and $\hat{p}$, we can see that the coherent states are in a sense the "semiclassical" states of the Hilbert space. The Heisenberg uncertainty principle tells us that we cannot know $\hat{q}$ and $\hat{p}$ precisely at the same time for a quantum system. The more precisely we know the position, the less precisely we can know the momentum. Formally this is given by the inequality:

$$\Delta\hat{q}\Delta\hat{p} \geq \frac{\hbar}{2}. \tag{2.23}$$

For the coherent states, the uncertainty is given by

$$\begin{aligned}
(\Delta\hat{q})^2 &= \langle\hat{q}^2\rangle - \langle q\rangle^2 \\
&= \frac{\hbar}{2}\langle\alpha|\hat{a}^2 + \hat{a}^{\dagger 2} + \hat{a}\hat{a}^\dagger + \hat{a}^\dagger\hat{a}|\alpha\rangle - 2\hbar\mathrm{Re}(\alpha)^2 \\
&= \frac{\hbar}{2}(|\alpha|^2 + \alpha^2 + \alpha^{*2} + |\alpha|^2 + 1) - 2\hbar\mathrm{Re}(\alpha)^2 \\
&= \hbar/2 \qquad (2.24) \\
(\Delta\hat{p})^2 &= \langle\hat{p}^2\rangle - \langle p\rangle^2 \\
&= -\frac{\hbar}{2}\langle\alpha|\hat{a}^2\hat{a}^{\dagger 2} - \hat{a}\hat{a}^\dagger - \hat{a}^\dagger\hat{a}|\alpha\rangle - 2\hbar\mathrm{Im}(\alpha)^2 \\
&= \frac{\hbar}{2}(|\alpha|^2 - \alpha^2 - \alpha^{*2} + |\alpha|^2 + 1) - 2\hbar\mathrm{Im}(\alpha)^2 \\
&= \hbar/2 \qquad (2.25) \\
(\Delta\hat{q})^2(\Delta\hat{p})^2 &= \frac{1}{4}\hbar^2. \qquad (2.26)
\end{aligned}$$

The coherent states minimise the Heisenberg uncertainty principle, they are the most classical states of the Hilbert space. We can visualise what a coherent state looks like in the classical phase space easily using the "ball and stick" analogy that is commonly referred to in quantum optics (shown in Fig 2.3). The coherent state is a ball displaced from the origin by complex amplitude $\alpha$. The size of the ball is determined by the uncertainty in $\hat{q}$ and $\hat{p}$.

What does the wavefunction of a coherent state look like in the position and momentum bases? The wavefunction in quantum mechanics is complex so we must look at the probability distribution instead. For comparison with the classical phase space we look at the marginals $|\langle q|\alpha\rangle|^2$ and $|\langle p|\alpha\rangle|^2$. The wave function in coordinate space is given by the overlap of the coherent state with the coordinate basis:

$$\langle q|\alpha\rangle = (\pi)^{-1/4}e^{\{-ip_0q_0/2 + ip_0q - (q-q_0)^2/2\}}. \tag{2.27}$$

In momentum space we similarly have

$$\langle p|\alpha\rangle = (\pi)^{-1/4}e^{\{ip_0q_0/2 - iq_0p - (p-p_0)^2/2\}}. \tag{2.28}$$

This shows that the quadrature probability distributions $|\langle q|\alpha\rangle|^2$ and $|\langle p|\alpha\rangle|^2$ are Gaussian, centred around the displaced point $\alpha = q_0 + ip_0$.

Let us now consider the overlap of two coherent states in the classical phase space:

$$\langle\alpha_2|\alpha_1\rangle = e^{-i(q_1p_2 - p_1q_2)/2}e^{-\{(q_2-q_1)^2 + (p_2-p_1)^2\}/4}, \tag{2.29}$$

which gets smaller exponentially fast as the coordinate distance between the two states

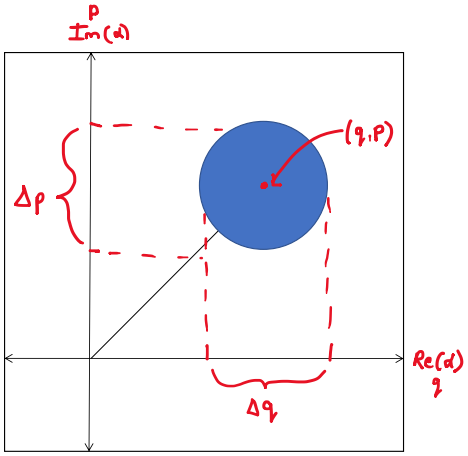


**Figure 2.3:** The coherent state can be easily visualised in phase space by a ball and stick analogy. In the complex phase space of $\alpha$, the coherent state is given by a ball that is centred around the point $(\mathrm{Re}(\alpha), \mathrm{Im}(\alpha)) = (\langle\hat{q}\rangle, \langle\hat{p}\rangle)$. The width of the ball is given by the uncertainty in $\hat{q}$, $\hat{p}$ which is equal. In the classical limit, the ball becomes a point that is infinitely narrow in phase space.

gets larger. Larger coordinate distance leads to a state that is somewhat more classical as the interference between the two states diminishes. The greater the distance between the two coherent states, the more classical they appear. The distance in classical phase space tends to larger values as the classical limit is approached. The space of coherent states is the classical phase space that is embedded in the infinite dimensional quantum Hilbert space. In the case at hand, we have a 2 dimensional flat plane. The metric for the space spanned by $q$ and $p$ gives the distance metric which we will use for calculating Lyapunov exponents. This metric is given as the distance in phase space:

$$\mathrm{d}s^2 = \frac{1}{2}(\mathrm{d}q^2 + \mathrm{d}p^2). \tag{2.30}$$

The benefit of considering coherent states is that there is a one-to-one mapping between the space of coherent states and the classical phase space. A point in the classical phase space corresponds to a coherent state.

### 2.3.6 Semiclassical limit

As the system becomes more classical, we can approximate our wave function by a Gaussian function in the classical phase space. We have just seen that coherent states are in a sense the classical states in the space of quantum states and that they saturate the Heisenberg uncertainty relation. However they are not the only states that do this. Coherent states are special because they also satisfy $\Delta q = \Delta p$ but we make the more general assumption that the semiclassical state will be a Gaussian in phase space. This assumption is also valid for squeezed states where the uncertainty in one observable is less than the canonical conjugate observable. This approximation is valid in the semiclassical regime where there is minimal quantum interference effects from superpositions but where there is still uncertainty in the observables of the system. The classical limit is then approached by taking the variance of the Gaussian to zero. For a Gaussian wavefunction, we can describe the state by just the expectation values $\hat{q}$ and $\hat{p}$, the variances $V_q$, $V_p$ and the

covariance $V_{qp} = \frac{1}{2}(\langle\hat{q}\hat{p}\rangle + \langle\hat{p}\hat{q}\rangle - \langle\hat{q}\rangle\langle\hat{p}\rangle$. This approximation is valid when there is no quantum superposition states. When the state is coherent or a squeezed coherent state it can be approximated as a Gaussian wavepacket [102]

$$\psi(q,t) = (2\pi\mu)^{-1/4}\exp\{i[A(x-q)^2 + p(x-q)]\}, \tag{2.31}$$

which implies the relations

$$\begin{aligned}
\langle\Delta\hat{q}^{2m}\rangle &= \frac{(2m)!\mu^m}{m!2^m}, &(2.32)\\
\langle\Delta\hat{q}^{2m+1}\rangle &= 0, &(2.33)\\
4\mu\langle\Delta\hat{p}^2\rangle &= \hbar^2 + \alpha^2, &(2.34)\\
\langle\Delta\hat{q}\Delta\hat{p} + \Delta\hat{p}\Delta\hat{q}\rangle &= \alpha, &(2.35)
\end{aligned}$$

where

$$A = \frac{1}{4\mu}(i+\alpha). \tag{2.36}$$

### 2.3.7 Visualising quantum states

We have shown above how the classical and quantum phase spaces can be connected through coherent states, and that these states can be visualised in phase space by looking at the marginals. But we also require a general method to visualise arbitrary states in phase space. In order to compare general quantum states with the classical dynamics, we require a quantum phase space distribution. Though in general the distribution can be negative for quantum mechanics and the probability distribution cannot be a true probability distribution because of incompatibility of the canonically conjugate observables $\hat{q}$ and $\hat{p}$. However, it is still useful to describe quantum states with quasi-probability distributions. Here we will introduce the density matrix formalism of quantum states that we will see again in chapter 3. The general description of a quantum state is a density matrix $\hat{\rho}_S$, with components giving the probabilities $p_i$ of being in the associated pure states $|\psi_i\rangle$:

$$\hat{\rho}_S = \sum_i p_i|\psi_i\rangle\langle\psi_i|, \tag{2.37}$$

where the probabilities are positive $p_i > 0$ and must sum to give $\sum_i p_i = 1$. We introduce this here because it will ensure we understand the following methods of visualising quantum states. In general, a quantum state may not always be a pure state and in that case, the density operator formalism is required.

#### Wigner Function

One of the quasi probability distributions used to visualise states is the Wigner function [151], which is given by

$$W(q,p) = \frac{1}{2\pi}\int_{-\infty}^{+\infty} e^{ipx}\langle q - \tfrac{x}{2}|\hat{\rho}|q + \tfrac{x}{2}\rangle \mathrm{d}x. \tag{2.38}$$

The Wigner function takes a Hilbert space state $\hat{\rho}$ and transforms it to a classical phase space function which has the following properties:

- Its real for Hermitian $\hat{\rho}$. $W^*(q,p) = W(q,p)$

- Its normalised. $\int_{-\infty}^{+\infty}\int_{-\infty}^{+\infty} W(q,p)\mathrm{d}q\mathrm{d}p = 1$.
- It is easy to calculate expectation values for the state. For an operator $\hat{F}$, the overlap formula gives $\mathrm{tr}\{\hat{\rho}\hat{F}\} = 2\pi\int_{-\infty}^{+\infty}\int_{-\infty}^{+\infty} W(q,p)W_F(q,p)\mathrm{d}q\mathrm{d}p$, where $W_F(q,p)$ is the Wigner function for the operator $\hat{F}$
- The Wigner function cannot be completely positive in general.
- $|W(q,p)| \leq 1/\pi$ (proven with the Schwarz inequality).

One of the benefits of the Wigner function as a tool for visualising quantum states, as we will see in examples below, is that it allows us to visualise and quantify the degree of "quantum-ness" of the state which can be seen from the presence of interference fringes that come from quantum superpositions. We will make use of this in Chapters 4 & 5. The degree of "quantum-ness" (ie. how nonclassical the state is) can be quantified by the amount of negativity in the Wigner function [69].

**Examples of Wigner Functions**

- For the vacuum state we have

$$W_0(q,p) = \frac{1}{\pi}\exp(-q^2-p^2) \tag{2.39}$$

- The coherent state is a displaced vacuum state with complex coherent amplitude $\sqrt{2}\alpha = q_0 + ip_0$.

$$\begin{aligned} W_D(q,p) &= \frac{1}{2\pi}\int_{-\infty}^{+\infty} e^{ipx}\langle q-\frac{x}{2}|\hat{\mathcal{D}}\hat{\rho}\hat{\mathcal{D}}^\dagger|q+\frac{x}{2}\rangle\mathrm{d}x \\ &= \frac{1}{2\pi}\int_{-\infty}^{+\infty} e^{i(p-p_0)x}\langle q-\frac{x}{2}-q_0|\hat{\rho}|q+\frac{x}{2}-q_0\rangle\mathrm{d}x \\ &= W(q-q_0,p-p_0), \end{aligned} \tag{2.40}$$

  So the Wigner function for a coherent state is given by $W(q,p) = 1/\pi\exp(-(q-q_0)^2-(p-p_0)^2)$. This looks exactly as what we have shown above in Fig. 2.3. The ball and stick is the Wigner function of a coherent state in phase space.

- Now if we consider the superposition of two coherent states located at different positions in the phase space, we have what is known as a cat state [59], named as such after Schrödinger's thought experiment: (which will be discussed in much greater detail in the next chapter).

$$W(q,p) \propto e^{-(q-q_0)^2-p^2} + e^{-(q+q_0)^2-p^2} + 2e^{-q^2-p^2}\cos(2pq_0), \tag{2.41}$$

  where we can see the interference fringes from the coherent superposition. The Wigner function for the cat state is shown in Fig. 2.4. The Wigner function displays quadrature amplitudes, their fluctuations and possible interferences.

**Husimi Q function**

What if we want something that is strictly positive? Something that more resembles a classical probability distribution. If we smooth the Wigner function by convolving it with a

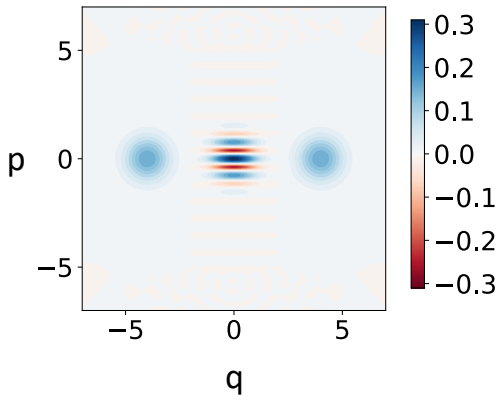


**Figure 2.4:** The cat state can be best visualised with the Wigner function. This is what it looks like in the phase space. As you can see the state is made up of the two coherent states in the superposition and the interference fringes that are a clear sign of the quantum superposition state.

Gaussian distribution we can achieve this, and we end up with the Husimi Q function [65]. What this gives is the overlap of the quantum state with a coherent state centred at the same point in phase space:

$$Q(q,p) = \frac{1}{\pi}\int_{-\infty}^{+\infty}\int_{-\infty}^{+\infty} W(q',p')e^{-(q-q')^2-(p-p')^2}\mathrm{d}q'\mathrm{d}p'. \tag{2.42}$$

The Q function gives the probability distribution for finding coherent states $|\alpha\rangle$ in the state $\hat{\rho}$.

$$\begin{aligned} Q(q,p) &= \frac{1}{2\pi}\mathrm{tr}\{\hat{\rho}|\alpha\rangle\langle\alpha|\} \\ &= \frac{1}{2\pi}\langle\alpha|\hat{\rho}|\alpha\rangle. \end{aligned} \tag{2.43}$$

The Husimi Q function is non-negative and normalised to unity. With the Husimi Q function we can no longer quantify how quantum the state is since we cannot see the interference fringes. A superposition state will look the same as a classical mixture of coherent states. But it can be seen as a more classical probability distribution since the probability is no longer negative.

### Example of Q function

As an example we bring back the Schrödinger cat state:

$$Q(\alpha) \propto e^{-|\alpha-\alpha_0|^2} + e^{-|\alpha+\alpha_0|^2} + 2e^{-|\alpha|^2-|\alpha_0|^2}\cos(2\mathrm{Im}(\alpha^*\alpha_0)). \tag{2.44}$$

An exponentially small bump proportional to $\exp(-|\alpha|^2)$ is all that is left of the interference structure in the Q function and the more macroscopic the cat state, the smaller the bump. So the Q function cannot clearly discriminate between macroscopic superpositions and statistical mixtures. This means that the Q function is not suitable to demonstrate the "quantum-ness" of the quantum state. For this reason we will not use it in our treatment of the Duffing Oscillator, however it is useful to highlight the advantages of the Wigner

function for some things.

## 2.4 Models of chaotic systems

In this thesis we will focus on the quantum version of two different chaotic models of interest, the Duffing oscillator (Ch. 4& 5) and the driven top (Ch. 6). In this section we will discuss the physics needed to describe these two systems. For the Duffing oscillator we have already described a lot of what is necessary in the previous sections, we require the physics of the harmonic oscillator. While for the driven top we must introduce some new physics and a new phase space for the classical limit.

### 2.4.1 The Duffing oscillator

The first system we will consider is the Duffing oscillator, which can be physically described by a single particle in a double well potential. The quantum state can be described by the Harmonic oscillator basis states given in section 2.3.1 and the classical phase space is the 2D plane given by $x$ and $p$ in section 2.3.5.

### 2.4.2 The driven top

The second system we will focus on in this thesis is the driven top, which can be physically described by the Bose-Hubbard dimer [89] or as a collection of two level atoms or as the spin of a single atom. All of these systems share the same physics that can be described by an SU(2) algebra and the angular momentum operators. Let us focus on the description of a Bose-Hubbard dimer. Physically this is the collection of atoms in two lattice sites that are free to interact with each other and tunnel between the two wells. For this realisation we have two bosonic modes. The two-mode Fock state is

$$|n_a\rangle \otimes |n_b\rangle = \frac{(\hat{a}^\dagger)^{n_a}}{\sqrt{n_a!}} \frac{(\hat{b}^\dagger)^{n_b}}{\sqrt{n_b!}} |0,0\rangle \equiv |n_a, n_b\rangle. \tag{2.45}$$

Atoms cannot be created or destroyed so the total number $N = n_a + n_b$ is fixed. By imposing the fixed number constraint we take the infinite space spanned by $|n_a, n_b\rangle$ and define the subspace spanned by $N+1$ basis vectors $|N-n, n\rangle$ $[n = 0, 1, ..., N]$ which are sometimes called Dicke states.

The Bose-Hubbard model can become quite complex with high numbers of atoms and lattice sites. Fortunately for the case of two bosonic modes, the system can be conveniently described by the SU(2) algebra which makes things a bit simpler. For three bosonic modes (three lattice sites) the system could be described by an SU(3) algebra and in general N lattice sites can be descibed by SU(N) algebra.

The Hamiltonian for the Bose-Hubbard dimer is

$$\hat{H} = \alpha \hat{a}^\dagger \hat{a} + \beta \hat{b}^\dagger \hat{b} + \gamma(\hat{a}^\dagger \hat{b} + \hat{b}^\dagger \hat{a}), \tag{2.46}$$

where $\alpha$ and $\beta$ correspond to the energy of the modes $a$ and $b$, with the number of particles in mode $a$ given by $\hat{n} = \hat{a}^\dagger \hat{a}$ acting on a particular state and similar for mode $b$. The $\gamma$ term describes the interaction between the two modes. Rather than looking at the action of the individual atoms, we can conveniently cast this system into a problem of pseudo-angular

momentum using the Jordan-Schwinger decomposition and use SU(2) algebra instead.

$$\begin{aligned}\hat{J}_x &= \frac{1}{2}\left(\hat{a}^\dagger\hat{b} + \hat{b}^\dagger\hat{a}\right)\\ \hat{J}_y &= \frac{1}{2i}\left(\hat{b}^\dagger\hat{a} - \hat{a}^\dagger\hat{b}\right)\\ \hat{J}_z &= \frac{1}{2}\left(\hat{a}^\dagger\hat{a} - \hat{b}^\dagger\hat{b}\right).\end{aligned} \tag{2.47}$$

The Hermitian angular momentum operators obey the commutation relation

$$[\hat{J}_i, \hat{J}_j] = i\varepsilon_{ijk}\hat{J}_k. \tag{2.48}$$

The basis states of the SU(2) angular momentum states are also the eigenstates of the number difference operator

$$\hat{J}_z|N-n, n\rangle = m|N-n, n\rangle, \tag{2.49}$$

where

$$m = \frac{1}{2}(n_a - n_b) = \frac{N}{2} - n. \tag{2.50}$$

We usually denote the eigenstates of the number difference (Dicke states) as $|j, m\rangle$ where $j = N/2$ is the total spin of the system. The $N+1$ unique eigenvalues take values in integer steps between $-j \leq m \leq j$. The maximal state $|j, j\rangle$ has all bosons in one mode and the minimal state $|j, -j\rangle$ has all bosons in the other mode. The raising and lowering operators for the spin are $\hat{J}_+ = \hat{a}^\dagger\hat{b}$ and $\hat{J}_- = (\hat{J}_+)^\dagger$, in terms of the Hermitian operators they are given as

$$\begin{aligned}\hat{J}_- &= \hat{J}_x - i\hat{J}_y\\ \hat{J}_+ &= \hat{J}_x + i\hat{J}_y.\end{aligned} \tag{2.51}$$

Analogous to the creation and annihilation operators for a single oscillator, they act to raise and lower the spin of the system, or for a two mode bosonic system, they take bosons from one mode to the other mode and vice versa.

$$\hat{J}_-|j, m\rangle = \sqrt{J(J+1) - m(m-1)}|j, m-1\rangle \tag{2.52}$$

$$\hat{J}_+|j, m\rangle = \sqrt{J(J+1) - m(m+1)}|j, m+1\rangle, \tag{2.53}$$

so that $\hat{J}_+|j, j\rangle = 0$ and $\hat{J}_-|j, -j\rangle = 0$, in the same way that we cannot apply the annihilation operator on the vacuum state.

For $\hat{J}_z, \hat{J}_+$ and $\hat{J}_-$, we have

$$[\hat{J}_z, \hat{J}_\pm] = \pm\hat{J}_\pm \quad \text{and} \quad [\hat{J}_+, \hat{J}_-] = 2\hat{J}_z. \tag{2.54}$$

### 2.4.3 Coherent spin states

The operator that gives the displacement in the SU(2) phase space is given by a rotation operation on the surface of the sphere. SU(2) is isomorphic to SO(3), so the classical phase space is the space of rotations on the surface of the sphere. We face the same problem as with classical rotations on a 2-sphere in that the operation of rotation is not unique. In an analogous way to Glauber coherent states, the coherent states for the SU(2) group can

be given as the rotation of a maximal spin state to a coherent spin state (CSS) [110]

$$\hat{\mathcal{R}}(\theta,\phi)|j,j\rangle = e^{(-i\phi\hat{J}_z)}e^{(-i\theta\hat{J}_y)}|j,j\rangle, \tag{2.55}$$

where $|j,j\rangle$ is the state of all the bosons in one of the wells. Because SU(2) is isomorphic to SO(3) this can be understood easily as the rotation of the CSS from about the $\hat{J}_y$ axis by the angle $\theta$ and then another rotation applied about the $\hat{J}_z$ axis by the angle $\phi$. In the limit of large $j$ the rotation becomes equivalent to the displacement operator given in Eq. 2.18. In the classical limit, the conjugate pair is $\cos(\theta), \phi$, this gives the two dimensional plane on which the classical state lies. As we approach the classical limit (as $N/2 = j \to \infty$) the surface of the sphere starts to look more and more like a 2D flat space. One possible uncertainty relation for the SU(2) algebra is given by

$$(\Delta\hat{J}_x)^2(\Delta\hat{J}_y)^2 \geq \frac{1}{4}\langle\hat{J}_z\rangle^2, \tag{2.56}$$

and once again the general CSS in SU(2) saturates the relation giving the minimum uncertainty state. The classical states for the SU(2) system (and the minimal uncertainty states) will be Gaussians on the classical phase space given by the surface of the sphere. Analogous to the Glauber coherent states, we have spin coherent states:

$$|j,\theta,\phi\rangle = \sum_{m=-j}^{j}\sqrt{\binom{2j}{j-m}}\sin\left(\frac{\theta}{2}\right)^{j-m}\cos\left(\frac{\theta}{2}\right)^{j+m}e^{i(j-m)\phi}|jm\rangle. \tag{2.57}$$

The metric for this space is given by the arc length on the surface of the sphere.

$$\mathrm{d}s^2 = \frac{j}{2}(\mathrm{d}\theta^2 + \sin^2(\theta)\mathrm{d}\phi^2). \tag{2.58}$$

### 2.4.4 Husimi Q function for SU(2)

In much the same way as the Husimi Q function for the Glauber coherent states, the Husimi Q function for an SU(2) system is the overlap of the state with a coherent spin state (CSS) which is given by

$$Q(\theta,\phi) = \frac{2J+1}{4\pi}\langle\alpha(\theta,\phi)|\hat{\rho}|\alpha(\theta,\phi\rangle. \tag{2.59}$$

The visualisation of the Husimi Q function for a coherent spin state in SU(2) is given in fig. 2.5. If we took the system to the limit of large $j$, this would look much the same as the pictorial representation for the Glauber Coherent state in $q,p$ phase space as a circle in the 2D space.

## 2.5 Evolution of Closed Quantum Systems

A closed quantum system is completely isolated from its surrounding environment. Think for example of an atom (or a cat, or a universe) in a box with no interaction with anything outside the box. The evolution of such a system is unitary which means there is no loss of information about the state and the process is reversible. The continuous time evolution of the closed system is given by the well known differential equation known as the Schrödinger

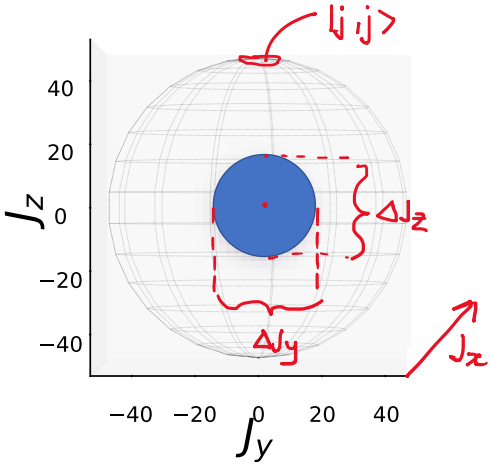


**Figure 2.5:** A coherent spin state on the surface of the sphere for $N = 100$ bosons. This coherent spin state is made by the rotation of the maximal state $\hat{\mathcal{R}}(\theta, \phi)|j, j\rangle$, with the parameter choice $(\theta = \pi/2,\ \phi = 0)$ which corresponds to a rotation about the $\hat{J}_y$ axis of $\theta = \pi/2$.

equation

$$i\hbar \frac{\mathrm{d}|\psi\rangle}{\mathrm{d}t} = \hat{H}|\psi\rangle, \tag{2.60}$$

where $\hbar$ is Planck's constant and $H$ is the Hamiltonian of the closed system. Solving the Schrödinger equation will give the state at time $t$:

$$|\psi(t)\rangle = \hat{U}(t, t_0)|\psi(t_0)\rangle, \tag{2.61}$$

where $\hat{U}(t, t_0)$ is the unitary operation that takes the state from time $t_0$ to $t$ and for a time-independent Hamiltonian, is given by

$$\hat{U}(t, 0) = e^{\frac{-i}{\hbar}\hat{H}(t-t_0)}. \tag{2.62}$$

In the next chapter we will look at what happens when we open the quantum system to interactions with an environment, which we will need in order to connect the quantum dynamics with the chaos found in the classical limit.

# 3

# Background II: Evolution of Open Quantum Systems

In the previous chapter, we introduced classical chaos and the usual methods for studying it. We also introduced the mathematical framework we will need for dealing with quantum states and quantum mechanics and the evolution of a closed quantum system. In this chapter we can now dive into the dynamics of open quantum systems . In this thesis, we are interested in the nonlinear dynamics of chaotic systems and how this emerges from the quantum system as we go towards the classical limit. We are specifically interested in the emergence of chaos in open quantum systems that are continuously monitored. In order to look at the dynamics of open quantum systems, we need to know how an open quantum system evolves and how we can obtain the state of a quantum system at some time. In section 3.1 we will introduce a quantum system interacting with an environment and discuss the evolution of an open quantum system. In section 3.2, we discuss the evolution of a quantum system under measurement which is one of the main focuses of this thesis and therefore an important section for the rest of the thesis. We will look at projection measurements and the measurement postulate and then cover the continuous measurement of open quantum systems.

## 3.1 Open Quantum Systems

No quantum system is ever truly isolated from the surrounding environment, and if we want to look at the dynamics of a quantum system in nature, often we need to also consider the effect that the environment has on the quantum system. Think again of a cat in a box, that box is sitting in a bigger box (also known as the universe) and the universe and the cat in the box can interact with each other, for example electromagnetic waves of light could penetrate the box and heat it up. When the principal system interacts with the external environment, information is shared between the two which can couple the systems and lead to entanglement. If the state of the environment and the coupling is known, then we can treat the two systems as sub-systems of one larger system. The evolution of the total system will remain unitary. However, if the state of the environment is ignored,

information about the state of the system of interest (and coherence) will be lost. This loss process is referred to as decoherence and is an irreversible process that generally (but not always) leads to the state of the quantum system becoming a classical mixture. When this is the case, we can no longer express the state of the principal system as a pure state vector $|\psi\rangle$. Recall from section 2.3.7 that in this case we describe the quantum state in the density operator formalism (Eq. 2.37). The density operator formalism can express a pure state as well as a mixed state for the system of interest and is more general than the state vector formalism.

In chapter 2 we briefly discussed the evolution of a closed quantum system. We can redo this in the density operator formalism to obtain the same thing. The evolution of the density operator for a closed system is given by

$$\hat{\rho}_T(t) = \hat{U}\hat{\rho}_T\hat{U}^\dagger, \tag{3.1}$$

where $T$ stands for the total system and the equation of motion of the total system is now given by the Von-Neumann equation

$$\frac{\mathrm{d}\hat{\rho}_T(t)}{\mathrm{d}t} = -\frac{i}{\hbar}[\hat{H}, \hat{\rho}_T(t)]. \tag{3.2}$$

In practice it can be near impossible to keep track of all information lost to the environment, inevitably leading to some amount of decoherence. It can also be quite challenging to model the evolution of the total system, especially when the environment coupled to the principal system has many degrees of freedoms. This motivates a simpler model for the approximate evolution of the principal system where the information lost to the environment is disregarded. This evolution is described by what is known as a master equation.

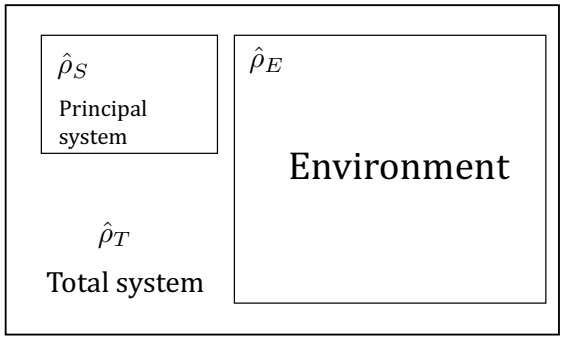


**Figure 3.1:** Open quantum system coupled to the environment. Both are sub systems of a much larger system.

### 3.1.1 Derivation of the Markovian master equation

The following derivation is based on the derivation given in the Wiseman and Milburn textbook [158] and the Breuer and Petruccione textbook [12]. As stated above, the evolution of the total system can be difficult to solve when the environment, often referred to a reservoir or bath, is much larger system than the principal system. In quantum optics we often regard a principal system coupled to a heat bath constructed of many harmonic oscillators. In this case, the problem can be much simpler if we disregard the information

lost to the environment and model the approximate evolution of the principal system with loss. If we focus solely on the principal quantum system with state $\hat{\rho}_S$, the evolution will no longer be unitary. To begin with, the reduced density matrix (the state of the principal system) with loss to the environment is given by tracing out the environmental degrees of freedom.

$$\hat{\rho}_S(t) = \mathrm{Tr}_E[\hat{\rho}_T] = \sum_j \langle e_j|\hat{\rho}_T(t)|e_j\rangle, \tag{3.3}$$

where the Hilbert spaces for the system and environment are $\mathcal{H}_S$ and $\mathcal{H}_E$ respectively and $\{|e_j\rangle\}$ is an orthonormal basis of $\mathcal{H}_E$. For the total closed system, the Hilbert space is $\mathcal{H}_S \otimes \mathcal{H}_E$ and the Hamiltonian is given by

$$\hat{H} = \hat{H}_S + \hat{H}_E + \hat{H}_I, \tag{3.4}$$

where $\hat{H}_S$ and $\hat{H}_E$ are the free Hamiltonians of the system and environment (we define $\hat{H}_0 = \hat{H}_S + \hat{H}_E$ to be the interaction-free/time-independent Hamiltonian) and are in general well understood and $H_I$ is the interaction term which is usually a more complicated perturbation on the system. We assume that the system and environment are initially uncorrelated, that is, the initial condition is a product state $\hat{\rho}_T(0) = \hat{\rho}_S(0) \otimes \hat{\rho}_E$. In the Schrödinger picture, the evolution of the total system is given by Eq. 3.2. It is useful to move into the interaction frame and split the Hamiltonian into the time-independent terms and the time dependent terms. In the interaction frame, we use

$$\hat{H}_I(t) = e^{i\hat{H}_0 t/\hbar}\hat{H}_I e^{-i\hat{H}_0 t/\hbar}, \tag{3.5}$$

so that the Schrödinger picture equation becomes

$$\frac{\mathrm{d}\hat{\rho}_{T(IF)}}{\mathrm{d}t} = -\frac{i}{\hbar}[\hat{H}_{I(IF)}, \hat{\rho}_{T(IF)}], \tag{3.6}$$

and the solution to Eq. 3.2 is found by

$$\hat{\rho}_T(t) = e^{-i\hat{H}_0 t/\hbar}\hat{\rho}_{T(IF)}(t)e^{i\hat{H}_0 t/\hbar}. \tag{3.7}$$

We will drop the $(IF)$ notation from here on since we will remain in the interaction picture for the rest of the derivation. Solving Eq. 3.6 implicitly we obtain:

$$\hat{\rho}_T(t) = \hat{\rho}_T(0) - \frac{i}{\hbar}\int_0^t ds\,[\hat{H}_I(s), \hat{\rho}_T(s)]. \tag{3.8}$$

Substituting Eq. 3.8 back into Eq. 3.2 and taking the partial trace over the environmental degrees of freedom, we get

$$\frac{\mathrm{d}\hat{\rho}_S}{\mathrm{d}t} = -\frac{1}{\hbar^2}\int_0^t ds\,\mathrm{Tr}_E\{[\hat{H}_I(t), [\hat{H}_I(s), \hat{\rho}_T(s)]]\}, \tag{3.9}$$

where $\mathrm{Tr}_E\{[\hat{H}_I(t), \hat{\rho}_T(0)]\} = 0$ is assumed. This assumption can be made because we assume the two systems are initially uncorrelated and the interaction Hamiltonian acts on both subspaces (see below for the decomposition). This may be valid experimentally if we have sufficiently weak coupling between the environment and the system.

Now we make the Born approximation, we assume the correlations between the subsystems are negligible at all times $\hat{\rho}_T(t) \approx \hat{\rho}_S(t) \otimes \hat{\rho}_E$. Meaning that the coupling between

the environment and system is sufficiently weak at all times and the environment is not affected greatly by the system. Again, this is valid assuming we have a very large environment coupled to the system. The equation of motion then becomes

$$\frac{\mathrm{d}\hat{\rho}_S}{\mathrm{d}t} = -\frac{1}{\hbar^2}\int_0^t ds\, \mathrm{Tr}_E\{[\hat{H}_I(t), [\hat{H}_I(s), \hat{\rho}_S(s)\otimes\hat{\rho}_E]]\}. \tag{3.10}$$

In this form, the future evolution of the system depends on the past state for times $s < t$. This can be understood intuitively if we think in terms of the information that is transferred to the environment. The environment retains a memory given by the information that is transferred and that means that the information can be transferred back to the system. We can simplify this further by assuming that the system is only affected by the present state. This is valid so long as the state does not change much in the time that the environment correlations take to decay (the correlation time). In many cases, the environment correlation time is much shorter than the timescale of the system so this is valid and we can treat the environment effectively as memoryless. This will give us the Redfield master equation:

$$\frac{\mathrm{d}\hat{\rho}_S}{\mathrm{d}t} = -\frac{1}{\hbar^2}\int_0^t ds\, \mathrm{Tr}_E\{[\hat{H}_I(t), [\hat{H}_I(s), \hat{\rho}_S(t)\otimes\hat{\rho}_E]]\}. \tag{3.11}$$

We have assumed so far that the state does not change much within the correlation time of the environment; we can take it a step further by neglecting change altogether within the correlation time by making a course graining in time. This is done by replacing the top limit of the integral with $\infty$. And for convenience we replace $s$ with $t - s$.

$$\frac{\mathrm{d}\hat{\rho}_S}{\mathrm{d}t} = -\frac{1}{\hbar^2}\int_0^\infty ds\, \mathrm{Tr}_E\{[\hat{H}_I(t), [\hat{H}_I(t-s), \hat{\rho}_S(t)\otimes\hat{\rho}_E]]\}. \tag{3.12}$$

The two-step approximation described in Eqs. 3.11 and 3.12 is known as the Markov approximation. We now have an equation that is suitable for weak coupling and memoryless dynamics, and we will use the Markovian evolution for the entirety of this thesis. The Markovian approximation is generally a valid approximation for a lot of systems that we can engineer. While not all systems can be modelled by making this assumption, and a lot of work is currently being done for non-Markovian systems, we will not encounter them in this thesis.

### 3.1.2 Lindblad Master Equation

Throughout this thesis we will use the Master equation in Lindblad form [81] (also referred to as the Gorini-Kossakowski-Sudarshan-Lindblad (GKSL) equation) which we can arrive at by making the Born, Markov and secular approximations on the evolution of our system. This form of the Master equation is easily solvable and valid for the systems we will cover in this thesis. The final steps to arrive at the Lindblad Master equation from Eq. 3.12 requires the secular approximation. The interaction Hamiltonian can be decomposed in terms of the operators of the system and environment

$$\hat{H}_I = \sum_i \hat{A}_i \otimes \hat{E}_i \tag{3.13}$$

where $\hat{A}_i$ ($\hat{E}_i$) are Hermitian operators of the system (environment). We assume the spectrum of $\hat{H}_s$ is discrete and write the system operator in terms of eigenoperators of the system.

$$\hat{A}_i = \sum_\omega \hat{A}_i(\omega) = \sum_\omega \hat{A}_i^\dagger(\omega). \tag{3.14}$$

Rewriting the interaction Hamiltonian in terms of the eigenoperators and moving to the interaction picture where the eigenoperators are simply given by $\hat{A}_i(\omega) = e^{-i\omega t}\hat{A}_i(\omega)$, we get

$$\begin{aligned}\frac{\mathrm{d}\hat{\rho}_S}{\mathrm{d}t} = &-\frac{1}{\hbar^2}\sum_{i,j}\sum_{\omega,\omega'}\int_0^\infty ds\,(e^{i\omega t}\hat{A}_i^\dagger(\omega)e^{i\omega'(t-s)}\hat{A}_j(\omega')\hat{\rho}_s(t) \\ &- e^{-i\omega'(t-s)}\hat{A}_j(\omega')\hat{\rho}_s(t)e^{i\omega t}\hat{A}_i^\dagger(\omega))\langle\hat{E}_i^\dagger(t)\hat{E}_j(t-s)\rangle + H.c.\end{aligned} \tag{3.15}$$

$$\begin{aligned}= &\frac{1}{\hbar^2}\sum_{i,j}\sum_{\omega,\omega'}\int_0^\infty ds\,e^{i\omega' s}\langle\hat{E}_i^\dagger(t)\hat{E}_j(t-s)\rangle e^{i(\omega-\omega')t}(\hat{A}_j(\omega')\hat{\rho}_s(t)\hat{A}_i^\dagger(\omega) \\ &- \hat{A}_i^\dagger(\omega)\hat{A}_j(\omega')\hat{\rho}_s(t)) + H.c.\end{aligned} \tag{3.16}$$

where $\hat{E}_i(t) = e^{i\hat{H}_E t}\hat{E}_i e^{-i\hat{H}_E t}$ are the environment operators in the interaction frame and $\langle\hat{E}_i^\dagger\hat{E}_j\rangle = \mathrm{Tr}_E\{\hat{E}_i^\dagger\hat{E}_j\}$. Now the secular approximation is made by assuming that the timescale of the system $\tau_s \approx |\omega-\omega'|^{-1}$ for $\omega \neq \omega'$ is much larger than the relaxation time scale of the open system $\tau_R$ so that we can neglect all exponentials with frequencies $\omega \neq \omega'$ because they oscillate fast and average out to zero. If we define the environment correlation function as $\Gamma_{ij}(\omega) = \int_0^\infty ds e^{i\omega s}\langle\hat{E}_i^\dagger(t)\hat{E}_j(t-s)\rangle$ then we have

$$\frac{\mathrm{d}\hat{\rho}_S}{\mathrm{d}t} = \frac{1}{\hbar^2}\sum_{i,j}\Gamma_{ij}(\omega)\left(\hat{A}_j(\omega)\hat{\rho}_s(t)\hat{A}_i^\dagger(\omega) - \hat{A}_i^\dagger(\omega)\hat{A}_j(\omega)\hat{\rho}_s(t)\right) + H.c. \tag{3.17}$$

Decomposing the environment correlation function into its real and imaginary components $\Gamma_{ij}(\omega) = \frac{1}{2}\gamma_{ij}(\omega) + iS_{ij}(\omega)$, we have

$$\dot{\hat{\rho}} = -\frac{i}{\hbar}[\hat{H}_{LS},\hat{\rho}_s] + \frac{1}{\hbar^2}\sum_\omega\sum_{i,j}\gamma_{ij}(\omega)\left(\hat{A}_j(\omega)\hat{\rho}_s(t)\hat{A}_i^\dagger(\omega) - \frac{1}{2}\{\hat{A}_i^\dagger(\omega)\hat{A}_j(\omega),\hat{\rho}_s(t)\}\right), \tag{3.18}$$

where $\hat{H}_{LS}$ is the Lamb shift Hamiltonian given by

$$\hat{H}_{LS} = \sum_\omega\sum_{i,j}S_{ij}(\omega)\hat{A}_i^\dagger(\omega)\hat{A}_j(\omega), \tag{3.19}$$

and $S_{ij}(\omega) = \frac{1}{2i}[\Gamma_{ij}(\omega) - \Gamma_{ij}^*(\omega)]$, and $\gamma_i j(\omega) = \Gamma_i j(\omega) + \Gamma_j i^*(\omega)$. If we now diagonalise the coefficient matrix, we end up with the GKSL form of the master equation

$$\dot{\hat{\rho}} = -\frac{i}{\hbar}[\hat{H}_{LS},\hat{\rho}_s] + \frac{1}{\hbar^2}\sum_{\omega,k}\gamma_k(\omega)\left(\bar{\hat{A}}_k(\omega)\hat{\rho}_s(t)\bar{\hat{A}}_k^\dagger(\omega) - \frac{1}{2}\{\bar{\hat{A}}_k^\dagger(\omega)\bar{\hat{A}}_k(\omega),\hat{\rho}_s(t)\}\right). \tag{3.20}$$

### 3.1.3 Example: Spontaneous Emission of a Two Level Atom

Let us now look at the example of a two level atom interacting with a surrounding electromagnetic field that is much larger than the system. The atom can spontaneously emit a photon if it decays to the ground state. This photon could go in any direction. The

Hamiltonian for the environment in this case with $k$ field modes is just given by a sum of harmonic oscillators (let us set $\hbar = 1$ for convenience)

$$\hat{H}_E = \sum_k \omega_k \hat{b}_k^\dagger \hat{b}_k, \tag{3.21}$$

where $\hat{b}_k^\dagger$ and $\hat{b}_k$ are the creation and annihilation operators for the $k$th mode, which are independent of all other modes. The free Hamiltonian for the two level atom is given by

$$\hat{H}_S = \frac{\omega_s}{2}\hat{\sigma}_z, \tag{3.22}$$

where $\omega_s$ is the natural frequency of the atom. This Hamiltonian describes the dynamics of the closed system, which is just the precession around the $\hat{\sigma}_z$ axis on the Bloch sphere. The interaction Hamiltonian that describes the interaction between the system and environment in this case is given by the coupling of the atom to the field modes, which will be the electric dipole coupling

$$\hat{H}_I = \sum_k (g_k \hat{b}_k + g_k \hat{b}_k^\dagger)(\hat{\sigma}_+ + \hat{\sigma}_-), \tag{3.23}$$

where $g_k$ is the coefficient of the $k$th mode that depends on the structure of the mode and $\hat{\sigma}_+$ and $\hat{\sigma}_-$ are the raising and lowering operators for the atom, given by $\hat{\sigma}_- = |g\rangle\langle e|$ and $\hat{\sigma}_+ = (\hat{\sigma}_-)^\dagger$. Moving into the interaction frame, the interaction Hamiltonian is

$$\begin{aligned}\hat{H}_I &= \sum_k (g_k \hat{b}_k e^{-i\omega_k t} + g_k \hat{b}_k^\dagger e^{i\omega_k t})(\hat{\sigma}_+ e^{i\omega_s t} + \hat{\sigma}_- e^{-i\omega_s t}) \\ &= \sum_k g_k \hat{b}_k \hat{\sigma}_+ e^{-i(\omega_k-\omega_s)t} + g_k \hat{b}_k^\dagger \hat{\sigma}_- e^{i(\omega_k-\omega_s)t} + g_k \hat{b}_k \hat{\sigma}_- e^{-i(\omega_k+\omega_s)t} + g_k \hat{b}_k^\dagger \hat{\sigma}_+ e^{i(\omega_k+\omega_s)t}.\end{aligned} \tag{3.24}$$

Now we make the rotating wave approximation. The terms with $\omega_k + \omega_a$ will rotate very fast ($\approx 10^{15} s^{-1}$) over the timescale of the radiative decay ($\approx 10^8 s^{-1}$) so that they will average out to zero. Next we make the Born approximation and obtain

$$\frac{\mathrm{d}\hat{\rho}_S}{\mathrm{d}t} = -\int_0^t \mathrm{d}s\{\Gamma(t-s)[\hat{\sigma}_+\hat{\sigma}_-\hat{\rho}_S(s) - \hat{\sigma}_-\hat{\rho}_S(s)\hat{\sigma}_+] + \text{H.c.}, \tag{3.25}$$

where H.c. is the hermitian conjugate term and

$$\Gamma(\tau) = \sum_k g_k^2 e^{-i(\omega_k-\omega_s)\tau}. \tag{3.26}$$

Next we make the Markov approximation and replace the sum in Eq. 3.26 by the integral

$$\Gamma(\tau) = \int_0^\infty \mathrm{d}\omega \rho(\omega) g(\omega)^2 e^{i(\omega_s-\omega)\tau}, \tag{3.27}$$

where $\rho(\omega)$ is the density of field modes as a function of frequency. Our master equation then becomes

$$\dot{\rho} = -i[\hat{H}_{LS}, \hat{\rho}_S] + \gamma \mathcal{D}[\hat{\sigma}_-]\hat{\rho}_S, \tag{3.28}$$

where $\gamma$ is the radiative decay rate, $\hat{H}_{LS} = \frac{\Delta\omega_a}{2}\hat{\sigma}_z$ and the superoperator $\mathcal{D}$ is defined as

$$\mathcal{D}[\hat{L}]\hat{\rho} = \left(\hat{L}\hat{\rho}\hat{L}^\dagger - \frac{1}{2}\{\hat{L}^\dagger\hat{L}, \hat{\rho}\}\right). \tag{3.29}$$

The real parameters $\Delta\omega_a$ and $\gamma$ are defined as

$$\Delta\omega_a - i\frac{\gamma}{2} = -i\int_0^\infty \Gamma(\tau)\mathrm{d}\tau. \tag{3.30}$$

### 3.1.4 Open quantum system treatment of a Bose Einstein condensate

One particular system of interest that we will refer to for experimental realisations in this thesis is a Bose Einstein Condensate (BEC). A BEC is a collection of atoms that can act as a single boson, with all atoms in the same quantum state, ie. the ground state of the harmonic trap (as we will see in Ch. 4 and 5). But it can also act in the same way as a system of many two level atoms in the case where we have two modes (Eq. 2.46) with the same SU(2) algebra (as we will see in Ch. 6).

#### Dephasing

The process of dephasing is described by the Lindblad Master equation as

$$\dot{\rho} = \gamma\mathcal{D}[\hat{J}_z]\hat{\rho}. \tag{3.31}$$

We will focus more on the effects of dephasing in Chapter 6.

#### Super radiance

At sufficiently low temperatures, the process of superradiance can be described by the Lindblad Master equation

$$\dot{\rho} = \gamma\mathcal{D}[\hat{J}_-]\hat{\rho}, \tag{3.32}$$

The process of superradiance describes the collective emission of light from an ensemble of atoms in the BEC.

## 3.2 Measurement of a Quantum System

### 3.2.1 Projection Measurements and the Measurement Postulate

The measurement postulate for quantum mechanics is given as follows [96]. Quantum measurements are described by a collection $\{\hat{M}_m\}$ of measurement operators. There are $m$ possible outcomes from the measurement with probability $p(m)$ of occurring

$$p(m) = \langle\psi|\hat{M}_m^\dagger\hat{M}_m|\psi\rangle. \tag{3.33}$$

The state of the system after a measurement is given by

$$\frac{\hat{M}_m|\psi\rangle}{\sqrt{\langle\psi|\hat{M}_m^\dagger\hat{M}_m|\psi\rangle}}. \tag{3.34}$$

The probabilities for the measurement outcomes must sum to $\sum_m p(m) = 1$ and so the completeness equation

$$\sum_m \hat{M}_m^\dagger \hat{M}_m = \hat{I}, \tag{3.35}$$

must be satisfied. Projective measurements are the special case of the measurement postulate where the measurement operators $\hat{M}_m$ are orthogonal projectors (Hermitian and $\hat{M}_m \hat{M}_n = \delta_{m,n} \hat{M}_m$).

We should also account for mixed states in our definition and so a more general form of the measurement postulate is given in density matrix formalism. For an initial state $\hat{\rho}$, the probability of an outcome occurring is given by

$$P(m) = Tr[\hat{M}_m \hat{\rho} \hat{M}_m^\dagger], \tag{3.36}$$

and the new state after the outcome has occurred is now

$$\hat{\rho}(m) = \frac{\hat{M}_m \hat{\rho} \hat{M}_m^\dagger}{P(m)}. \tag{3.37}$$

### 3.2.2 Continuous Measurement of Open Quantum Systems

Measurement of a quantum system usually disturbs the system in question, collapsing the wave-function. But often, this consequence is unwanted in an experiment where we want to control the quantum system for some purpose or we wish to understand the dynamics of the system and how the state evolves. In these cases we want the weakest disturbance to the system possible in order to estimate the state without destroying it. This kind of measurement is called a weak measurement, where instead of projectively measuring the system, the environment surrounding the system is measured to gain information about the state of the system (note that this is not the same as Ahranov's version of weak measurement [1]). Let us go back to the cat in the box once again. Consider this scenario,

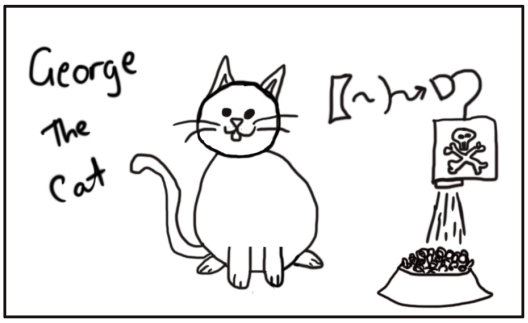


**Figure 3.2**: The cat, let us call him George.

Schrödinger's cat is sitting in a box with a vial of poison and a hammer. The hammer is connected to a Geiger counter with a small amount of radioactive substance in it. If a radioactive atom decays and the geiger counter detects a photon, then the hammer will drop, resulting in the death of the cat. If there is no detection, then the cat is still alive. Considering the box as the quantum system, the cat is in a superposition of alive and dead until a measurement is made. A projective measurement is made if the box is opened, the result will either be a dead cat or a living cat. Now let's assume that we don't want to

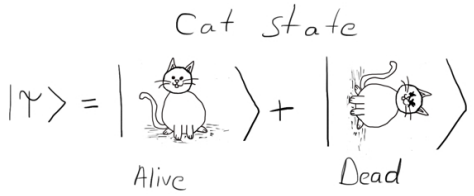


**Figure 3.3**: The cat is in a superposition of alive and dead state.

open the box to find out if our cat is dead or alive. What we can do instead of looking in the box is look at how the box is interacting with the environment. In this case the environment is a mouse that will go through the box and come out the other side. This cat, like most cats, is fond of playing with mice (and eating them, yuck!) so whatever happens to the mouse, we will gain some knowledge about the state of the cat. If the cat is alive, then the mouse will surely be eaten before it can escape the box. But this would still be a projective measurement, and if we want to not destroy the superposition state, we only want to weakly interact with the cat, so the mouse and cat will weakly interact. There is a probabilistic chance that the cat will decide to eat the mouse, and so there is a probabilistic chance that we will know the cat is alive. And if the cat is dead, the mouse

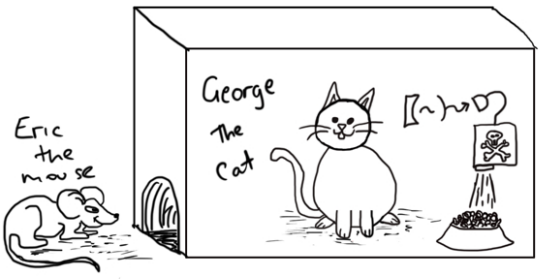


**Figure 3.4:** We can send a mouse into the box to determine whether the cat is probabilistically alive or dead.

will certainly be happy and continue on its way through and out of the box. We know with some probability what has happened and we did not need to look at the cat! Now if we need to know the state of the cat over time, we can send a continuous stream of mice into the box and see what happens to the mice. But the system is quantum so there will be some effect of the environment back on the system that will affect how the system evolves. We are dealing with weak measurement so there is still some degree of projection here. Some assumptions need to be made if we are to believe that the mouse has little effect on the state of the cat. For a weak measurement we assume that the environment-system interaction is weak, meaning the coupling between them is very small. This analogy is not 100% accurate but its a nice introduction to weakly destructive measurements for the purpose of this thesis.


**Figure 3.5:** Send in a bunch of mice and we know with greater probability what the state of the cat is.

## 3.3 Conditional evolution and quantum trajectories

From our cat and mouse analogy, it should be apparent that when we are dealing with the evolution of quantum systems under measurement, we are talking about a probabilistic process. When we use measurement devices such as a photon detector, the probabilistic nature of the measurement requires us to build a stochastic formalism into the evolution. Now we move onto the evolution of a quantum system that is conditioned by the measurement outcomes. And because the act of measurement itself can effect the state of a quantum system, we will have some sort of back-action that is applied to the system by the act of measurement. A lot of the following section follows closely from Wiseman's texbook [158] which is an excellent reference for quantum trajectories.

A quantum trajectory is the path taken by the quantum state that is conditioned by the continuous measurement of the system. It is also called an unraveling of the master equation. The unconditional state of a quantum system is given by an ensemble of quantum states that lead to the density matrix $\hat{\rho} = \sum_k p_k |\psi_k\rangle\langle\psi_k|$. As we saw earlier the evolution of the density matrix is given by the Master equation (Eq. 3.20), and this can be thought of as the evolution of an ensemble of pure quantum states. Each state in the ensemble can correspond to a particular realisation of the continuous measurement of the system. There is a one-to-infinitely many mapping from the density matrix to the weighted ensemble [156] which means there is an infinite number of ways we can unravel the Master equation.

If the system begins in a pure state, then it will remain pure as we continuously monitor the environment (assuming perfect detection efficiency of course). For an ensemble of unraveled states, we require that the stochastic average reproduces the unconditional density matrix for each time $t$:

$$E[|\psi(t)\rangle\langle\psi(t)|] \equiv \hat{\rho}(t), \tag{3.38}$$

where $E$ denotes the ensemble average with respect to the noise process. In general, the evolution of a quantum trajectory is given by a nonlinear Stochastic Schrödinger equation

(SSE) [156, 158]

$$\frac{\mathrm{d}|\psi\rangle}{\mathrm{d}t} = -i\hat{H}_\psi|\psi\rangle + \mathrm{noise}_\psi, \tag{3.39}$$

where $\hat{H}_\psi$ is a non-Hermitian effective Hamiltonian that depends on the state. Let us begin with some examples of different unravelings. Then we will move onto a more general form for the SSE.

### 3.3.1 Example: Photodetection of a Two Level Atom in a Cavity

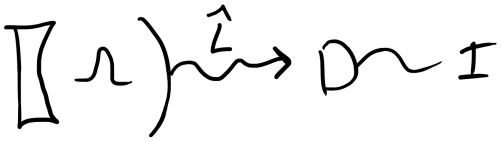

**Figure 3.6:** Photodetection of the the environment surrounding the two level system. We can refer back to our cat in a box once again for analogy. The two level atom in this case is the cat and the cavity surrounding the atom is our box. Light can escape our box/cavity and we are able to detect it (our mice are equivalent to light).

Recall from the previous section that the evolution of an open quantum system that consists of the two level atom coupled to the electromagnetic field is given by the master equation in Lindblad form

$$\dot{\hat{\rho}} = -\frac{i}{\hbar}[\hat{H}, \hat{\rho}] + \gamma\mathcal{D}[\hat{\sigma}_-]\hat{\rho}, \tag{3.40}$$

where $\hat{L} = \gamma\hat{\sigma}_-$ describes the interaction with the field modes.

Let us now consider how we can measure the conditional state of the atom by weakly measuring the environment. One possible way of doing this is to use photodetectors to detect any photons that are emitted by the atom. Now if the atom emits a photon, the atom will have gone from an excited state $|e\rangle$ to the ground state $|g\rangle$. Of course when this happens, the photon will be emitted in any possible direction in space so it would be nearly impossible to detect the photon with a single photodetector. We can make the system simpler by placing the atom inside a cavity constructed from two mirrors, one completely reflective and one leaky to transmission. The environment with which the atom interacts is now the few (or single) modes in the cavity. Inside the cavity, any emitted photons will be channelled out through the leaky mirror with a decay rate $\gamma$ for the atom. In order for the approximations that give the Lindblad Master equation to be valid in this case, we need to make some assumptions on the rate of emission from the cavity, namely that the photons escape quickly compared to the atomic frequency so that the photons do not re-interact with the two level atom.

The quantum measurement resulting from the photodetection of the cavity emission can be described by a set of measurement operators $\{\hat{M}_m\}$ which act on the state space of the two level atom. For the specific case of the two level atom in a leaky cavity, a click on the detector occurs when the atom emits a photon and as a result jumps to the ground state. This measurement result is given by the jump operator

$$\hat{M}_1 = \sqrt{\gamma_-\mathrm{d}t}\hat{\sigma}_-, \tag{3.41}$$

with $\gamma_-$ describing the decay rate to the ground state and we now have a $\sqrt{\mathrm{d}t}$ term since

we are continuously measuring over the inifinitesimal time interval d$t$. Upon inspection, it is easy to see that this single measurement outcome does not satisfy the completeness equation (3.35). And the reason for this is simple: This is not the only possible measurement outcome for the photodetection. We are still measuring the system in some way even when we do not detect a photon, the photodetector is switched on for more than the infinitesimal time interval, so what is going on? During the time where no photons are detected, we are still gaining information about the state of the system. The probability that the system is in the ground state increases as time progresses with no detections. The no-click operator

$$\hat{M}_0 = I - \left(\frac{\hat{R}}{2} + i\hat{H}\right) \mathrm{d}t, \tag{3.42}$$

will clearly satisfy completeness if $\hat{R} = \gamma_- \hat{\sigma}_-^\dagger \hat{\sigma}_-$ is chosen. This outcome occurs with a probability that is equal to $1 - O(\mathrm{d}t)$.

The detection occurs randomly with a rate $p(1)/\mathrm{dt}$, and we call this event a quantum jump corresponding to a jump in the quantum state of the system. For each run of the measurement, a new trajectory is obtained. A trajectory resulting from the photodetection is stochastic in nature due to the random nature of the wavefunction collapse. So for $N(t)$ photodetections up to time $t$, d$N(t)$ will be a stochastic increment which is Poisson distributed [16], obeying the following equations [158]:

$$\mathrm{d}N(t)^2 = \mathrm{d}N(t), \tag{3.43}$$

and

$$\mathrm{E}[\mathrm{d}N(t)] = \langle \hat{M}_1^\dagger \hat{M}_1 \rangle, \tag{3.44}$$

where the first equation signifies that it can only be 0 or 1 (click or no-click) in an infinitesimal time interval. The second equation gives the classical expectation (E[...]) or mean of d$N$ as the probability of detecting a photon given by the quantum expectation value ($\langle ... \rangle$). The change to the state vector as a result of a click operation in the interval $\mathrm{d}N(t) = 1$ is given by

$$|\psi_1(t + \mathrm{d}t)\rangle = \frac{\hat{M}_1|\psi(t)\rangle}{\sqrt{\langle\psi(t)|\hat{M}_1^\dagger \hat{M}_1|\psi(t)\rangle}} = \frac{\hat{\sigma}_-|\psi(t)\rangle}{\sqrt{\langle\psi(t)|\hat{\sigma}_-^\dagger \hat{\sigma}_-|\psi(t)\rangle}}, \tag{3.45}$$

and the result of a no-click operation in the interval $\mathrm{d}N(t) = 0$ is given by

$$|\psi_0(t + \mathrm{d}t)\rangle = \frac{\hat{M}_0|\psi(t)\rangle}{\sqrt{\langle\psi(t)|\hat{M}_0^\dagger \hat{M}_0|\psi(t)\rangle}} = \{\hat{I} - \mathrm{d}t[i\hat{H} + \tfrac{1}{2}\hat{\sigma}_-^\dagger \hat{\sigma}_- - \tfrac{1}{2}\langle\hat{\sigma}_-^\dagger \hat{\sigma}_-\rangle]\}|\psi(t)\rangle, \tag{3.46}$$

where the denominator is expanded to first order in d$t$. The nonlinear evolution of the state is given by the SSE

$$\mathrm{d}|\psi(t)\rangle = \left[\mathrm{d}N(t)\left(\frac{\hat{\sigma}_-}{\sqrt{\langle\hat{\sigma}_-^\dagger \hat{\sigma}_-\rangle(t)}} - I\right) + [1 - \mathrm{d}N(t)]\mathrm{d}t\left(\frac{\langle\hat{\sigma}_-^\dagger \hat{\sigma}_-\rangle(t)}{2} - \frac{\hat{\sigma}_-^\dagger \hat{\sigma}_-}{2} - i\hat{H}\right)\right]|\psi(t)\rangle. \tag{3.47}$$

The solution to this equation is a quantum trajectory and it preserves the purity of the state. Since d$N(t)$ is of the order of d$t$, we can say that any terms of higher order in

$\mathrm{d}t$ (eg. $\mathrm{d}N(t)\mathrm{d}t$) is much smaller than $\mathrm{d}t$ and is negligable in the above equation. The general form of the nonlinear SSE is given by:

$$\mathrm{d}|\psi(t)\rangle = \left[\mathrm{d}N(t)\left(\frac{\hat{L}}{\sqrt{\langle\hat{L}^\dagger\hat{L}\rangle(t)}} - I\right) + \mathrm{d}t\left(\frac{\langle\hat{L}^\dagger\hat{L}\rangle(t)}{2} - \frac{\hat{L}^\dagger\hat{L}}{2} - i\hat{H}\right)\right]|\psi(t)\rangle, \tag{3.48}$$

where the jump operator is given by $\hat{M}_1 = \sqrt{\mathrm{d}t}\hat{L}$. In density matrix formalism, the evolution is given by the stochastic master equation (SME):

$$\mathrm{d}\hat{\pi} = \{\mathrm{d}N(t)\mathcal{G}[\hat{L}] - \mathrm{d}t\mathcal{H}[i\hat{H} + \tfrac{1}{2}\hat{L}^\dagger\hat{L}]\}\hat{\pi}, \tag{3.49}$$

where the superoperators $\mathcal{G}$ and $\mathcal{H}$ are defined by:

$$\mathcal{G}[\hat{G}]\hat{\rho} = \frac{\hat{G}\hat{\rho}\hat{G}^\dagger}{\mathrm{Tr}[\hat{G}\hat{\rho}\hat{G}^\dagger]} - \hat{\rho}, \tag{3.50}$$

$$\mathcal{H}[\hat{G}]\hat{\rho} = \hat{G}\hat{\rho} + \hat{\rho}\hat{G}^\dagger - \mathrm{Tr}[\hat{G}\hat{\rho} + \hat{\rho}\hat{G}^\dagger]\hat{\rho}. \tag{3.51}$$

In order to get back the Lindblad master equation from this unraveling, we must take the ensemble average:

$$\hat{\rho}(t) = \mathrm{E}[\hat{\pi}(t)]. \tag{3.52}$$

The point of this example is to introduce the stochastic nature of quantum measurement which we will discuss further soon. Throughout this thesis we will not be dealing with jump processes, but rather the smooth and continuous function given by diffusive evolution. So let us move onto an example of a system where this is possible.

### 3.3.2 Example: Homodyne Detection

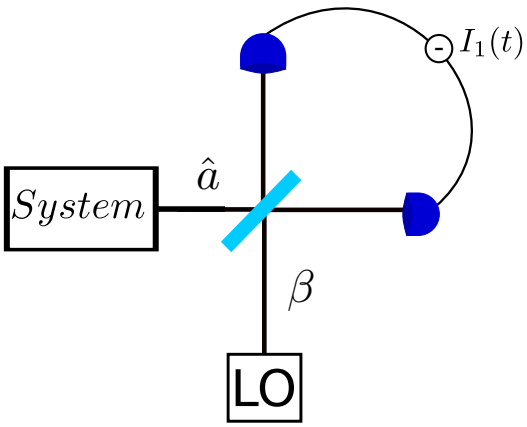


**Figure 3.7**: Simple homodyne detection scheme in quantum optics.

Let us start with our system being a leaky cavity again where the system of interest interacts only with a single mode of light. Then the coupling operator that describes the interaction is $\hat{L} = \sqrt{\gamma}\hat{a}$, where $\hat{a}$ is the annihilation operator for the single mode of light. Our system could be anything, for example a two level atom in a cavity or the single mode

of light in the cavity. Now suppose we combine the signal with a much stronger continuous classical field $\beta = |\beta| \exp(i\phi)$ called a local oscillator (LO). This type of measurement is known as a simple homodyne detection (shown in the schematic in Fig. 3.7). The output from the cavity and the LO are combined in a beam splitter before being detected by a single photodetector. The photodetector is only able to count the number of photons that hit the detector $N$ (the current is given by $I = \mathrm{d}N(t)/\mathrm{d}t$). After the linear combination of the light mode and the LO, the detector will see the current given by the expectation value of the number operator. The measurement operator for a detection event is then

$$\hat{M}_1 = \sqrt{\mathrm{d}t}(\sqrt{\gamma}\hat{a} + \beta) \tag{3.53}$$

and when there is no detection event, the measurement operator is

$$\hat{M}_0 = \hat{I} - \mathrm{d}t[i\hat{H} + \tfrac{1}{2}(\sqrt{\gamma}\hat{a}\beta^* - \sqrt{\gamma}\hat{a}^\dagger\beta) + \tfrac{1}{2}(\sqrt{\gamma}\hat{a}^\dagger + \beta^*)(\sqrt{\gamma}\hat{a} + \beta)] \tag{3.54}$$

The rate of photodetections is given by

$$\begin{aligned} \mathrm{E}[\mathrm{d}N(t)/\mathrm{d}t] &= \langle \hat{M}_1^\dagger \hat{M}_1 \rangle = \langle (\sqrt{\gamma}\hat{a}^\dagger + \beta^*)(\sqrt{\gamma}\hat{a} + \beta) \rangle \\ &= \langle \gamma \hat{a}^\dagger \hat{a} + \sqrt{\gamma}(\hat{a}^\dagger \beta + \beta^* \hat{a}) + \beta^* \beta \rangle. \end{aligned} \tag{3.55}$$

We assume that the classical field is much larger than the output of the cavity so $\hat{a}^\dagger\hat{a}$ is much smaller than $\beta^*\beta$. So then we have a large constant plus a term that is proportional to the quadratures of the system plus a small term. The phase of the LO is now important as it decides what the information we will gain from the measurement. For instance, if $\beta$ is real ($\phi = 0$), then the middle term is $\sqrt{\gamma}|\beta|\langle\hat{x}\rangle$ and if $\beta$ is imaginary ($\phi = \pi/2$), then the middle term is $\sqrt{\gamma}|\beta|\langle\hat{p}\rangle$, where we define the quadratures of the system to be $\hat{x} = \hat{a}^\dagger + \hat{a}$ and $\hat{p} = i(\hat{a}^\dagger - \hat{a})$. The conditional evolution of the state is now given by

$$\begin{aligned} \mathrm{d}|\psi(t)\rangle = \big[\mathrm{d}N(t) &\left( \frac{\sqrt{\gamma}\hat{a} + \beta}{\sqrt{\langle (\sqrt{\gamma}\hat{a}^\dagger + \beta^*)(\sqrt{\gamma}\hat{a} + \beta) \rangle}} - \hat{I} \right) \\ &+ \mathrm{d}t \left( \frac{\gamma\langle \hat{a}^\dagger \hat{a} \rangle}{2} - \frac{\gamma \hat{a}^\dagger \hat{a}}{2} + \frac{\sqrt{\gamma}\langle \hat{a}^\dagger \beta + \beta^* \hat{a} \rangle}{2} - \sqrt{\gamma}\hat{a}^\dagger \beta - i\hat{H} \right) \big] |\psi(t)\rangle. \end{aligned} \tag{3.56}$$

This is another unraveling of the master equation. As we mentioned at the beginning of this chapter, these unravelings are not unique. By this we mean that by taking the ensemble average we will get back to the same master equation. This is essentially ignoring the measurement results from the detector. However, different measurement schemes result in different evolutions of the single trajectories and a single unraveling will correspond to a particular method of measurement. What we can take away from this example is that by using homodyne detection, we are able to change the way we measure the system without changing the measurement setup, this will be important later on, but we will come back to this in section 3.3.5.

### 3.3.3 Weiner noise process

If we consider the limit where the amplitude of $\beta$ goes to infinity, the number of photodetections will also go to infinity, but the effect that each one has on the evolution will go to zero and we will end up with a photocurrent rather than a series of photo-detections. This

leads to a smooth evolution that is continuous in time [16]. In the limit where the number of detections $\delta N$ is very large, the variance of $\delta N$ will be dominated by the poissonian number statistics of the local oscillator which will be approximately gaussian due to the large number of counts. In this case the statistics of $\delta N$ is consistant with a random gaussian variable [157]. In the limit $\beta \to \infty$, the point process photocurrent can be replaced by a continuous photocurrent with white noise. Removing the constant local oscillator contribution yields

$$J(t) = \sqrt{\gamma}\langle \hat{a}^\dagger e^{i\phi} + \hat{a}e^{-i\phi}\rangle_J(t) + \xi(t), \tag{3.57}$$

where $\xi(t) = \mathrm{d}W/\mathrm{d}t$. Here $\mathrm{d}W$ is an infinitesimal Wiener increment that satisfies the following properties

$$\mathrm{d}W(t)^2 = \mathrm{d}t \tag{3.58}$$
$$\mathrm{E}[\mathrm{d}W(t)] = 0. \tag{3.59}$$

For pure initial states, this evolution can be described by the SSE

$$\mathrm{d}|\psi_J(t)\rangle = -i\hat{H}|\psi\rangle\mathrm{d}t - \frac{1}{2}\left(\hat{a}^\dagger\hat{a} - 2\langle(\hat{a}^\dagger e^{i\phi} + \hat{a}e^{-i\phi})/2\rangle_J(t)\hat{a} + \langle(\hat{a}^\dagger e^{i\phi} + \hat{a}e^{-i\phi})/2\rangle_J^2(t)\right)|\psi_J(t)\rangle + [\hat{a} - \langle(\hat{a}^\dagger e^{i\phi} + \hat{a}e^{-i\phi})/2\rangle_J(t)]|\psi_J(t)\rangle\mathrm{d}W(t). \tag{3.60}$$

The evolution is now diffusive rather than given by quantum jumps.

### 3.3.4 Ito stochastic integration

The above equation is an Ito stochastic differential equation [25]. In ordinary stochastic integration, there is the choice of two integration methods, Ito and Stratonovich. The Ito form has several mathematical advantages, because the increment is independent of the integration variable and it is easy to derive. Ito calculus is an extension of ordinary calculus with a small correction to what we would expect from ordinary calculus rules. There are numerical methods to calculate stochastic differential equations in either Ito or Stratonovich form, however, in this thesis we will be using the numerical software package XMDS2 [24] which requires equations in Stratonovich form.

The general SSE in Ito form for multiple Lindblad operators $\hat{L}_k$ is given as:

$$\mathrm{d}|\psi\rangle = -i\hat{H}|\psi\rangle\mathrm{d}t + \sum_k\left(-\frac{\hat{L}_k^\dagger\hat{L}_k}{2} + \langle\hat{L}_k^\dagger\rangle\hat{L}_k - \frac{\langle\hat{L}_k^\dagger\rangle\langle\hat{L}_k\rangle}{2}\right)|\psi\rangle\mathrm{d}t + \sum_k\left(\hat{L}_k - \langle\hat{L}_k\rangle\right)|\psi\rangle\mathrm{d}\xi_k. \tag{3.61}$$

The noise term $\mathrm{d}\xi$ is a complex Wiener process with zero mean ($\mathrm{E}[\mathrm{d}\xi]= 0$) and correlations given by

$$\mathrm{d}\xi\,\mathrm{d}\xi^* = \mathrm{dt} \qquad \text{and} \qquad \mathrm{d}\xi\,\mathrm{d}\xi = u\mathrm{d}t, \tag{3.62}$$

and now the difference between Ito and ordinary calculus will become clearer with the equation of motion for the expectation of an operator, which is given by:

$$\mathrm{d}\langle\hat{G}\rangle = \langle\mathrm{d}\psi|\hat{G}|\psi\rangle + \langle\psi|\hat{G}|\mathrm{d}\psi\rangle + \langle\mathrm{d}\psi|\hat{G}|\mathrm{d}\psi\rangle, \tag{3.63}$$

where the state evolves via eq. 3.61.

In the density matrix formalism, the state $\hat{\rho}$ evolves via a stochastic master equation (SME):

$$\mathrm{d}\hat{\rho}(t) = -i[\hat{H}, \hat{\rho}(t)]\mathrm{d}t + \mathrm{d}t \sum_k \mathcal{D}[\hat{L}_k]\hat{\rho}(t) + \sum_k \mathcal{H}[\hat{L}_k \mathrm{d}\xi_k]\hat{\rho}(t), \tag{3.64}$$

and we define the superoperators:

$$\mathcal{D}[\hat{L}]\hat{\rho} \quad = \hat{L}\hat{\rho}\hat{L}^\dagger - \frac{1}{2}\{\hat{L}^\dagger\hat{L}, \hat{\rho}\}, \tag{3.65}$$

$$\mathcal{H}[\hat{L}\mathrm{d}\xi]\hat{\rho} \quad = \hat{L}\hat{\rho}\mathrm{d}\xi + \hat{\rho}\hat{L}^\dagger\mathrm{d}\xi^* - \mathrm{Tr}[\hat{L}\hat{\rho}]\hat{\rho}\mathrm{d}\xi - \mathrm{Tr}[\hat{L}^\dagger\hat{\rho}]\hat{\rho}\mathrm{d}\xi^*, \tag{3.66}$$

where $\{...\}$ is the anti commutator: $\{\hat{A}, \hat{B}\} = \hat{A}\hat{B} + \hat{B}\hat{A}$. The first superoperator $\mathcal{D}$ is the decoherence term and the second superoperator $\mathcal{H}$ is usually referred to as the innovation term since this is the information that is obtained from the measurement. In this case the equation of motion for an operator is given by

$$\mathrm{d}\langle\hat{G}\rangle = \mathrm{Tr}[\hat{G}\mathrm{d}\hat{\rho}]. \tag{3.67}$$

### 3.3.5 Parametrisation of the measurement

From the homodyne example shown above, we can see that for diffusive measurement processes, the information that is gained from the measurement can be chosen by a single parameter. This will be important for our investigation since we wish to look at the effect that the measurement choice itself has on the evolution of chaotic dissipative systems. We also showed for the general SSE above that the choice of the complex noise increment $\mathrm{d}\xi$ is arbitrary with freedom to choose $u$ where the complex number $u$ must satisfy the condition $|u| \leq 1$ [118, 156]. In this thesis we are interested in dissipative chaotic systems and it is natural to consider diffusive quantum trajectories (i.e. with diffusive noise) in this case and so we will focus solely on these from now on. We will also assume perfect monitoring of the environment throughout this thesis which will make things simple. As discussed above, we are continuously monitoring the environment that is coupled to the system. By doing this we are continuously applying a projective measurement on the state of the environment which will result in the purification of the state of the system. In this thesis we will consider the case where $u \equiv |u| \exp^{-2i\phi}$. We can then write the complex Wiener process as

$$\mathrm{d}\xi = e^{-i\phi}\left(\sqrt{\frac{1+|u|}{2}}\,\mathrm{d}W_1 + i\sqrt{\frac{1-|u|}{2}}\,\mathrm{d}W_2\right), \tag{3.68}$$

where $\mathrm{d}W_1$ and $\mathrm{d}W_2$ are independent real Wiener processes. Note that the amplitude $|u|$ and phase $\phi$ fully characterize the noise process and therefore different choices of $u$ correspond to particular ways of unraveling the master equation into stochastic trajectories. Physically, different $u$ and $\phi$ correspond to different choices of continuous monitoring [117, 156]. Note that the often used form of this is the quantum state diffusion equation (QSD) [125, 13, 105] for which $|u| = 0$. In this case there is a complex noise $\mathrm{d}\xi = \mathrm{d}W_1 + i\mathrm{d}W_2/\sqrt{2}$. At this point it is important to recognise that $u$, more than providing a convenient mathematical parametrization of the unravelings, also bears a direct connection to a physical way of continuously monitoring the quantum system [156]. For example, if the dissipation operator $\hat{L}$ describes an optical channel observed using the scheme shown in Fig. 3.8, there is a direct relationship between the beam splitter ratios

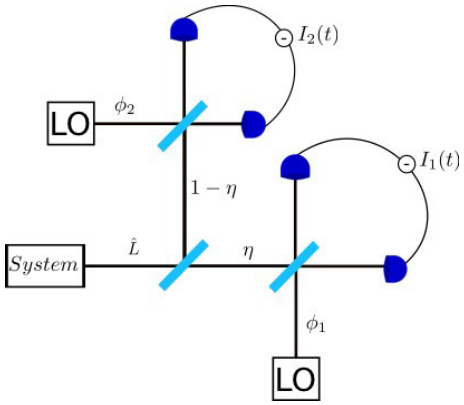


**Figure 3.8:** Monitoring scheme for the unraveling parametrisation in terms of $u$. The first beam splitter has transmittance $\eta$ while the ones at the detectors end are balanced. The local oscillators (LO) used in the homodyne-like measurements have phases $\phi_1$ and $\phi_2$.

and phases indicated in the figure and the value of $u$ corresponding to that measurement:

$$u^* = \eta e^{2i\phi_1} + (1-\eta)e^{2i\phi_2}, \tag{3.69}$$

and the complex Wiener noise can be written as

$$\mathrm{d}\xi^* = \sqrt{\eta}e^{i\phi_1}\mathrm{d}W_1 + \sqrt{1-\eta}e^{i\phi_2}\,\mathrm{d}W_2. \tag{3.70}$$

By comparing equation (3.68) with equation (3.70), we can immediately establish a direct connection between $u$ and the physical parameters $\eta$, $\phi_1$ and $\phi_2$ of the monitoring. Note that these diffusive quantum trajectories correspond to homodyne-like measurements that are routinely implemented in quantum optical setups and that have been measured recently in superconducting qubit systems [93, 119, 15]. The QSD type evolution corresponds to the case of heterodyne detection where there is a 50:50 split at the first beam splitter.

### 3.3.6 Stratonovich form

As we stated above, for the numerical calculations done in XMDS2 we require the stochastic differential equations in Stratonovich form. This can be easily done by a correction term to the equations. Note that there are in fact other integration methods that work for Ito form [121].

#### Stratonovich correction

The Stratonovich correction to the stochastic Ito differential equation is derived below. Going between Ito and Stratonovich requires a correction term

$$X \circ \mathrm{d}Y = X\mathrm{d}Y + \frac{1}{2}\mathrm{d}X\mathrm{d}Y, \tag{3.71}$$

where the term on the left is the Stratonovich form and the first term on the right is the Ito form and the last term is the correction term to obtain Stratonovich. For the nonlinear SSE, we have a stochastic term in Ito form given by

$$X\mathrm{d}Y = (\hat{L} - \langle L\rangle)|\psi\rangle\mathrm{d}\xi, \tag{3.72}$$

where $(\hat{L} - \langle\hat{L}\rangle)|\psi\rangle$ is $X$ and $\mathrm{d}\xi$ is $\mathrm{d}Y$. For Stratonovich form we calculate the correction.

$$\begin{aligned} X\mathrm{d}Y &= X \circ \mathrm{d}Y - \frac{1}{2}\mathrm{d}X\mathrm{d}Y \\ &= (\hat{L} - \langle\hat{L}\rangle)|\psi\rangle \circ \mathrm{d}\xi - \frac{1}{2}\mathrm{d}[(\hat{L} - \langle\hat{L}\rangle)|\psi\rangle]\mathrm{d}\xi. \end{aligned} \tag{3.73}$$

Since we are in the Schrödinger picture, the state is dependent on time, so $\mathrm{d}\hat{L}|\psi\rangle = \hat{L}\mathrm{d}|\psi\rangle$. However, the expectation $\langle\hat{L}\rangle$ is state dependent and so will evolve in time. So we have

$$\begin{aligned} -\frac{1}{2}\mathrm{d}[(\hat{L} - \langle\hat{L}\rangle)|\psi\rangle]\mathrm{d}\xi = \\ -\frac{1}{2}\hat{L}\mathrm{d}|\psi\rangle\mathrm{d}\xi + \frac{1}{2}(\mathrm{d}\langle\hat{L}\rangle)|\psi\rangle\mathrm{d}\xi + \frac{1}{2}\langle\hat{L}\rangle\mathrm{d}|\psi\rangle\mathrm{d}\xi + \frac{1}{2}(\mathrm{d}\langle\hat{L}\rangle)\mathrm{d}|\psi\rangle\mathrm{d}\xi. \end{aligned} \tag{3.74}$$

The last term is here because we are still using $\mathrm{d}|\psi\rangle$ in Ito form, but it is easy to see that this term will disappear because there will be no terms of $O(\mathrm{d}t)$ or lower. The other terms will give us corrections, but it is also easy to see that the only surviving terms from these will be $\mathrm{d}\xi\mathrm{d}\xi = u\mathrm{d}t$ and $\mathrm{d}\xi^*\mathrm{d}\xi = \mathrm{d}t$ since any higher order terms disappear. Now let us work through the terms that will survive one at a time.

$$\begin{aligned} -\frac{1}{2}\hat{L}\mathrm{d}|\psi\rangle\mathrm{d}\xi &= -\frac{1}{2}\hat{L}(\hat{L} - \langle\hat{L}\rangle)|\psi\rangle\mathrm{d}\xi\mathrm{d}\xi \\ &= -\frac{u}{2}(\hat{L}^2 - \hat{L}\langle\hat{L}\rangle)|\psi\rangle\mathrm{d}t. \end{aligned} \tag{3.75}$$

And then for the next term we use Eq. 3.63 for the equation of motion of an operator:

$$\begin{aligned} \frac{1}{2}(\mathrm{d}\langle\hat{L}\rangle)|\psi\rangle\mathrm{d}\xi &= -\frac{1}{2}\left(\langle\mathrm{d}\psi|\hat{L}|\psi\rangle + \langle\psi|\hat{L}|\mathrm{d}\psi\rangle + \langle\mathrm{d}\psi|\hat{L}|\mathrm{d}\psi\rangle\right)|\psi\rangle\mathrm{d}\xi, \\ &= -\frac{1}{2}\left(\langle\psi|(\hat{L}^\dagger - \langle\hat{L}^\dagger\rangle)\hat{L}|\psi\rangle\mathrm{d}\xi^* + \langle\psi|\hat{L}(\hat{L} - \langle\hat{L}\rangle)|\psi\rangle\mathrm{d}\xi\right)|\psi\rangle\mathrm{d}\xi, \\ &= -\frac{1}{2}\left(\langle\hat{L}^\dagger\hat{L}\rangle - \langle\hat{L}^\dagger\rangle\langle\hat{L}\rangle + u(\langle\hat{L}^2\rangle - \langle\hat{L}\rangle^2)\right)|\psi\rangle\mathrm{d}t. \end{aligned} \tag{3.76}$$

Then the final term is $\frac{1}{2}\langle\hat{L}\rangle\mathrm{d}|\psi\rangle\mathrm{d}\xi$

$$\begin{aligned} \frac{1}{2}\langle\hat{L}\rangle\mathrm{d}|\psi\rangle\mathrm{d}\xi &= \frac{1}{2}\langle\hat{L}\rangle(\hat{L} - \langle\hat{L}\rangle)|\psi\rangle\mathrm{d}\xi\mathrm{d}\xi \\ &= \frac{u}{2}\left(\langle\hat{L}\rangle\hat{L} - \langle\hat{L}\rangle^2\right)\mathrm{d}t. \end{aligned} \tag{3.77}$$

So the Stratonovich correction term is given by:

$$-\frac{1}{2}\mathrm{d}X\mathrm{d}Y = \frac{1}{2}\left(\langle\hat{L}^\dagger\hat{L}\rangle - \langle\hat{L}^\dagger\rangle\langle\hat{L}\rangle - u\left[\hat{L}^2 - 2\hat{L}\langle\hat{L}\rangle - \langle\hat{L}^2\rangle + 2\langle\hat{L}\rangle^2\right]\right)|\psi\rangle\mathrm{d}t. \tag{3.78}$$

**Stochastic Schrödinger equation in Stratonovich form**

Now that we have calculated the correction term, we can express the SSE in Stratonovich form:

$$\mathrm{d}|\psi\rangle = \left(-i\hat{H} - \frac{\hat{L}^\dagger\hat{L}}{2} + \frac{\langle\hat{L}^\dagger\hat{L}\rangle}{2} + \langle\hat{L}^\dagger\rangle\hat{L} - \langle\hat{L}^\dagger\rangle\langle\hat{L}\rangle\right)|\psi\rangle\mathrm{d}t \\ - \frac{u}{2}\left(\hat{L}^2 - 2\hat{L}\langle\hat{L}\rangle - \langle\hat{L}^2\rangle + 2\langle\hat{L}\rangle^2\right)|\psi\rangle\mathrm{d}t + \left(\hat{L} - \langle\hat{L}\rangle\right)|\psi\rangle \circ \mathrm{d}\xi. \quad (3.79)$$

**Linear SSE**

The SSE we have presented so far is the normalised, nonlinear version of the equation. There is however another version that is linear and unnormalised which can be easier to numerically integrate [156]. The quantum trajectory is invariant under the global gauge transformation

$$|\psi(t)\rangle \to e^{i\chi(t)}|\psi(t)\rangle = |\phi(t)\rangle, \quad (3.80)$$

where $\chi(t)$ is a complex function. Using this, we can derive a new SSE that is easier for numerical calculations and will be used for simulations throughout this thesis

$$\mathrm{d}|\bar{\phi}(t)\rangle = \mathrm{d}t(-i\hat{H} - \frac{1}{2}\hat{L}_k^\dagger\hat{L}_k + J_k^*\hat{L}_k)|\bar{\phi}(t)\rangle, \quad (3.81)$$

where $|\bar{\phi}(t)\rangle$ is unnormalised and $J_k^* = (\langle\hat{L}_k^\dagger\rangle + \langle\hat{L}_k\rangle u)\mathrm{d}t + \mathrm{d}\xi$ is the complex current that comes from the measurement. This equation is in Ito form, in order to numerically integrate, we apply the Stratonovich correction to the equation giving us

$$\mathrm{d}|\bar{\phi}(t)\rangle = \mathrm{d}t(-i\hat{H} - \frac{1}{2}\hat{L}_k^\dagger\hat{L}_k - \frac{u}{2}\hat{L}_k^2 + J_k^*\hat{L}_k)|\bar{\phi}(t)\rangle. \quad (3.82)$$

Since the state is unnormalised, a normalisation step must be done every time step of the simulation.

# Part I

# Dynamics of quantum chaotic systems

# 4

# Measurement of a Quantum Duffing Oscillator

Now that we have introduced both the tools to describe quantum states and the evolution of quantum states under continuous measurement, we can finally start to delve into the purpose of this thesis; to investigate how continuous measurement impacts the emergence of chaos in an open quantum system. In this chapter, we do this by specialising to a very simple model that presents chaos in the classical limit (the Duffing oscillator), one that is easily modelled in the classical and quantum regimes and has a clear transition between the two that is governed by a single parameter. There are many ways to continuously monitor a quantum system. For concreteness, we choose a homodyne measurement scheme where a single parameter can change the quadrature that is being continuously measured and effectively changes the information received from the measurement signal.

This chapter contains work that has been published in:
*'Tuning quantum measurements to control chaos'*, **J. K. Eastman**, J. J. Hope, A. R. R. Carvalho, Scientific Reports, **7**, 44684 (2017). DOI: https://doi.org/10.1038/srep44684

## 4.1 Introduction

Understanding how classical dynamics emerge from the more fundamental quantum theory has proven to be a subtle problem when the system in question exhibits chaos in the classical limit. Coherent interference effects lead to a rapid breakdown of the correspondence between the classical and quantum dynamics. The inclusion of decoherence effects destroys the interference and is a crucial step to achieve a smooth quantum to classical transition [100, 28, 166, 55, 103, 18].

Many studies of classically chaotic systems undergoing environmental coupling have focused on the ensemble average behaviour given by the master equation and the comparison of the classical phase space with its quantum counterpart via Wigner functions. Others have adopted an approach based on continuously monitored quantum systems [27, 131, 13, 117, 6, 47, 54, 68]. As a reminder from chapter 3, the monitoring is said to produce an "unraveling" of the master equation in terms of individual stochastic quantum trajectories that evolve conditioned on the measurement record. Using this approach, it has been shown that the Poincaré section (see chapter 1) of a single quantum trajectory

reproduces the corresponding classical strange attractors in the macroscopic limit [131, 13], even when considering a few different monitoring strategies [117]. It also allowed a quantitative comparison between classical and quantum Lyapunov exponents as the effective size of the system varies [6, 99, 54, 68]. In general, when the classical motion is large compared to the quantum noise induced by the stochastic nature of the trajectories, the quantum Lyapunov exponent approaches the classical value [6], while there is a crossover to the quantum regime where noise predominates and chaos is suppressed [99]. Interestingly, positive Lyapunov exponents have been found away from the classical limit [54] but perhaps even more surprising is the fact that they have also been reported for parameters where the corresponding classical system is regular [68, 107].

These results show not only that the onset of chaos at the quantum level is possible, but also that it has a rich behaviour due to the interplay between the strength of the nonlinear dynamics and the amount of noise introduced by the measurement back action. But quantum mechanics allows us to go beyond that and explore more complex scenarios where, even when the form and strength of the system-environment interaction are kept unchanged, different choices of measurement schemes can have a drastic effect on the dynamics of the system. This is the purpose of this contribution: we show that the Lyapunov exponent of the quantum system is sensitive to the choice of monitoring strategy and, consequently, one can control the degree of chaos in the system by tuning an easily accessible measurement parameter. Our results show that this effect originates from a fine balance between two competing factors: the appearance of interference at the quantum level due to the underlying classical nonlinear dynamics, and the effectiveness of certain monitoring schemes in destroying these very same interference fringes.

## 4.2 Quantum Duffing Oscillator

We begin by considering a driven-damped Duffing oscillator [30], a model that has been extensively used in the investigation of chaotic dynamics in open quantum systems [108, 99, 113, 13, 125]. The model consists of a particle that oscillates in a double-well potential that is periodically tilted by an external driving force with amplitude $g$ and frequency $\Omega$. The dimensionless quantum Hamiltonian describing this model is given by

$$\hat{H} = \frac{1}{2}\hat{P}^2 + \frac{\beta^2}{4}\hat{Q}^4 - \frac{1}{2}\hat{Q}^2 + \frac{\Gamma}{2}(\hat{Q}\hat{P} + \hat{P}\hat{Q}) - \frac{g}{\beta}\hat{Q}\cos(\Omega t), \tag{4.1}$$

where time is in units of the trap period $2\pi/\omega_0$ and $\hat{Q} = \hat{x}/\sqrt{\hbar/(m\omega_0)}$ and $\hat{P} = \hat{p}/\sqrt{\hbar m\omega_0}$ are, respectively, the dimensionless position and momentum operators for a single particle of mass $m$. The first term in the Hamiltonian describes the kinetic energy, the quartic and quadratic terms in $\hat{Q}$ describe the double-well potential, and the last term describes the periodic driving of the particle. The term with the coefficient $\Gamma$ is not essential for chaos in this system, instead it works to effectively mix dissipation in $\hat{Q}$ and $\hat{P}$ which prevents the wavefunction from spreading too much in phase space and lowers the computational requirements for simulations. The dimensionless parameter $\beta^2 = \hbar/(ml^2\omega_0)$ defines the scale of the phase space relative to Planck's constant [13, 99, 68] (where $l$ characterizes the size of the system). A larger $\beta$ is therefore associated with a regime where quantum fluctuations have a larger effect on the oscillator dynamics. Thus, by tuning $\beta$ we can study the transition from the quantum regime to the classical regime ($\beta \to 0$).

To include damping, we model the quantum dynamics as an open quantum system

as we saw in section 3.1 through the master equation (3.20) where dissipation effects arise from choosing the system-environment coupling, $\hat{L} = \sqrt{\Gamma}(\hat{Q} + i\hat{P}) = \sqrt{2\Gamma}\hat{a}$, to be proportional to the annihilation operator of the harmonic oscillator.

In the classical limit ($\beta \to 0$), we can make the identifications $\langle\hat{Q}\rangle \to x_{cl}$ and $\langle\hat{P}\rangle \to p_{cl}$ such that the equations of motion for $\langle\hat{Q}\rangle$ and $\langle\hat{P}\rangle$ correspond to the dimensionless classical dynamics given by [13, 99, 68, 33]

$$\ddot{x}_{cl} + 2\Gamma\dot{x}_{cl} + \beta^2 x_{cl}^3 - x_{cl} = \frac{g}{\beta}\cos(\Omega t). \tag{4.2}$$

Although the scaling factor $\beta$ is crucial in determining the role of quantum effects in the dynamics, classically it is a trivial scaling factor due to the definition of $x_{cl}$ and $p_{cl}$. Indeed, for rescaling $X \equiv \beta x_{cl}$, the classical equation of motion is independent of $\beta$. Note also that the quantum dissipation, given in terms of $\hat{L}$, is symmetric with respect to position and momentum. The extra term proportional to the damping rate $\Gamma$ in the Hamiltonian (4.1), breaks this symmetry in such a way that the dissipative force is proportional to the velocity, exactly as expected in the classical limit.

Depending on the parameters, the classical model described by Eq. (4.2) exhibits chaotic dynamics as illustrated by the strange attractor in phase space shown by the black dots in Fig. 4.1. The steady state of the Wigner function, obtained by numerically solving Eq. (3.20), is also shown in Fig. 4.1 for the same set of parameters and different values of the scaling parameter $\beta$. This illustrates that the Wigner function of the ensemble-averaged quantum state broadly matches the strange attractor as $\beta \to 0$, which is a signature of chaotic dynamics and shows the emergence of chaos for the open quantum system. However, the degree of chaos cannot be quantified via the unconditional dynamics of Eq. (3.20), since any two initial states evolve to the same asymptotic state, giving a negative Lyapunov exponent. This does *not* mean that chaos is not present; indeed, the same problem would arise in classical chaos if one decided to calculate classical Lyapunov exponents by using the separation of average trajectories over a classical ensemble, rather than the separation of two classical trajectories. To define the degree of chaos via a *quantum* Lyapunov exponent, we need to use a conditional quantum trajectory approach that has a direct comparison with the classical trajectory approach [131, 125, 7, 48].

## 4.3 Continuous Measurement of the Duffing Oscillator

The final step in the description of our model is to move from the master equation (3.20), which corresponds to the ensemble averaged evolution of the open quantum system, to an equation that describes a single realisation of the quantum system being continuously monitored. Such a description is given by quantum trajectories governed by a stochastic Schrödinger equation (SSE). As said in the previous chapter, we are focusing solely on diffusive trajectories of the kind given by Eq. (3.61). Note that the amplitude $|u|$ and phase $\phi$ fully characterise the noise process and therefore different choices of $u$ correspond to particular ways of unraveling the master equation into stochastic trajectories.

Previous works on quantum Lyapunov exponents and the quantum to classical transition have adopted a fixed monitoring strategy (a particular case of Eq. (3.61) for a given choice of $u$ and $\hat{L}$ operator) corresponding to either a continuous position measurement ($u = 1$ and $\hat{L} = \hat{x}$) [6, 54] or to the quantum state diffusion (QSD) model ($u = 0$) [99, 68].

In what follows, we choose $u = \exp(-2i\phi)$ so that $\mathrm{d}\xi = \exp(-i\phi)\,\mathrm{d}W$, where $dW$ is a real noise of zero mean and $dW^2 = dt$. Physically, this choice corresponds to a

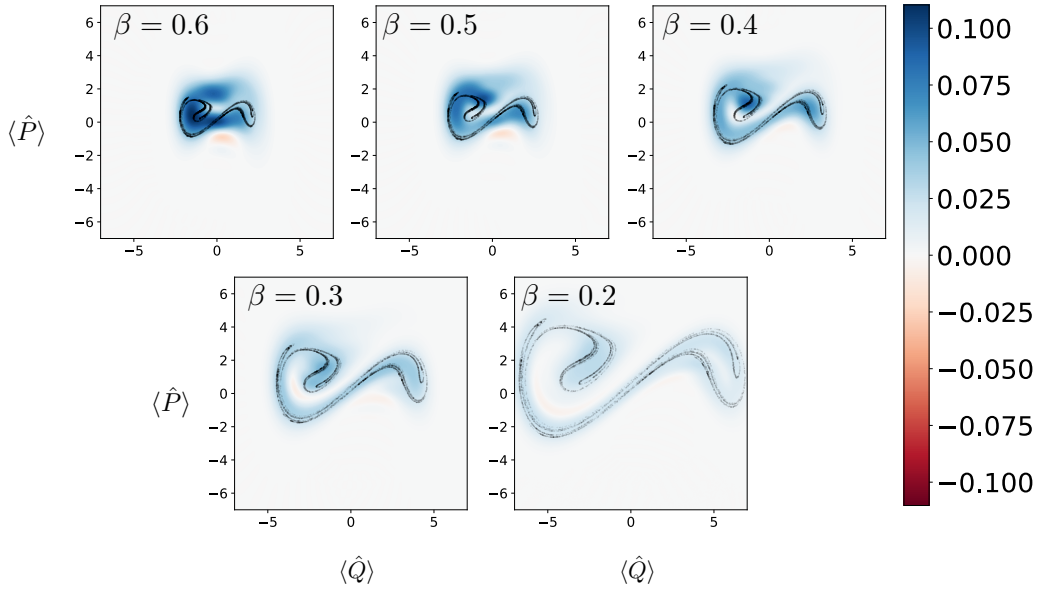


**Figure 4.1:** Wigner function for the steady state of the unconditional dynamics given by the master equation (3.20), for the dimensionless parameters $\Gamma = 0.10$, $g = 0.3$, $\Omega = 1$, and for several values of $\beta$ transitioning from quantum ($\beta = 0.6$) to semiclassical ($\beta = 0.2$). The Poincaré section of the classical Duffing oscillator is also overlaid for these parameters (black dots). The system exhibits chaos for these parameters, as seen by the emergence of the strange attractor and the positive Lyapunov exponent $\lambda_{cl} = 0.16$. Here the Wigner function for the unconditional state also follows the shape of the strange attractor in phase space, which is a signature of chaotic dynamics. The shape of the strange attractor becomes pronounced as $\beta$ decreases.

continuous measurement of the quadrature operator $\hat{X}_\phi = [\exp(-i\phi)\hat{a} + \exp(i\phi)\hat{a}^\dagger]/\sqrt{2}$. Experimentally, this could be achieved by performing a standard balanced homodyne detection on the output of the system, as shown in Fig. 5.1. The output channel $\hat{L} = \sqrt{2\Gamma}\hat{a}$ is combined with a local oscillator (LO) of phase $\phi$ at a beam splitter, while the readings at the detectors are subtracted to yield a measurement signal $I\mathrm{d}t = \sqrt{\Gamma}\langle \hat{X}_\phi \rangle + \mathrm{d}W$ [156]. The phase $\phi$ of the LO is a controllable parameter that determines the quadrature to be measured. For instance, $\phi = 0$ results in a measurement of $\hat{Q} = \hat{X}_{\phi=0}$, whereas $\phi = \pi/2$ gives a measurement of $\hat{P} = \hat{X}_{\phi=\pi/2}$.

## 4.4 Quantum Lyapunov Exponents

Within the context of quantum chaos, this quantum trajectory approach has proven useful in the investigation of the quantum-classical transition [131, 13, 117, 118, 47]. Furthermore, it offers a way to calculate quantum Lyapunov exponents, thereby unambiguously quantifying the degree of chaos within the system [6, 99, 54, 68, 33, 108]. Similar to the classical protocol [159], this is done by following the separation of two initially close wave-packet centroids in phase space $(\langle \hat{Q} \rangle, \langle \hat{P} \rangle)$ evolving according to Eq. (3.61) under the same noise realization [33, 108].

Specifically, the quantum Lyapunov exponent is defined as

$$\lambda = \lim_{t\to\infty} \lim_{d_0\to 0} \frac{\ln(d_t/d_0)}{t}, \tag{4.3}$$

where $d_t = [\Delta Q(t)^2 + \Delta P(t)^2]^{1/2}$ is the dimensionless phase-space distance between two quantum trajectories with differences in the average position and average momentum of the two trajectories given by $\Delta Q(t) = \langle \hat{Q}_1 \rangle - \langle \hat{Q}_2 \rangle$ and $\Delta P(t) = \langle \hat{P}_1 \rangle - \langle \hat{P}_2 \rangle$, respectively. The two quantum trajectories are initially prepared in coherent states displaced (in phase space) from each other by a small distance $d_0 = d_{t=0}$ (i.e., $|\alpha_1\rangle = |\alpha\rangle$ and $|\alpha_2\rangle = |\alpha + d_0\rangle$), and then evolved stochastically via Eq. (3.61) under the same noise realization, which corresponds to the same measurement record.

We are now in the position to investigate the dynamics of a chaotic quantum Duffing oscillator under continuous monitoring. To establish a quantitative picture of the level of chaos in the dynamics, we calculate the quantum Lyapunov exponent. For the numerical calculations, one of the trajectories is periodically reset towards the other one to remain within the linear regime using the displacement operator [125], and $\log(d_t/d_0)$, calculated before every reset, is averaged over time. Convergence occurs within 500 cycles of the driving term, and the final Lyapunov exponent is obtained after averaging over multiple realisations (20 runs) of the stochastic noise. The numerical calculations can be computationally intensive as the size of the system is increased. However, since the state in a chaotic system is confined to the strange attractor, we need only a large enough basis size to encompass this region of phase space for a given choice of $\beta$. In this work we vary the scaling parameter from $\beta = 1$ to 0.1, which requires a range of basis size from $N = 35$ to 200 (using the harmonic oscillator energy eigenstates). Note that this computation could be made more efficient by using a moving basis [125], however we did not use this for the purpose of this work.

The effect of the monitoring angle on the quantum Lyapunov exponents is shown in Fig. 4.2-d for $\Gamma = 0.10$, $g = 0.3$, $\Omega = 1$, and $\beta = 0.3$. The quantum dynamics is chaotic ($\lambda > 0$) for most choices of the phase $\phi$, with the quantum Poincaré section (Fig. 4.2-b) roughly following the classical strange attractor, which is shown in Fig. 4.2-a for comparison. For $\phi \approx \pi/2$, however, the quantum attractor is significantly blurred (Fig. 4.2-c) leading to a strong suppression of chaos. This shows that we can tune the behaviour of the system from chaotic to regular by simply changing which quadrature is measured in the homodyne setup.

It is evident that in the classical limit, there is no dependence on the monitoring scheme, so there must be a value of $\beta$ beyond which the choice of monitoring can have an effect on the complex behaviour of the system. To investigate that, we plotted in Fig. 4.3 the quantum Lyapunov exponents for $\phi = \pi$ (dashed black) and $\phi = \pi/2$ (solid red), corresponding approximately to the maximum and minimum values of $\lambda$, as a function of our macroscopicity parameter $\beta$. The curves show that for large $\beta$, the quantum Lyapunov exponent is always negative and it is not significantly affected by the choice of $\phi$. This is the region where the quantum noise is dominant, chaos is suppressed, and the exact form of the monitoring is irrelevant. In the opposite limit, the quantum curve is always positive and should approach the classical value of $\lambda_{cl} = 0.16$ for small enough $\beta$. This region also shows very little dependence with $\phi$, but now for a different reason: in this limit the classical dynamics prevails over the quantum noise and the choice of measurement ceases to affect the system. However, there is an intermediate region, highlighted in Fig. 4.3, where there is a noticeable dependence on $\phi$. This is exactly the window of the macroscopicity parameter where controlling the onset of chaos through quantum measurements is possible.

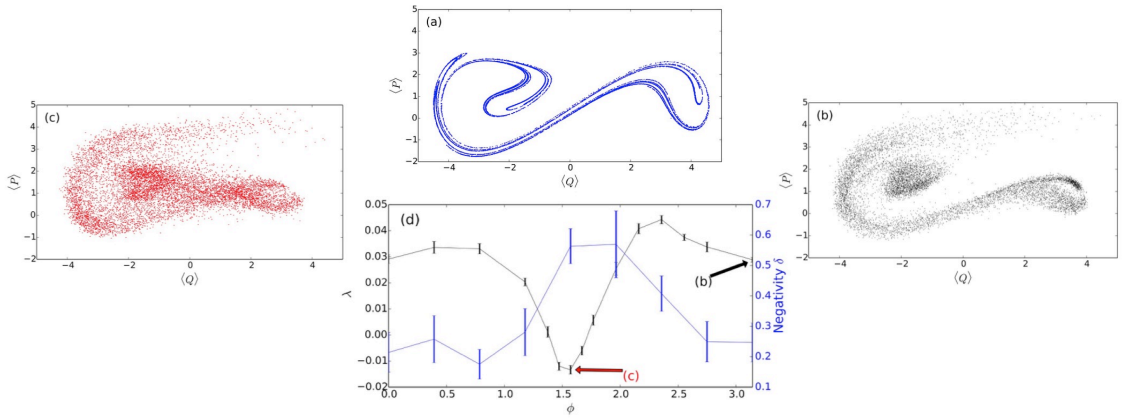


**Figure 4.2:** (a) Strange attractor for the classical Duffing oscillator with parameters $\Gamma = 0.10$, $g = 0.3$ and $\Omega = 1$. (b) Quantum Poincaré section for a single trajectory with 1000 points for $\phi = \pi$ with points taken once every driving period ($t = 2\pi n$). (c) Quantum Poincaré section for $\phi = \pi/2$. (d) Average Lyapunov exponent $\lambda$ (black curve) and average negativity $\delta$ (blue curve) as a function of $\phi$ for $|u| = 1$, $\beta = 0.3$, $\Gamma = 0.10$, $g = 0.3$ and $\Omega = 1$. The averages are constructed from the Lyapunov exponents and negativities calculated for 20 different individual trajectories. Error bars are given by the standard error in the mean. The arrows indicate the choice of $\phi$ that correspond to the Poincaré sections in (b) and (c). For (b), (c) and (d), with the choice $\beta = 0.3$, a basis size of $N = 65$ is used.

## 4.5 Semiclassical approach: comparison with Gaussian wave packet dynamics

To utilise this window of control and predict the monitoring parameters that provide minimum or maximum Lyapunov exponents for a given chaotic system, one first needs to understand the physical mechanism behind this dependency with the angle $\phi$. A first hint towards the explanation comes from considering the semiclassical results shown by the top two curves in Fig. 4.3, obtained using a Gaussian approximation [102]. In this approximation, we restrict the wavefunction to always be of a form expressed mathematically as a Gaussian function. Doing so leads to higher-order moments that can be described by just the mean and the variance and the covariance of the Gaussian wavefunction. We can fully describe the dynamics in this limit with the 5 equations of motion given for the centroid ($\langle\hat{Q}\rangle$, $\langle\hat{P}\rangle$) and the variances ($\mathrm{Var}_Q$, $\mathrm{Var}_P$, $\mathrm{Var}_{QP}$). We will use the replacement variables $x = \langle\hat{Q}\rangle$, $p = \langle\hat{P}\rangle$ for the semiclassical equations.

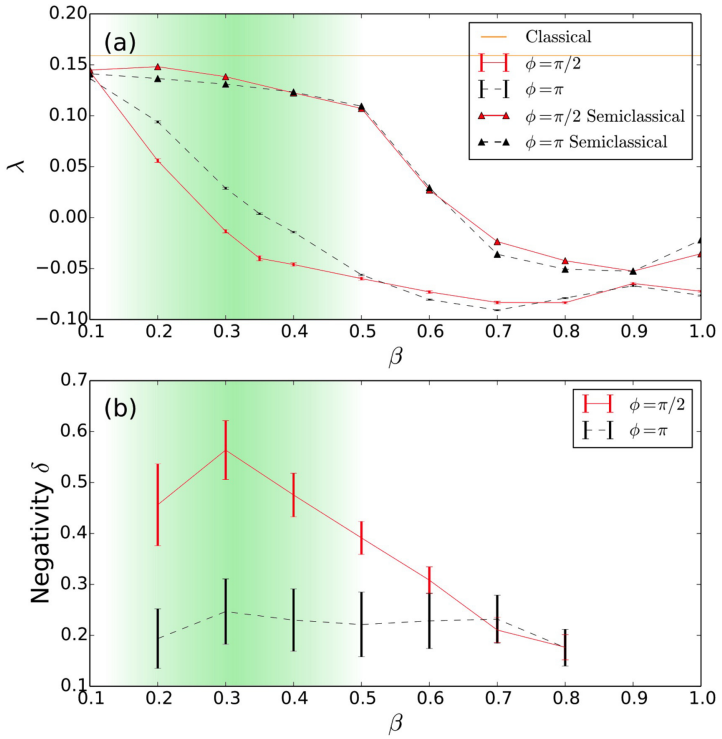


**Figure 4.3:** (a) Average quantum Lyapunov exponent $\lambda$ for $|u| = 1$, $\Gamma = 0.10$, $g = 0.3$ and $\Omega = 1$. The points are constructed from averaging 20 different noise realisations, each starting with a pair of coherent states. Error bars give the standard error from the mean. In (a) $\lambda$ is shown as a function of the macroscopicity parameter $\beta$ for the full quantum simulation with two values of the phase $\phi = \pi$ (black, dashed) and $\phi = \pi/2$ (red, solid). The straight line at the top corresponds to the classical Lyapunov exponent $\lambda_{cl} = 0.16$ for these parameters. $\lambda$ is also plotted as a function of $\beta$ using a semiclassical approximation (triangles) to obtain the equations of motion, again with the same phases. (b) Negativity $\delta$ of the Wigner function, is averaged over the 20 trajectories for the same parameters and phases as in (a) and plotted as a function of $\beta$. The region where we see a qualitative, pronounced difference between monitoring strategies (roughly between $\beta = 0.2$ and 0.4) is highlighted in green.

The equations of motion are found in Ito form using Eq. (3.63) and using the fact that we have a pure state ($\langle \hat{G} \rangle = \langle \psi(t)|\hat{G}|\psi(t)\rangle$). So that in the semiclassical limit, the

equations of motion in Stratonovich form for the Duffing oscillator are given by

$$\frac{\mathrm{d}x}{\mathrm{d}t} = p + \sqrt{\Gamma}(\cos(\phi)(-1+2V_x) - 2\sin(\phi)V_{xp})\mathrm{d}W, \tag{4.4}$$

$$\frac{\mathrm{d}p}{\mathrm{d}t} = \frac{g}{\beta}\cos(\Omega t) + x - \beta^2(x^3+3xV_x) - 2\Gamma p + \sqrt{\Gamma}(\sin(\phi)(1-2V_p) + 2\cos(\phi)V_{xp})\mathrm{d}W, \tag{4.5}$$

$$\begin{aligned}\frac{\mathrm{d}V_x}{\mathrm{d}t} &= 2V_{xp} + \frac{1}{2}\Gamma\left[1-4(V_{xp}^2 - V_x + V_x^2)\right] \\ &\quad + \frac{1}{2}\Gamma\left[\cos(2\phi)(-1+4(V_{xp}^2+V_x-V_x^2)) + 4\sin(2\phi)(-V_{xp}+2V_{xp}Vx)\right],\end{aligned} \tag{4.6}$$

$$\begin{aligned}\frac{\mathrm{d}V_x}{\mathrm{d}t} &= 2V_{xp} - 6\beta^2 V_{xp}(x^2+V_x) + \frac{1}{2}\Gamma\left[1-4V_p-4V_p^2-4V_{xp}^2\right] \\ &\quad + \frac{1}{2}\Gamma\left[\cos(2\phi)(1-4V_p+4V_p^2-4V_{xp}^2) + 4\sin(2\phi)(-V_{xp}+2V_{xp}Vp)\right],\end{aligned} \tag{4.7}$$

$$\begin{aligned}\frac{\mathrm{d}V_{xp}}{\mathrm{d}t} =& -2\Gamma\left[V_{xp}(V_p+V_x) - \cos(2\phi)V_{xp}(Vp-Vx) - \frac{1}{4}\sin(2\phi)(1-2V_p+4V_{xp}^2-2V_x+4V_x^2)\right] \\ &+ V_p + V_x - 3\beta^2 V_x(x^2+V_x).\end{aligned} \tag{4.8}$$

From inspection of the Lyapunov exponent for the Gaussian approximation (Fig. 4.3), We can see that in the classical limit, the semiclassical and quantum results both agree, tending towards the classical Lyapunov exponent. However, further into the quantum regime, the semiclassical tends to overshoot the quantum Lyapunov exponent, showing us the breakdown of the approximation in this regime. The semiclassical dynamics are still useful in their own right in this regime, and they help us to understand what is going on for the quantum dynamics.

It is important to note that while the semiclassical results given by the Gaussian approximation are not necessary (we are able to solve the exact quantum dynamics in this regime) they do offer a valuable perspective of what is going on with the dynamics. We see a negligible difference between the Lyapunov exponents for the two curves, indicating that the difference we see in the quantum dynamics cannot be explained by the Gaussian approximation. This approximation retains the measurement terms and the stochastic aspect of the dynamics, but restricts the state to remain as a Gaussian in phase space. The latter aspect prevents the formation of the complex interference fringes that we see in the full quantum evolution (see Fig. 4.6) and indicates that the effect we observed is intrinsically quantum, arising from the interplay between the interference generated by the nonlinear dynamics and the way different monitoring strategies destroy them.

## 4.6 Negativity of the Wigner function

In order to assert that interference effects are indeed the key factor at play, we must quantify the level of interference present in the evolution. To do this we use the negativity of the Wigner function which has previously been proposed as an indicator of non-classicality [69] and is defined as $\delta_\psi = \int\int |W_\psi(q,p)|\,\mathrm{d}q\,\mathrm{d}p - 1$. Here, both the Wigner function and the negativity are calculated for the pure state $|\psi\rangle$ evolved in each individual quantum trajectory. The average negativity is then found by averaging over the 20 noise realisations $\delta = \sum_i^{M=20}\delta_{\psi_i}/M$. In Fig. 4.4, where we show the average negativity as a function of time, we see that for both choices of monitoring angles in the figure (red curve for $\phi = \pi/2$

and black for $\phi = \pi$) the negativity starts from zero (initial coherent state) and has a surge at around $0.8\Omega t$. This is the time taken for the quantum state to start probing the shape of the classical stange attractor and start developing fringes in the Wigner function. After this build up period, the effect of the monitoring on the dynamics becomes evident: For $\phi = \pi/2$ the negativity fluctuates around higher values than for $\phi = \pi$. To make a connection with the Lyapunov exponents calculated previously, we averaged the negativity from Fig. 4.4 for the last two forcing periods and plotted the results in Fig. 4.2-d. We see a clear anti-correlation between the negativity and the quantum Lyapunov exponents, which is also observed for the different values of $\beta$ in Fig. 4.3. The large negativity at $\phi \approx \pi/2$ explains the dip in the Lyapunov exponent: The larger the interference effects, the further the quantum system is from the classical behaviour, leading to a stronger suppression of chaos.

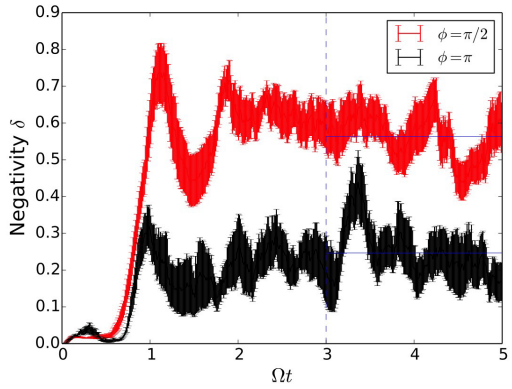


**Figure 4.4:** Evolution of the negativity of the Wigner function for $\phi = \pi/2$ (red) and $\phi = \pi$ (black) averaged over 20 noise realisations. The horizontal lines show the average negativity for the last 2 forcing periods, a value that is used in Fig. 4.2-d. We see that smaller (higher) values of negativity correspond to higher (smaller) values of the Lyapunov exponents.

The remaining issue to be explained is why the suppression is stronger at that particular measurement angle. The best way to understand the role of the phase $\phi$ is to examine a simple class of states that present interference. Here we look at superpositions of coherent states in the form $|\psi_0\rangle = c_+|\alpha\rangle + c_-|-\alpha\rangle$ (Schrödinger cat state), with $\alpha = |\alpha|e^{i\varphi}$. The interference fringes in these states have a well defined structure, being aligned along the direction defined by the angle $\varphi$. The evolution of the state conditioned on the measurement only is given by Eq. (3.61) with $\hat{H} = 0$. Looking just at the noise term $(\hat{a} - \langle\hat{a}\rangle)|\psi\rangle \mathrm{d}\xi$ for $|u| = 1$, we have

$$\mathrm{d}|\psi_0\rangle = |\alpha|\left(c_+ e^{i(\varphi-\phi)}|\alpha\rangle - c_- e^{i(\varphi-\phi)}|-\alpha\rangle\right)\mathrm{d}W, \tag{4.9}$$

where we have assumed that the initial coefficients are equal ($c_+ = c_-$) and that $\alpha$ is large, such that $\langle-\alpha|\alpha\rangle \approx 0$.

For each term, the evolution is given by

$$\mathrm{d}c_+ = c_+|\alpha|e^{i(\varphi-\phi)}\mathrm{d}W, \tag{4.10}$$

$$\mathrm{d}c_- = -c_-|\alpha|e^{i(\varphi-\phi)}\mathrm{d}W. \tag{4.11}$$

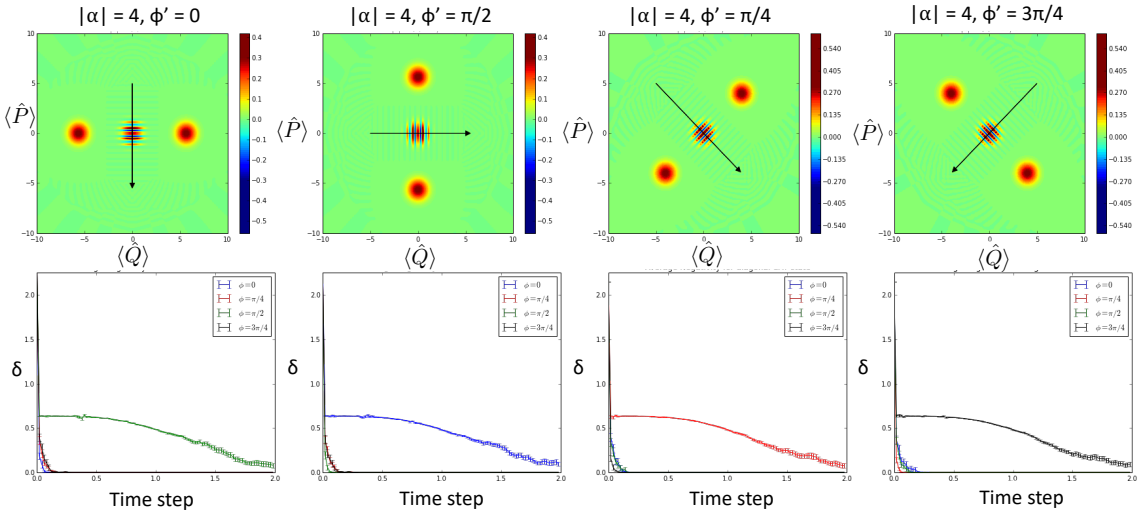


**Figure 4.5:** Decay of negativity for four orientations of a cat state in phase space and four different choices of measurement phase. The evolution of the state is given solely by the dissipation and the measurement ($\hat{H} = 0$). The above panels show the Wigner function for each initial cat state orientation while the lower panels show the corresponding decay rate of the negativity calculated over the evolution time for four different monitoring angles: $\phi = 0$(blue), $\phi = \pi/4$(red), $\phi = \pi/2$(green) and $\phi = 3\pi/4$(black). The direction perpendicular to the orientation of the fringes (given by the arrow in the top panel) corresponds to the slowest decay of negativity.

From these equations one can see that when the monitoring angle $\phi$ is parallel to the interference fringes ($\varphi - \phi = 0$), then in a short time the system stochastically evolves to one of the components of the original superposition and interference fringes quickly disappear. On the other hand, when the measurement direction is perpendicular to the fringes ($\varphi - \phi = \pi/2$), the short term evolution corresponds to a phase rotation between the two components and the fringes survive for longer. Therefore, the efficacy of the the stochastic term in equation (3.61) in eliminating interference depends directly on the alignment between $\phi$ and $\varphi$. This can be seen in Fig. 4.5 where we have plotted the initial Wigner functions for four orientations of cat states in phase space (top panels) and the corresponding decay rate of the negativity calculated over the evolution time for four different monitoring angles (bottom panels): $\phi = 0$(blue), $\phi = \pi/4$(red), $\phi = \pi/2$(green) and $\phi = 3\pi/4$(black). The direction perpendicular to the orientation of the fringes (given by the arrow in the top panel) corresponds to the slowest decay of negativity.

The alignment of the monitoring angle with the direction of the fringes, and the rate at which this localises the state explains the dependency of the quantum Lyapunov exponent with the monitoring parameter. Given the complexity of the dynamics and the geometric structure of the strange attractor in phase space, it is non-trivial to justify that there is a privileged direction where this effect can take place. However, by following the dynamics of the Wigner function for a single trajectory in real time, it is possible to distinguish certain structures that repeat over time. These structures, representing the stretching region around the origin and also the left and right bending regions of the classical strange attractor, are depicted in the snapshots of the Wigner function of Fig. 4.6. Even though the interference fringes in these plots are not perfectly aligned, they are concentrated in

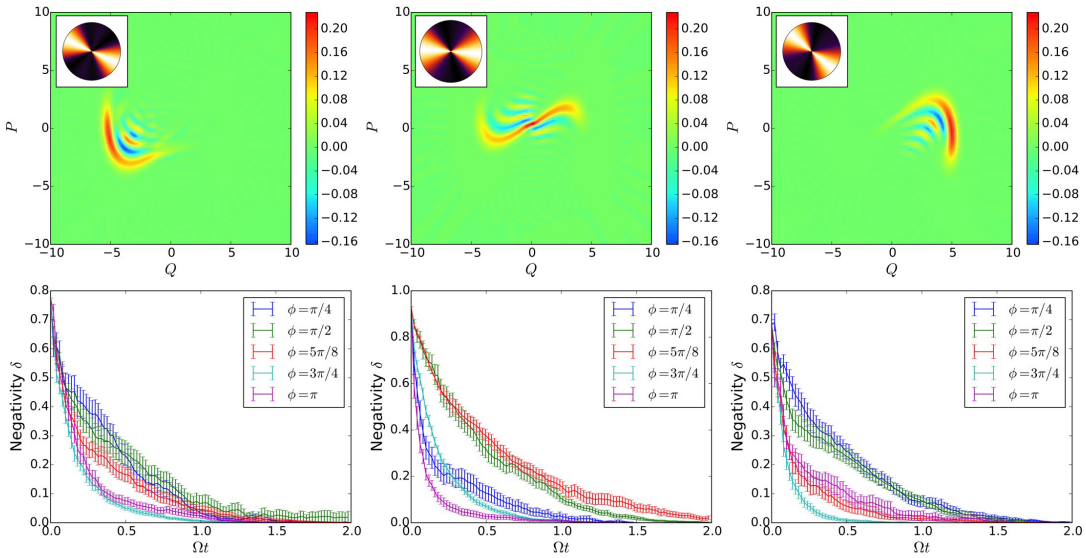


**Figure 4.6:** (Top) Snapshots of the Wigner function (for a single noise realisation of the quantum trajectory) for the full dynamics at three different times (for $\Gamma = 0.10$ and $\beta = 0.3$). These quantum states are chosen as the initial condition for the evolution shown in the three bottom panels. (Bottom) Decay of the negativity over time, with evolution of the state given solely by the dissipation and the measurement ($\hat{H} = 0$) from the initial condition given in the top panels. The decay plots are a result of averaging over 20 noise realisations. As in the case of cat states, negativity decays faster when the monitoring angle is parallel to the interference pattern, though it is not as obvious here. (Insets) These show the polar density plot for the decay rate of the negativity. These are found by fitting an exponential function to the curves in the bottom panels, with the minimum (maximum) decay rate corresponding to the darker (brighter) colours. These insets confirm that the direction of fastest decay is indeed parallel to the direction of the interference fringes.

the range of angles orthogonal to the ones that lead to higher negativity (around $\phi = \pi/2$). This dependency with the angle is quantified by calculating the decay rate of the negativity for the evolution of these states under monitoring dynamics only (bottom plots in Fig. 4.6), and they match the region where the Lyapunov exponent dips in Fig. 4.2-d.

Given the evidence presented so far, it is tempting to always associate the presence of negativity in the Wigner function with suppression of chaos. However, in certain cases a large negativity seems to be connected with enhancement of chaos, as shown in Fig. 4.7, where the quantum Lyapunov exponents for $\Gamma = 0.05$ are shown (all other parameters are as in Fig. 4.2) . This is an interesting case recently investigated by Pokharel *et al.* [107] where the classical dynamics is regular but chaos can emerge quantum mechanically. Although this seems to be a counter example to our discussion so far, the fact that the dependency of the Lyapunov exponent with the monitoring angle is also seen in the semiclassical calculations (see Fig. 4.7-b) indicates that a different mechanism is at play in this case, overshadowing the effects of negativity.

Indeed, simulations of the dynamics using the Gaussian approximation show that for the phase $\phi$ corresponding to the smallest value of the Lyapunov exponent, the semiclassical system remains most of the time concentrated along the classical stable orbit, rarely making incursions into the central region corresponding to the classical chaotic transient (see Fig. 4.8). In the stable region, the quantum state remains mostly Gaussian, explain-

ing the small values for the negativity. On the other hand, for the phase linked to the maximum Lyapunov exponent, the semiclassical system spends more time in the chaotic region, visiting the stable classical orbit from time to time, but eventually coming back. While visiting the chaotic region, the quantum state is allowed to stretch along the unstable direction and then fold, interfering with itself and producing negative values of the Wigner function. The existence of negative values is therefore a consequence of a semiclassical dynamical effect of the monitoring process which, for certain values of $\phi$, induces transitions between the coexisting regular and chaotic regions. These transitions seem to be related to the recent analysis of the quantum-classical correspondence in terms of transient chaos done by Wang *et al.* [148]. Note, however, that here the noise strength is fixed, it is therefore the form of the coupling between the noise and the system variables, determined by the measurement choice, that dictates the average time spent in each region. Once again, just a change in our measurement parameter allows us to radically alter the complexity of the dynamical evolution of the system.

In conclusion, our results show that the choice of monitoring plays a crucial role in the emergence of chaos in quantum systems, adding yet another layer of complexity to the already intriguing problem of the quantum to classical transition. We showed that the effect of the measurement choice on the quantum Lyapunov exponent manifests in two distinct ways: 1) at the semiclassical level, by inducing transitions between regions corresponding to a classical periodic orbit and a transient chaotic regime & 2) at the quantum level, by influencing the way interference fringes in the Wigner function are destroyed. In both cases, the more 'quantumness' in the system, as measured by the amount of negativity, the more its dynamical behaviour departs from the classical, by suppressing chaos in the latter and creating it in the former. In the case where the corresponding classical system is chaotic, the effectiveness of certain monitoring schemes in suppressing interference depends on the relative angle between the measurement direction and the fringes induced by the nonlinear dynamics. In this way, we have predictive power over the monitoring parameters that will lead to minimum or maximum quantum Lyapunov exponents by analysing the geometrical structure of the classical attractor. In both cases the system size and the form and amount of dissipation in the system are kept constant, so it is remarkable that we can manipulate the onset of complex behaviour in the system by tuning a purely quantum parameter associated with the appropriately chosen measurement scenario.

## 4.7 A different perspective on the semiclassical result for $\Gamma = 0.05$

The work discussed in this section comes from the paper:

*The effects of amplification of fluctuation energy scale by quantum measurement choice on quantum chaotic systems: Semiclassical analysis*, S. Greenfield, Y. Shi, **J. K. Eastman**, A. R. R. Carvalho, A. K. Pattanayak, Proceedings of the 5th International Conference on Applications in Nonlinear Dynamics, Springer, Cham, 72-83 (2019).

The main investigator for this work is S. Greenfield. This work offers more detail for the case of $\Gamma = 0.05$, where the classical limit is regular and the onset of chaos can be seen in the semiclassical regime. My contribution is the verification of the semiclassical results using the exact quantum dynamics. This section is included in the thesis for completeness. We refer to the paper itself for detailed equations, here we present a glimpse of the arguments.

Let us again focus on the case $\Gamma = 0.05$. Instead of looking at the evolution of five

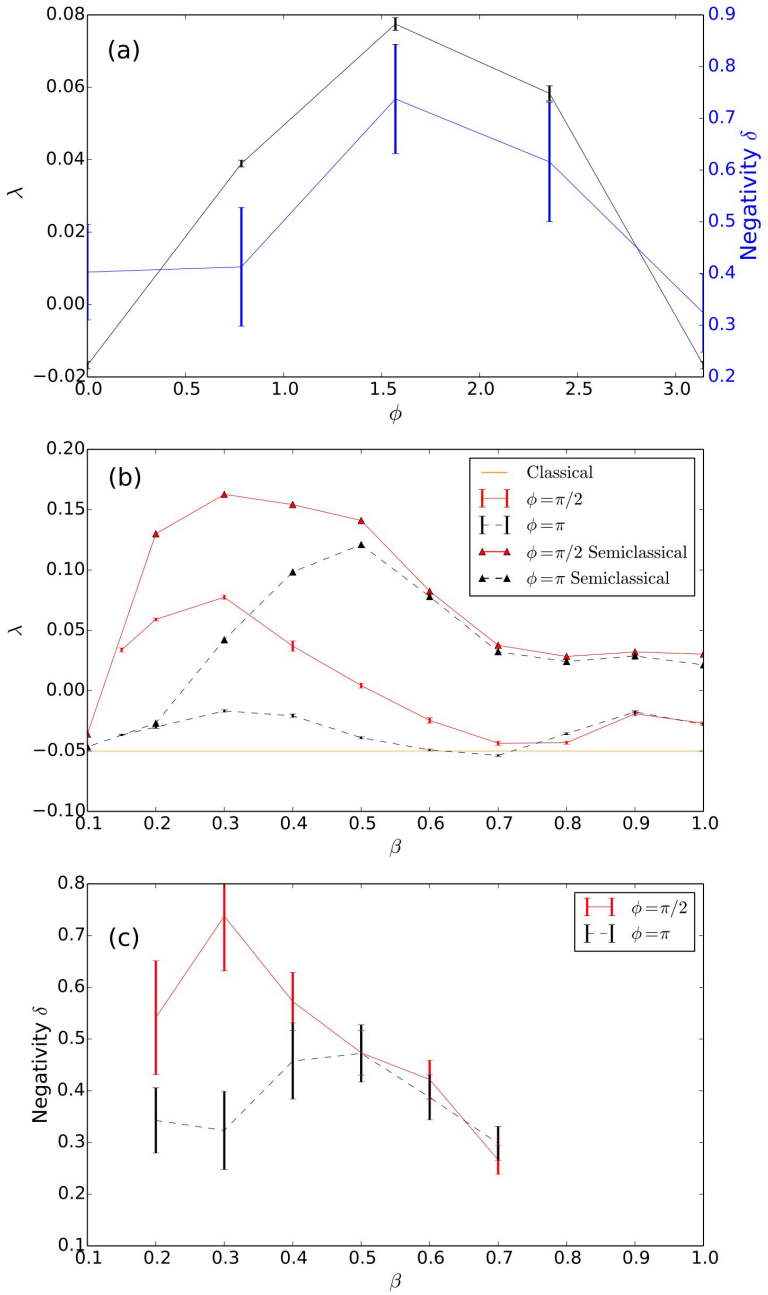


**Figure 4.7:** (a) Lyapunov exponent (black) and average negativity (blue) as a function of the monitoring parameter $\phi$ for $\Gamma = 0.05$. The Lyapunov exponents for $\phi = \pi$ (black, dashed) and $\phi = \pi/2$ (red, solid) are given in (b) as a function of the macroscopicity parameter $\beta$ for the quantum and semiclassical (triangles) for values from 0.1 to 1.0. The points here are constructed from 10 different noise realisations. The classical Lyapunov exponent in this case is $\lambda_{cl} = -0.05$ and is represented by the horizontal line in the plot. (c) Average negativity of the Wigner function as a function of $\beta$ for the same phases as in (b) . Each point is constructed from 20 different noise realisations. The error bars give the standard error in the mean.

coupled equations of motion that give the mean, variance and covariance, we consider

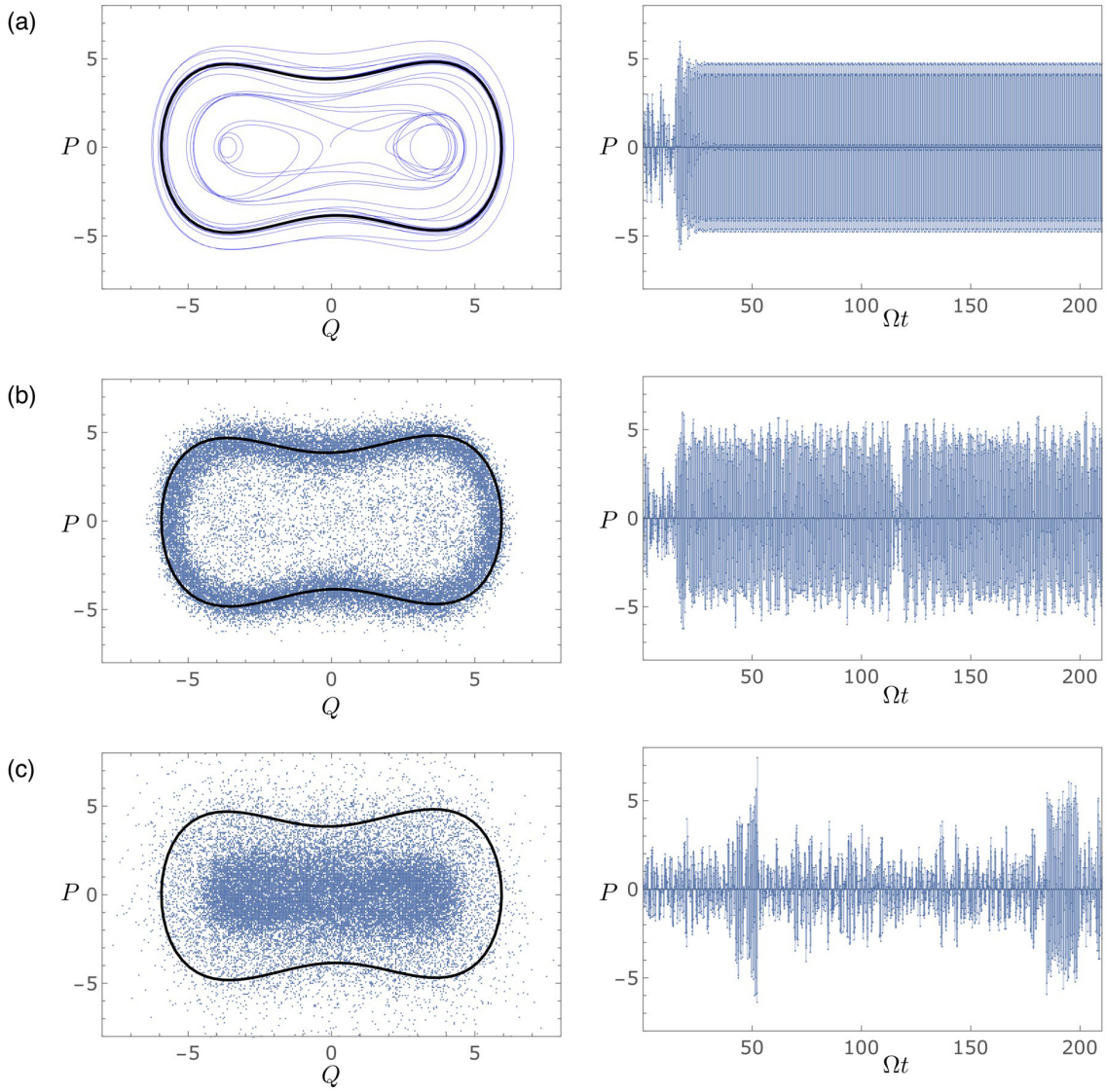


**Figure 4.8:** Phase space projection (left column) and momentum time series (right column) for: (a) classical; and semiclassical with (b) $\phi = \pi$ and (c) $\phi = \pi/2$. The bold black line corresponds to the classical dynamics with the transient removed. Classically, the central chaotic region is only visited in the initial transient before the system settles in its periodic behaviour. Semi-classically, the system can transition from one region to another. Different choices of the monitoring parameter $\phi$ induce preferences towards the classical periodic orbit (b), or the irregular region (c).

a different formalism where we describe the system as two coupled oscillators, the centroid oscillator $(x, p)$ and the 'quantum' spread oscillator $(\chi, \Pi)$ of the wave packet [102]. The spread oscillator is given by taking a change of variables for the variances given in section 4.5:

$$V_{QQ} = \chi^2, \tag{4.12}$$
$$V_{QP} = \chi\Pi, \tag{4.13}$$
$$V_{PP} = 1/4\chi^2 + \Pi^2. \tag{4.14}$$

In this formalism the effective time dependent Hamiltonian is given by the term for the

centroid oscillator, the term for the spread oscillator and the term that describes the coupling between the two. When we exclude coupling to the environment we have:

$$H(x, p, \chi, \Pi) = \frac{1}{2}p^2 + \frac{1}{2}\Pi^2 + U(x, \chi, t), \tag{4.15}$$

where $U(x, \chi, t)$ gives the 2D time dependent semiclassical potential

$$U(x, \chi, t) = U_1(x, t) + U_2(\chi) + U_{12}(x, \chi). \tag{4.16}$$

For the Duffing oscillator, the potential terms are given as

$$U_1(x, t) = -\frac{1}{2}x^2 + \frac{1}{4}\beta^2 x^4 + \frac{g}{\beta}x\cos\omega t, \tag{4.17}$$

$$U_2(\chi) = \frac{3}{4}\beta^2\chi^4 - \frac{1}{2}\chi^2 + \frac{1}{8\chi^2}, \tag{4.18}$$

$$U_{12}(x, \chi) = \frac{3}{2}\beta^2 x^2\chi^2. \tag{4.19}$$

The plots in Fig. 4.9 show the semiclassical potential $U(x, \chi)$ as a function of both $x$ and

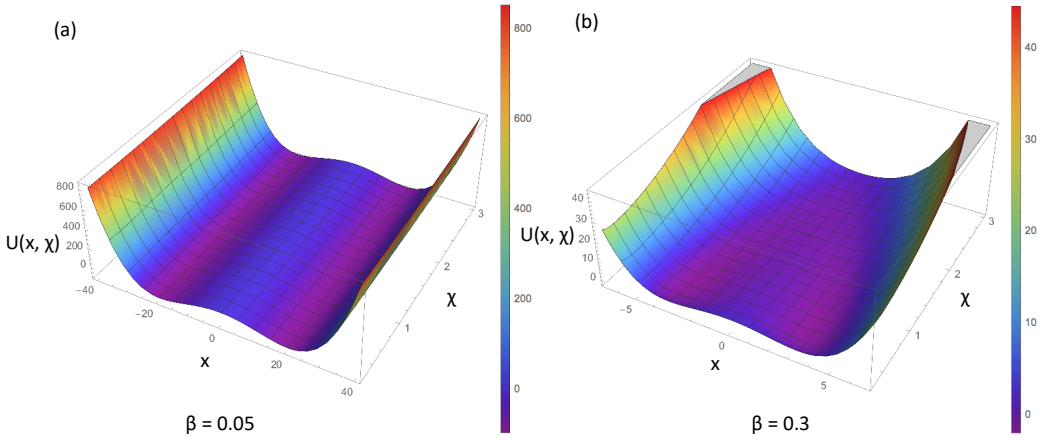


**Figure 4.9:** We plot the semiclassical potential given in Eq. (4.16) for two different values of $\beta$: (a) 0.05 and (b) 0.3. The plots show the semiclassical potential as a function of both $x$ and $\chi$ for both values of $\beta$, showing the change in the effective potential as the dynamics moves to a quantum regime. **This was produced by S. Greenfield.**

$\chi$ for both values of $\beta$, showing the change in the effective potential as the dynamics moves to a quantum regime. As a result of changing $\beta$, the move from a double well potential to a single well potential can be seen as as the quantum spread grows larger. This creates a non-classical path between the two wells, altering the dynamics of the quantum system. This effective potential assists in explaining why we see the onset of chaos in the quantum regime even when the classical limit is regular. The quantum system is able to 'tunnel' between the two wells (which is classically forbidden) for large $\chi$. This formalism also

enables us to understand the measurement dependence of the dynamics in this regime. Let us consider the equations of motion again. Using the above formalism, the wavefunction is accurately described by just four equations of motion instead of the five equations given in Eqs. **??**. The new 4D phase-space vector gives the following dynamics:

$$\begin{aligned}
\dot{x} &= p + \sqrt{\Gamma} N_x(\phi, \chi, \Pi) \mathrm{d}W \\
\dot{p} &= x - \beta^2 x^3 + \frac{g}{\beta}\cos(\Omega t) + \Gamma F_p + 3x\beta^2\chi^2 + \sqrt{\Gamma} N_p(\phi, \chi, \Pi)\mathrm{d}W \\
\dot{\chi} &= \Pi + \Gamma F_x(\phi, \chi, \Pi) \\
\dot{\Pi} &= \chi(-3\beta^2(x^2+\chi^2)+1) + \frac{1}{4\chi^3} + \Gamma F_\Pi(\phi, \chi, \Pi),
\end{aligned} \tag{4.20}$$

where the equations are described in terms of a generalised dissipative force $\mathbf{F}(\phi) = (F_x,\ F_p,\ F_\chi,\ F_\Pi)$ and noise $\mathbf{N}(\phi) = (N_x,\ N_p,\ N_\chi,\ N_\Pi)$ which is dependent on the back-action of the measurement. The noise terms couple only to the centroid oscillator $(x, p)$, with $N_\chi = N_\Pi = 0$ while the dissipative force terms that are dependent on $\phi$ couple only to the spread oscillator $(\chi, \Pi)$. It is particularly interesting to note that the $\phi$-dependent force acts to suppress large $\chi$ in the case of $\phi = 0$, leading to the suppression of the non-classical mechanism for inter-well transition. For the case of $\phi = \pi/2$ however, the forces that would suppress large $\chi$ are cancelled out by other dissipative forces which leads to the widely different dynamics of the system. This is easily seen from the numerical results shown in Fig. 4.10. The results plotted in this figure show the phase space portrait for

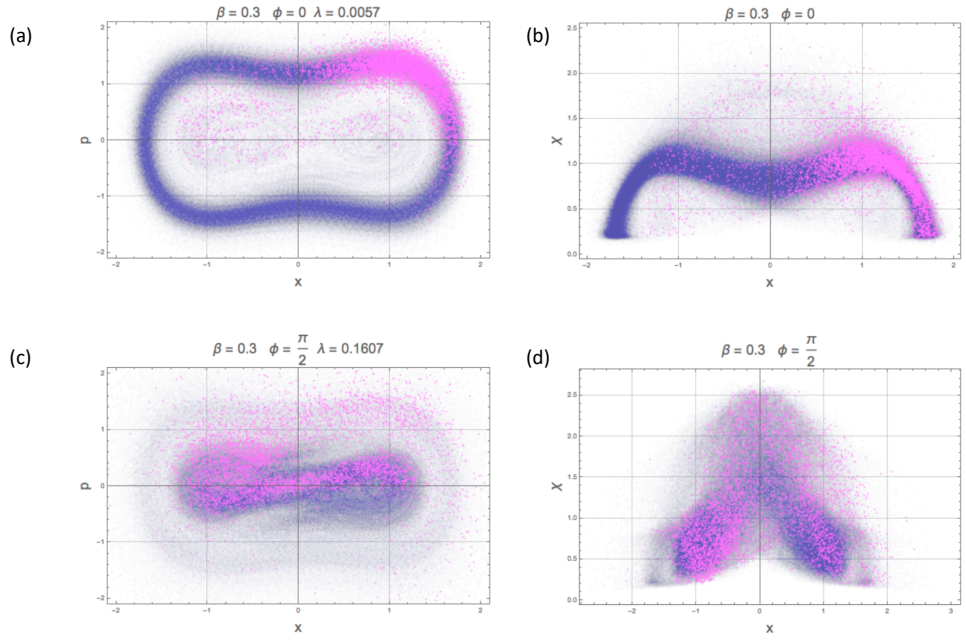


**Figure 4.10:** $(x,p)$ and $(x,\chi)$ phase space plots for both the trajectory (purple) and Poincaré section (pink) for the Semiclassical Duffing oscillator for the parameters $\beta = 0.3$, $\Gamma = 0.05$, $g = 0.3$ and $\Omega = 1$. This plot shows the results for both $\phi = 0$ (a) & (b) and $\phi = \pi/2$ (c) & (d). **This was produced by S. Greenfield.**

$(x, p)$ on the left and $(x, \chi)$ on the right for both the Poincaré section and the trajectory and for both choices of monitoring. These plots show frequent excursions to large values of $\chi$ are seen for $\phi = \pi/2$ and not for $\phi = 0$. This behaviour is verified by seeing the same result in the exact quantum dynamics shown in Fig. 4.11 where we have plotted $(\langle\hat{Q}\rangle, \langle\hat{P}\rangle)$

on the left and $(\langle\hat{Q}\rangle, \hat{\chi})$ on the right, where we have $V_Q = \langle\hat{Q}^2\rangle - \langle\hat{Q}\rangle^2$ and $\hat{\chi} = \sqrt{V_Q}$. Again we see the dynamics visiting large values of $\chi$ more often in the case of $\phi = \pi/2$.

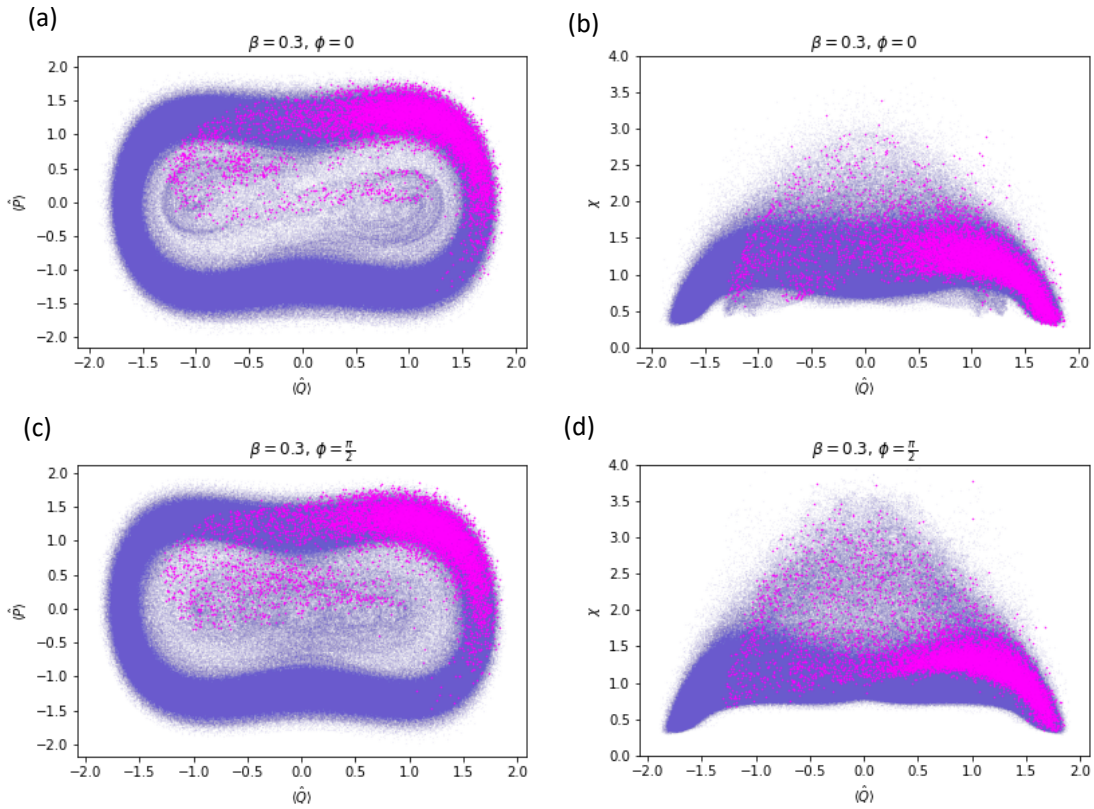


**Figure 4.11:** $(\langle\hat{Q}\rangle,\langle\hat{P}\rangle)$ and $(\langle\hat{Q}\rangle,\hat{\chi})$ phase space plots for both the trajectory (purple) and Poincaré section (pink) for the exact quantum dynamics of the Duffing oscillator for the parameters $\beta = 0.3$, $\Gamma = 0.05$, $g = 0.3$ and $\Omega = 1$. This plot shows the results for both $\phi = 0$ (a) & (b) and $\phi = \pi/2$ (c) & (d).

This means that while the semiclassical may not be a valid description of the dynamics of the quantum system, it can still accurately describe the mechanism by which the onset of chaos is seen for a given choice of monitoring angle. Large $\chi$ values lead to the non-classical mechanism of inter-well transitions that leads to chaotic dynamics. Excursions to large $\chi$ are suppressed in the $\phi = 0$ case due to the dissipative force that results from the measurement back-action.

# Part II

# Methods to control chaotic sytems

# 5

# Controlling Chaotic Systems with Adaptive Measurement Techniques

The previous chapter showed that the choice of measurement can affect the emergence of chaos. Here we use this information to find strategies to control chaos in experimental systems where the presence of chaos may or may not be desired, and so the ability to control the onset of chaos will assist greatly. This is done by using the measurement as a control knob to control the dynamics to either enhance or suppress chaos.

This chapter contains work that has been published in the following paper: *'Controlling chaos in the quantum regime using adaptive measurements'*, J. K. Eastman, S. S. Szigeti, J. J. Hope, A. R. R. Carvalho, Phys. Rev. A. **99**, 012111 (2018). DOI: https://doi.org/10.1103/PhysRevA.99.012111

## 5.1 Introduction

Quantum systems possess uniquely nonclassical properties, such as coherence and entanglement, which can be manipulated for applications including quantum computation [96, 60], quantum communication [57, 80], and quantum sensing [49, 106]. Designing controls that do this is a diverse and productive area of ongoing research [164, 147, 124, 95, 141, 52, 23, 62, 63, 139, 97, 165, 116]. However, these nonclassical properties also considerably modify the kinds of control strategies and mechanisms available to quantum systems.

One key example of the differences is the role of measurement. It is a given in classical control that one can measure the system and act upon it based on the information extracted about the system. However, for a quantum system measurement itself changes the state of the system and this has to be carefully accounted for in the design of many closed-loop control protocols [154, 155, 29, 58, 136, 56, 64]. Although measurement backaction is usually considered undesirable—an unwanted effect to be minimised—from another perspective measurement is an extra "control knob" unavailable in the classical context, which can be used to develop new control strategies for quantum dynamical systems [8, 140]. In particular, adaptive measurements have been used to improve phase estimation [153], in quantum state preparation [114], and to enhance the precision of quantum

measurements [61].

Here, we explore how this uniquely quantum knob can be used to control the dynamics of a chaotic system. Classically, controlling these systems is both a significant and non-trivial problem. In some situations it is desirable to induce chaotic dynamics, as in the case of embedding data into chaotic signals for secure transmission of information [76]. However, in other cases the task is to lock the system to stable orbits, as when aiming to regularise the behaviour of cardiac rhythms [40] or improve energy harvesting in cantilever devices [38, 75]. In many of these stabilisation problems, feedback methods are used to turn an originally unstable orbit embedded in the chaotic attractor into a regular one [101, 109]. In this work, we show that transitioning at will from chaos to regularity is possible by using a real-time adaptive measurement protocol. In particular, our protocol combines the tunability of quantum measurement backaction on the quantum state with the underlying geometry of the classical dynamical system. This opens up regimes of control not available to open-loop control schemes.

This quantum control strategy cannot be borrowed straightforwardly from an analogous classical problem, not only because of the aforementioned peculiarities of quantum measurement, but also due to subtleties associated with identifying emergent quantum chaotic orbits. In a closed quantum system, coherent interference effects cause a breakdown in the correspondence principle such that chaotic classical dynamics do not emerge when the underlying quantum model is taken to the macroscopic limit [35]. However, in *open* quantum systems, decoherence destroys such quantum interference effects [166], allowing emergent chaotic dynamics in the classical limit [100, 28, 166, 131, 55, 103, 18, 17]. In particular, by considering stochastic unravelings of an open quantum system, which are physically associated with making particular continuous measurements on the system [156, 158, 117], we can observe chaos in the conditional system dynamics [117, 131]. The stochastic unravelings allow chaos to be identified and quantified with the quantum Lyapunov exponent [6, 99, 54, 68, 108] and also provide the necessary ingredient for a closed-loop feedback control scheme.

In the previous chapter we showed that the behaviour of the system can be chaotic or not depending on the initial (and fixed) choice of measurement, due to the interplay between the interference effects induced by the nonlinear dynamics and the effectiveness of the measurement in destroying them. This sensitivity to measurement choice was shown to be absent both in the macroscopic limit, where the effects of quantum measurement are naturally expected to disappear, and in a highly-quantum regime, where noise dominates and measurement choice becomes irrelevant. Although the system behaves chaotically in the former case, as in the classical analog, in the latter, chaos is suppressed by quantum effects. As the main outcome of the control protocol presented here, we are able to show that a judicious real-time choice of measurement can induce chaotic behaviour deeper in the quantum regime, effectively pushing the quantum-classical boundary further towards the microscopic domain.

## 5.2 Adaptive measurement protocol for controlling chaos

To illustrate our adaptive protocol, we once again consider the driven-damped Duffing oscillator [30] given in Eq. 4.1. The continuous measurement approach described in Sec. 4.3 naturally sets the scene for our main result: the design of a protocol to control chaos by using a tunable, and experimentally accessible, parameter. The parameter in question, the LO phase $\phi$, is intrinsically linked to the measurement backaction, making our control

mechanism fundamentally quantum in nature.

The scheme we consider is shown in Fig. 5.1. The continuous monitoring of the system gives a measurement signal, $I(t)$, that allows for a real-time estimate of the quantum state. In possession of this information, one can then design a feedback action to influence the system. Motivated by the effect that measurement has on the system dynamics [33], here we propose to adaptively change the phase $\phi$ in real time, with the intent to control the Lyapunov exponent of the system.

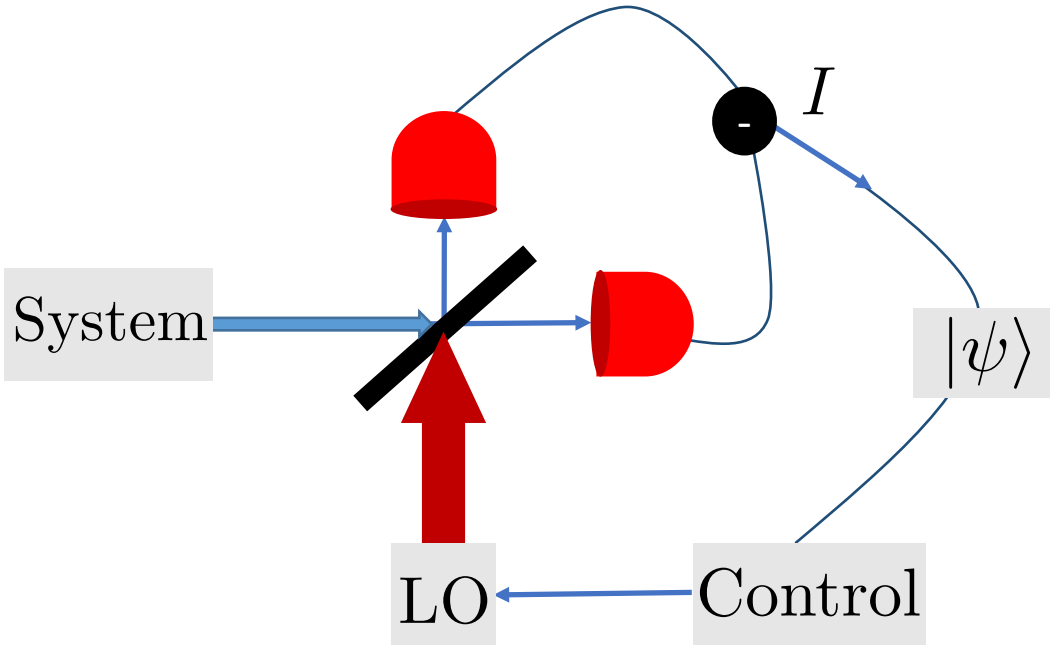


**Figure 5.1:** Adaptive measurement scheme in a quantum optics setup. The state-dependent controller chooses the LO phase $\phi$ at each time step in order to change the measurement backaction applied to the system, which changes the evolution as desired.

The design of an effective control strategy relies on first understanding how the feedback action affects the system. For that, we recall a fact observed in the previous chapter: The stretches and foldings induced by the chaotic dynamics generate interference fringes in the Wigner function of the system (see top panel of Fig. 5.2), and these lead to the suppression of chaos in the quantum regime. Since these interference fringes are associated with quantum coherence, destroying them shifts the dynamics towards the classical chaotic behaviour. Therefore, in order to enhance (suppress) chaos, our state-dependent controller chooses the LO phase $\phi$ such that the measurement destroys the interference fringes in the state's Wigner function at the fastest (slowest) possible rate. More precisely, this rate of fringe destruction is determined by the direction of the interference fringes in phase space ($\theta_f$) relative to the axis of measurement (determined solely by $\phi$), with fast destruction rates occurring when these axes are aligned. Our control protocol then consists of estimating the fringe structure in real time and picking a $\phi(t)$ that would maximise the control objective.

Automating the process of determining the direction of the interference fringes in the Wigner function can be done by examining the probability distributions for different

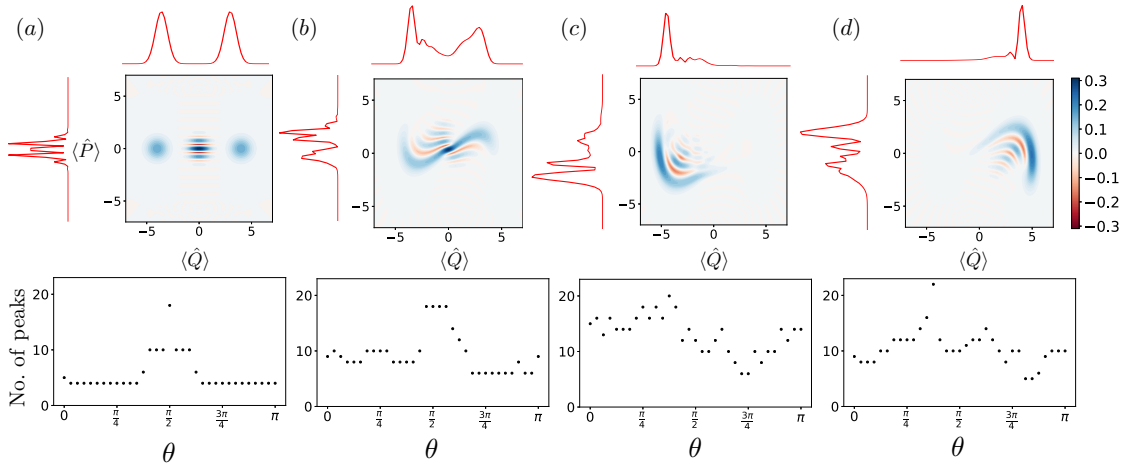


**Figure 5.2:** Wigner functions and corresponding phase quadrature projections $X_{\theta=0}$ and $X_{\theta=\pi/2}$ for (a) a Schrödinger cat state $|\psi_{cat}\rangle \propto |\alpha\rangle + |-\alpha\rangle$ and (b)-(d) three snap shots typically seen in the evolution of the quantum Duffing oscillator. Here $\theta = 0$ (top) and $\theta = \pi/2$ (side) are the only projections plotted. The number of peaks in the probability distributions is plotted as a function of quadrature $\theta$ for 32 different angles. The maximum in the number of peaks corresponds to the direction perpendicular to the interference fringes ($\theta_{\max} - \theta_f = \pi/2$). Note that the number of peaks in the bottom plots does not equal the number of peaks seen in the probability distributions. This is a numerical noise associated with counting every turning point and does not affect the outcome of the search.

quadrature measurements:

$$P_{X_\theta} \quad = \quad |\langle X_\theta|\psi\rangle|^2, \tag{5.1}$$

where $|X_\theta\rangle$ is an eigenstate of the quadrature operator $\hat{X}_\theta$. To understand how this can be used to estimate the fringe structure, let us look at the particular case of the Schrödinger cat state $|\psi_{cat}\rangle \propto |\alpha\rangle + |-\alpha\rangle$ shown in Fig. 5.2(a). Projection onto the $\hat{X}_0$ quadrature is given by the top red plot in Fig. 5.2(a). Here, a measurement of $\hat{X}_0$ distinguishes between the two coherent states, resulting in two peaks. In contrast, the projection onto the $\hat{X}_{\pi/2}$ quadrature (the red plot to the left of the Wigner function plot) reveals the overlap of the two coherent states, resulting in interference fringes and a large number of peaks. As shown directly below the Wigner function plot, looking at the number of peaks as a function of projection angle $\theta$ reveals that the peak distribution is narrowly centred around $\theta = \pi/2$ [the $\langle\hat{P}\rangle$ axis], which is perpendicular to the interference fringe axis. This shows that the angle that maximises the number of peaks ($\theta_{\max}$) is a good indicator of the direction that is perpendicular to the fringes in the Wigner function.

In the actual quantum Duffing oscillator, the nonlinear dynamics lead to interference fringe patterns with more complexity than those of a Schrödinger cat state. Examples of the Wigner functions for typical evolved states that arise during this evolution are plotted in Figs. 5.2(b)-5.2(d). Although more complicated, these Wigner functions still present a reasonably-well-defined direction in the fringe structure, which can be determined by finding the angle that leads to the maximum number of peaks in $P_{X_\theta}$, as explained above.

In summary, our protocol consists of the following steps:

(i) Starting from a given $|\psi(t)\rangle$, calculate $P_{X_\theta}$ for various $\theta$;

(ii) Count the number of peaks for each $P_{X_\theta}$ and find $\theta_{\max}$;

(iii) To maximize (minimize) the Lyapunov exponent, choose $\phi(t) = \theta_f = \theta_{\max} - \pi/2$ ($\phi(t) = \theta_{\max}$);

(iv) Use the value of $\phi(t)$ from (iii) in Eq. (3.61) to calculate the new state $|\psi(t+dt)\rangle$;

(v) Repeat steps (i) to (iv).

Full details of the numerical implementation of these steps are given in the following section.

## 5.3 Methods

We numerically simulated the SSE Eq. (3.61) on a finite subspace of $N$ energy eigenstates of the harmonic oscillator using the software package XMDS2 [24]. That is, we write the conditional state as $|\psi\rangle = \sum_{n=0}^{N-1} C_n(t)|n\rangle$ and numerically solve for the dynamics of the coefficients $C_n(t)$, governed by the set of Stratonovich stochastic differential equations

$$\begin{aligned}
\mathrm{d}C_n = -i\Big[&\tfrac{\beta^2}{4}\sqrt{(n+1)(n+2)(n+3)(n+4)}C_{n+4} + \sqrt{(n+1)(n+2)}\left(\tfrac{\beta^2}{4}(4n+6) - \tfrac{1}{2}(1+i\Gamma)\right)C_{n+2} \\
&- \tfrac{g}{\sqrt{2}\beta}\cos(\Omega t)\sqrt{n+1}C_{n+1} + \tfrac{\beta^2}{4}(6n^2+6n+3)C_n - \tfrac{g}{\sqrt{2}\beta}\cos(\Omega t)\sqrt{n}C_{n-1} \\
&+ \sqrt{n(n-1)}\left(\tfrac{\beta^2}{4}(4n-2) - \tfrac{1}{2}(1-i\Gamma)\right)C_{n-2} + \tfrac{\beta^2}{4}\sqrt{n(n-1)(n-2)(n-3)}C_{n-4}\Big]\mathrm{d}t \\
&- n\Gamma C_n \mathrm{d}t - e^{2i\phi}\Gamma\sqrt{(n+1)(n+1)}C_{n+2}\mathrm{d}t + 2\Gamma\left(\langle\hat{a}^\dagger\rangle + \langle\hat{a}\rangle\, e^{2i\phi}\right)\sqrt{n+1}C_{n+1}\mathrm{d}t \\
&+ \sqrt{2\Gamma}\sqrt{n+1}C_{n+1}\, e^{i\phi}\circ \mathrm{d}W, \quad (5.2)
\end{aligned}$$

where $\langle\hat{a}\rangle = \sum_{n=0}^{N-2}\sqrt{n+1}C_n^* C_{n+1}$ and $C_n = 0$ for all $n \geq N$. For our simulations, we use $N = 64$ basis states, a large enough number such that $|C_{N-4}|^2 + |C_{N-3}|^2 + |C_{N-2}|^2 + |C_{N-1}|^2 < 10^{-4}$ at all times, whilst still small enough to be numerically tractable.

For the adaptive protocol, we calculate the probability distribution for a number of quadratures, this is given by

$$\begin{aligned}
P_{X_\phi} &= |\langle X_\phi|\psi\rangle|^2 \\
&= \left|\sum_n C_n \psi_n(x) e^{-in\phi}\right|^2, \quad (5.3)
\end{aligned}$$

where $\psi_n(x)$ are the Hermite-Gauss functions:

$$\psi_n(x) = (2^n n!\sqrt{\pi})^{-1/2} e^{-x^2/2}\, \mathrm{H}_n(x), \quad (5.4)$$

where $\mathrm{H}_n(x)$ are Hermite polynomials.

We use a grid-based search algorithm to determine the optimum measurement phase for each time step. To do this, we use a finite difference method to calculate the derivative of the probability distribution Eq. (5.1) for an equidistant grid of LO angles $\phi \in [0, \pi]$, allowing the number of peaks in the distribution to be calculated. The angle $\theta_{\max}$ corresponding to the maximum number of peaks gives an axis perpendicular to the interference fringes ($\theta_f + \pi/2$). To enhance chaos we adjust the LO phase to $\phi = \theta_f$ (parallel to fringes), whereas to suppress chaos we choose $\phi = \theta_f + \pi/2$ (perpendicular to fringes) for

the next integration step of Eq. (5.2). In order for this grid-based search method to be effective, the grid of LO angles used needs to be of sufficiently high resolution. We found that when suppressing chaos ($\phi = \theta_f + \pi/2$), a grid of 32 angles was required, whereas for enhancing chaos ($\phi = \theta_f$) a coarser grid of 8 angles was sufficient.

We quantify the degree of chaos in our system by computing the quantum Lyapunov exponent as in the previous chapter, which is based on an adaptation of the usual classical procedure [159]. For our numerical calculations, one of the trajectories is periodically reset towards the other one to remain within the linear regime and $\log(d_t/d_0)$, calculated before every reset, is averaged over time. The perturbed trajectory after the reset is a displaced version of the trajectory of interest. The displacement is given by the initial distance $d_0$ in phase space, in the direction of expansion. The perturbed trajectory becomes $|\psi_2\rangle = D(\alpha)|\psi_1\rangle$, where $D(\alpha)$ is the displacement operator and $\alpha = d_0((\langle\hat{Q}_2\rangle + i\langle\hat{P}_2\rangle) - (\langle\hat{Q}_1\rangle + i\langle\hat{P}_1\rangle))/(d_t\beta)$ is the displacement in the direction of expansion.

The simulations are run over $10,000$ cycles of the driving term ($t = 10^4/\Omega$) for both the adaptive and the fixed LO cases, and the final Lyapunov exponent is averaged over multiple realizations (10 runs) of the stochastic noise.

## 5.4 Results

We implemented the adaptive measurement scheme described in Sec. 5.2 for a range of scaling parameters $\beta$ (spanning the transition from the quantum regime to the classical regime) and two distinguishable strategies: maximisation and minimisation of the Lyapunov exponent ($\lambda$). The results are shown in Fig. 5.3 for both cases, specifically, where the LO phase is set to always measure along an axis parallel ($\phi = \theta_f$, blue line, square points) or perpendicular ($\phi = \theta_f + \pi/2$, green line, crosses) to the interference fringes. To assess the effectiveness of our adaptive protocol, we compare with the best nonadaptive strategy by displaying the curves that maximise (black line, triangles) and minimise (red line, circles) $\lambda$ for a *fixed* LO phase.

The adaptive maximisation strategy leads to Lyapunov exponents that are always larger than the best fixed-angle scenario ($\phi = 0$). By destroying coherent interference effects and localising the state faster, the adaptive case allows the quantum system to track the classical chaotic dynamics more closely, increasing $\lambda$. Further evidence of this is provided by looking at the dynamical evolution of the Wigner function (see Fig. 5.4, top), showing states that are more localised and possess less interference, and are therefore more classical in nature. The opposite adaptive strategy, the one designed to suppress chaos, also works effectively, giving negative Lyapunov exponents for all values of $\beta$. In this case, the adaptive choice of monitoring angle leads to the preservation of quantum interference effects and therefore to highly nonclassical states with a large spread in phase space, as seen in the Wigner functions of Fig. 5.4 (bottom).

Interestingly, the adaptive $\lambda$-maximisation scheme gives positive Lyapunov exponents for much larger values of $\beta$ (up to 0.5), showing that the adaptive protocol pushes the emergence of chaos deep into the quantum regime—and much further than what is possible with a fixed LO phase. This is remarkable behaviour given that quantum noise is expected to dominate the dynamics at these large values of $\beta$, and so one would think that the choice of measurement is irrelevant. This is clearly the case for the fixed measurement (see Fig. 5.3), where the quantum Lyapunov exponent for all monitoring schemes other than $\lambda$-maximisation converge to roughly the same negative value, indicating regular dynamics. In stark contrast, our $\lambda$-maximisation protocol is able to sustain chaotic dynamics even

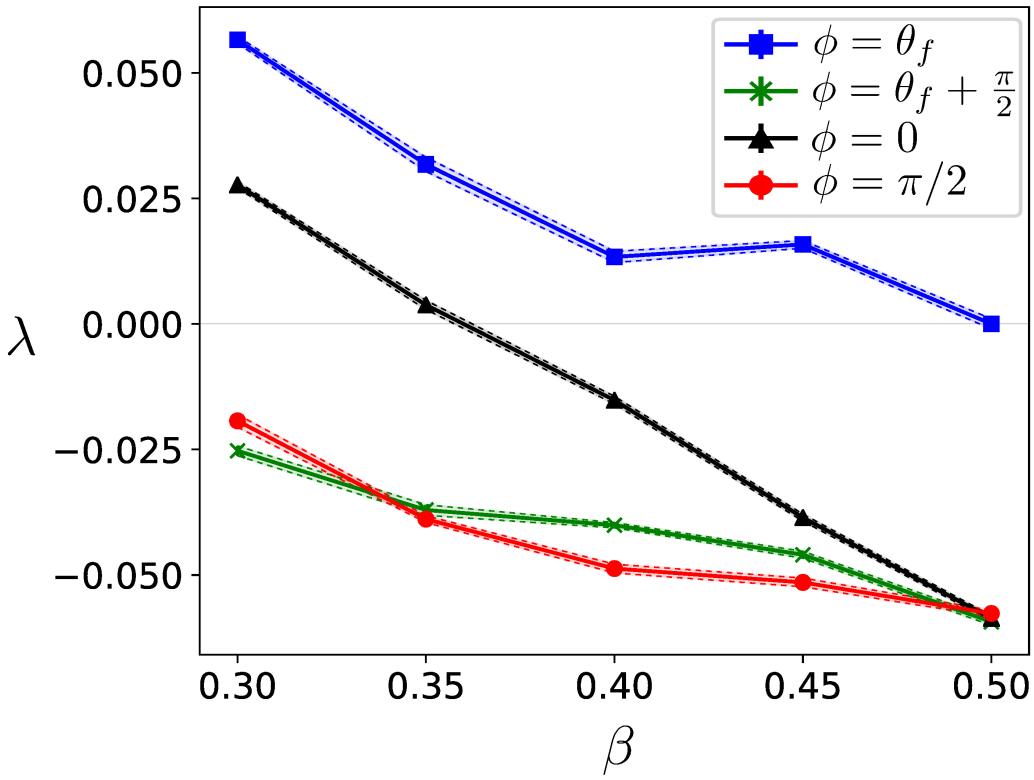


**Figure 5.3:** The quantum Lyapunov exponent ($\lambda$) as a function of $\beta$ for adaptive measurements ($\phi = \theta_f$, blue squares, and $\phi = \theta_f + \pi/2$, green crosses) and fixed LO measurements ($\phi = 0$, black triangles, and $\phi = \pi/2$, red circles). Here $\Gamma = 0.10$, $g = 0.3$ and $\Omega = 1$, and the classical system is chaotic with $\lambda_{cl} = 0.16$. Each point is averaged over 10 different noise realizations and the shaded area within the dashed lines signifies twice the standard error.

at this scale.

Although our adaptive $\lambda$-maximisation scheme can significantly enhance chaos, the adaptive $\lambda$-minimisation scheme does not provide significantly enhanced regularity over the fixed measurement. This is a consequence of using metric (5.1) to choose the measurement quadrature angle $\phi$ at each time point. The aim is to find the direction of interference fringes in the Wigner function, and choose a measurement angle parallel (perpendicular) to this direction in order to enhance (suppress) chaos. However, the metric (5.1) becomes less effective when the state is highly nonclassical and delocalised. This is shown clearly in the Wigner function plots of Fig. 5.4(b), in particular at time $\Omega t = 70$. In this case, the large degree of delocalisation means that there is no well-defined single direction of interference fringes. Consequently, in this regime the adaptive control does not provide a substantially improved performance over a fixed-angle measurement. When trying to suppress chaos by picking a measurement that has the least deleterious effect on quantum interferences, it is exactly this highly delocalised regime that is encouraged. Therefore, it is unsurprising that our adaptive measurement protocol provides little benefit over a fixed measurement angle, if the goal is to suppress chaos. In contrast, our metric is more effective when the Wigner function is localised and the fringe direction better defined [see Fig. 5.4(a) for $\Omega t = 70$]. This is the scenario arising from our strategy to enhance chaos: choosing measurements that destroy coherence and keep the state localised.

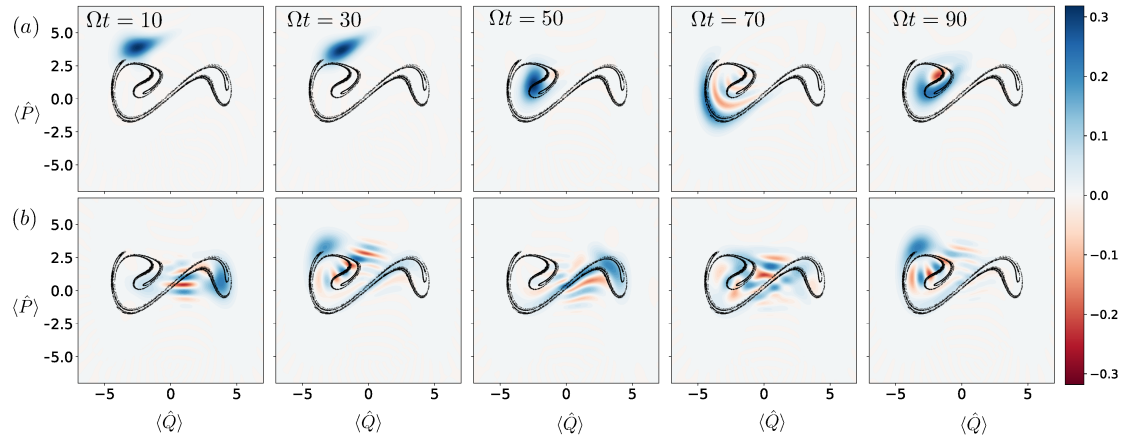


**Figure 5.4:** Snap shots of the Wigner function for the first 100 cycles of the driving for both adaptive measurements [(a) $\phi = \theta$, and (b) $\phi = \theta + \pi/2$]. The snap shots only show a single quantum trajectory (noise realisation); however, all trajectories have similar evolution to that depicted here. The corresponding Lyapunov exponents are (a) $\lambda = 0.057 \pm 0.001$ and (b) $\lambda = -0.025 \pm 0.001$.

## 5.5 Discussion

We briefly discuss the experimental prospects of realising both the driven-damped quantum Duffing oscillator and our adaptive measurement protocol. Superconducting circuits are excellent candidate systems, due to their flexible architecture, wide range of experimental parameters, and the existence of demonstrated continuous probing [149]. Specifically, superconducting circuits in a parallel circuit configuration (i.e., a rf-SQUID) could be used to experimentally realise a quantum Duffing oscillator [86, 113]. For the scheme proposed in Ref. [113], $\beta^2 = e^2/[3\hbar\omega C_p(1 - L_p/L_J)]$, where $\omega = 1/\sqrt{C_p L_p}$, $C_p$ is the capacitance of the Josephson junction in the circuit, $L_p^{-1} = L_J^{-1} - L_p^{-1}$ is the parallel inductance formed from the Josephson inductance $L_J$ and the geometric inductance $L_{pe}$, and $e$ is the charge of an electron. Using typical experimental parameters from Ref. [11], we estimate that $\beta \sim 0.4$ is currently achievable which, as shown in Fig. 5.3, is a regime ideally suited for observing measurement-dependent effects on the emergence of chaos.

Realising our scheme with ultracold atomic gases is another potential option. Ultracold atomic experiments have previously been used to experimentally investigate the emergence of chaos in the quantum kicked rotor [112, 31, 144]. A Bose-Einstein condensate (BEC) provides the high optical densities needed for real-time nondestructive imaging [150, 39]. A noninteracting BEC gives the single-particle behaviour required to realise the driven-damped quantum Duffing oscillator. A noninteracting gas can be achieved by using an extremely dilute sample or by extinguishing the interactions via a Feshbach resonance [87, 39]. The required double-well potential could be created by superimposing a Gaussian barrier on a harmonic potential:

$$\begin{aligned}\hat{V}_{\text{exp}} &= \frac{1}{2}m\omega_0^2\hat{x}^2 + Ae^{-\hat{x}^2/2\sigma^2} \\ &\approx \hbar\omega_0\left[\frac{1}{2}\left(1 - \frac{A}{m\omega_0^2\sigma^2}\right)\hat{Q}^2 + \frac{1}{4}\left(\frac{\hbar A}{2m^2\omega_0^3\sigma^4}\right)\hat{Q}^4\right].\end{aligned} \tag{5.5}$$

The choice of barrier height $A = 2m\omega_0^2\sigma^2$ realizes the needed potential [see Eq. (4.1)] with $\beta^2 = \hbar/(m\omega_0\sigma^2)$. There are a number of techniques for creating this potential, including

via an optical lattice [130] or spatial light modulation [45]. For the 780 nm transition of $^{85}$Rb, a barrier waist of $\sigma \sim 10\mu$m is easily achievable. For typical trapping frequencies $\omega_0 \in 2\pi \times [5, 100]$ Hz, this gives $\beta \sim 0.1 - 0.5$.

These simple estimates suggest that state-of-the-art experiments in both superconducting circuits and ultracold atomic gases are promising platforms for experimentally investigating the relationship between measurement and chaos, and are capable of observing chaotic dynamics deep within the quantum regime. Experimentally, one possible approach to infer the degree of chaos would be time series analysis [67, 146]. This requires acquisition of large data sets, which is possible in experiments, but computationally expensive for large-scale quantum simulations. Theoretically, it is much simpler to calculate Lyapunov exponents directly.

Although our initial investigations have revealed that this adaptive measurement scheme shows promise, our model did not include the effect of detection inefficiency. Detection inefficiency could affect both the emergence of chaotic dynamics and the effectiveness of our adaptive measurement protocol. For the quantum Duffing oscillator, numerical simulations have shown positive Lyapunov exponents with measurement efficiencies as low as 20% [113]. These Lyapunov exponents were also shown to be robust to small errors in the system parameters. Measurement efficiencies as high as 80% have been reported in recent superconducting circuit experiments [34]. Similar detection efficiencies are possible in BEC systems at the cost of introducing heating, the effects of which would require further investigation.

In addition to perfect detection efficiency, our model assumes that the underlying estimate of the system state used to effect feedback (through the choice of quadrature measurement angle) precisely corresponds to the underlying system state. Although conditional master equations are known to be robust to imperfections in such estimates, which arise due to imperfect estimates of the model parameters, technical noise sources, and time delays, relaxing this assumption through a system-filter separation would provide crucial detail needed for the experimental realisation of our adaptive measurement protocol [138].

This work has focused on the control of chaos with continuous measurement in a *single-particle* system. *Many-body* quantum chaos is a growing research field, due to its potential connections to random unitaries [37], information scrambling and holographic duality [85, 135, 88], nonequilibrium thermodynamics [94], and even quantum sensing [42]. Whether measurement can be used to meaningfully control chaos in many-body quantum systems is an intriguing question that warrants further investigation.

## 5.6 Conclusion

In this work we have shown that the degree of chaos in a quantum Duffing oscillator can be controlled by applying real-time state-dependent feedback via an adaptive measurement technique. The underlying mechanism for this control is the rate at which the measurement backaction destroys interference fringes in the state's Wigner function. By adaptively choosing measurements that are more (less) destructive, the dynamics more (less) closely resemble the corresponding classical trajectory, thereby enhancing (suppressing) chaos. Using this adaptive measurement technique, we have shown that the presence of chaos can be pushed further into the quantum regime. This regime is more easily accessible for certain experimental setups, potentially enabling new, detailed studies into the emergence of chaos in quantum systems.

# Part III

# Quantum Chaos in a Driven Top

# 6

# Chaos in a Continuously Monitored Quantum Driven top

Previously, our attention was focused on observing quantum chaos in a single-body quantum system interacting with an environment. Now that we are somewhat familiar with the role that measurement has to play in the emergence of chaos from a single-body quantum system, let us ask the question: Can we see a measurement dependence in a many-body quantum system? As mentioned in the previous chapter, the need to understand the measurement of many-body quantum chaos is motivated by the growing research that makes connections to many other areas of physics such as random unitaries [37], information scrambling and holographic duality [85, 135, 88], nonequilibrium thermodynamics [94], and quantum sensing [42]. In this chapter, we attempt to understand how continuous measurement plays a role in the emergence of chaos in a many-body system that is experimentally realisable with ultracold atoms: the quantum driven top. This is an interesting system to consider because, in contrast to the Duffing oscillator, the corresponding classical system for the driven top is a closed system with no dissipation. In this chapter we will investigate the continuous measurement of a quantum driven top. In the previous chapters, we saw that by considering an open system treatment of the Duffing oscillator, we were able to consolidate the dynamics of the quantum system with the classical system, allowing us to understand the emergence of chaos in the classical world. Unlike the Duffing oscillator, we start here with a system that is initially closed and by opening the quantum system to environmental interactions, we will consequently drive the system away from the chaotic system we wish to study. This is an important consideration, however, if we want to study the realistic observed dynamics of a continuously monitoring the quantum system. A fine balance comes between the benefits from opening the quantum system to observe the continuous dynamics and the effect this has on the degree of chaos present in the system. If the coupling to the environment is too strong, we will inevitably destroy the chaos that we wish to measure, but if the coupling is not strong enough, we will not be able to localise the quantum state in phase space and observe the dynamics that emerges from the classical chaos. We will be using the quantum driven top as our model system, where the top is continuously driven by a sinusoidal driving term. In the literature, the

system that is most regularly studied is the kicked top, where the top is kicked by delta kicks equally spaced in time [46, 19, 83, 53, 70, 90]. Perhaps because it is easily realised experimentally in many different experimental set ups from a collection of two level atoms, to a two mode BEC experiment [144], or even in the higher spin of a single atom [90]. All of these systems obey the same SU(2) physics and so all have the potential to realise the driven/kicked top. Recently the parameter sensitivity in the kicked top has been theoretically demonstrated to be useful for sensitivity in precision measurements [42]. This work showed that the amount of information that could be extracted about a parameter of the system (ie. the Fisher information) was increased when the Hamiltonian was that of a kicked top. The consequences of the presence of chaos in digital quantum simulations has been explored [128]. More closely related to the work presented in this thesis, the measurement of chaotic systems has been investigated by others using the Kicked top [163, 92]. However, what these works have not considered, and what is a large part of this thesis, is exactly what the effect of the measurement is on the emergence of chaos from the quantum regime, and in this chapter we tackle this question for the driven top as well. Is there some general effect that can be seen for different chaotic systems or is it entirely dependent on the system in question?

The driven top shares the same chaotic features as the kicked top and has recently been experimentally realised in an ultra-cold atomic experiment [144]. Since we have already considered a periodically driven system with the Duffing oscillator, we will also consider the periodically driven version of the top. The work in this thesis follows closely the experimental realisation of a driven top given in [144] and so we will be looking at the same system with the same parameters used in the paper.

## 6.1 Quantum Driven Top as a Driven Bose Hubbard Dimer

The experimental realisation of the quantum driven top can be done in a spinor Bose Einstein condensate that is driven by an external field. The Hamiltonian for this system is given by the Bose Hubbard Hamiltonian that describes bosonic atoms in a lattice potential. The following derivation comes from the paper by Xie *et al.* and the thesis by Tomkovič [160, 145].

### 6.1.1 Undriven Bose Hubbard Dimer

The general Hamiltonian for the bosonic atoms is given by

$$\hat{H} = \hat{H}_0 + \hat{H}_{coupl} + \hat{H}_{MF} + \hat{H}_{inter}, \tag{6.1}$$

where $\hat{H}_0$ describes the kinetic energy and trapping potential for the atoms

$$\hat{H}_0 = \sum_{i=1,2} \int \mathrm{d}^3 r \hat{\psi}_i^\dagger(r) \left( \frac{-\hbar^2}{2m} \nabla^2 + V(r) \right) \hat{\psi}_i(r). \tag{6.2}$$

$\hat{H}_{coupl}$ is the coupling term that describes the hopping between the two modes,

$$\hat{H}_{coupl} = \frac{-\hbar\Omega_R}{2} \int \mathrm{d}^3 r \left( \hat{\psi}_1^\dagger(r)\hat{\psi}_2(r)e^{i\Delta t} + \hat{\psi}_2^\dagger(r)\hat{\psi}_1(r)e^{-i\Delta t} \right), \tag{6.3}$$

in rotating frame approximation. $\hat{H}_{MF}$ describes the self interactions between atoms in the same mode.

$$\hat{H}_{MF} = \sum_{i=1,2} \frac{4\pi\hbar^2 a_{ii}}{2m} \int \mathrm{d}^3 r \hat{\psi}_i^\dagger(r)\hat{\psi}_i^\dagger(r)\hat{\psi}_i(r)\hat{\psi}_i(r), \tag{6.4}$$

where $a_{ii}$ is the intra-species scattering length. $\hat{H}_{inter}$ describes the collision of two particles in different spin states.

$$\hat{H}_{inter} = \frac{4\pi\hbar^2 a_{12}}{m} \int \mathrm{d}^3 r \hat{\psi}_1^\dagger(r)\hat{\psi}_2^\dagger(r)\hat{\psi}_1(r)\hat{\psi}_2(r), \tag{6.5}$$

where $a_{12}$ is the inter-species scattering length.

### Two mode model

We now move to a two mode model for this system:

$$\hat{\psi}_i = \Phi_0 \hat{a}_i, \tag{6.6}$$

where $\hat{a}_i^\dagger$ and $\hat{a}_i$ are the creation and annihilation operators for each mode and $\Phi_0$ is a scalar mode function. $\Phi_0$ is assumed to be equal for both spin species which us only valid in the miscible regime and is a good approximation if the trapping is very tight. Now the Hamiltonian terms become

$$\begin{aligned}
\hat{H}_0 &= E(\hat{a}_1^\dagger\hat{a}_1 + \hat{a}_2^\dagger\hat{a}_2) \\
\hat{H}_{coupl} &= -\frac{\Omega}{2}\left(\hat{a}_1^\dagger\hat{a}_2 e^{i\Delta t} + \hat{a}_2^\dagger\hat{a}_1 e^{-i\Delta t}\right) \\
\hat{H}_{MF} &= \chi_{11}\hat{a}_1^\dagger\hat{a}_1^\dagger\hat{a}_1\hat{a}_1 + \chi_{22}\hat{a}_2^\dagger\hat{a}_2^\dagger\hat{a}_2\hat{a}_2 \\
\hat{H}_{inter} &= 2\chi_{12}\hat{a}_1^\dagger\hat{a}_2^\dagger\hat{a}_1\hat{a}_2,
\end{aligned} \tag{6.7}$$

with

$$\begin{aligned}
E &= \int \mathrm{d}^3 r \Phi_0^* \left(-\frac{\hbar^2}{2m}\nabla^2 + V(r)\right)\Phi_0 \\
\chi_{ij} &= \frac{4\pi\hbar^2 a_{ij}}{2m}\int \mathrm{d}^3 r |\Phi_0|^4 \\
\Omega &= \hbar\Omega_R \int \mathrm{d}^3 r \Phi_0^*\Phi_0
\end{aligned} \tag{6.8}$$

Using the Jordan-Schwinger decomposition from Eqs. 2.47, we now arrive at a Hamiltonian that is a lot simpler, given in terms of the angular momentum operators

$$\hat{H} = \chi\hat{J}_z^2 - \Omega\hat{J}_x + \delta\hat{J}_z \tag{6.9}$$

with

$$\begin{aligned}
\delta &= \Delta + (2J-1)(\chi_{22} - \chi_{11}) \\
\chi &= \chi_{11} + \chi_{22} - 2\chi_{12} \\
&= \frac{1}{2}(g_{11} + g_{22} - 2g_{12})\int \mathrm{d}^3 r |\Phi_0|^4
\end{aligned} \tag{6.10}$$

where $g_{ij} = 4\pi\hbar^2 a_{ij}/m$. The rescaled equations are then

$$\tilde{\chi} = \frac{\chi}{2\pi\hbar} \tag{6.11}$$

$$\tilde{\Omega} = \frac{\Omega}{2\pi\hbar} \tag{6.12}$$

$$\tilde{\delta} = \frac{\delta}{2\pi\hbar} \tag{6.13}$$

$$\hat{\mathcal{J}}_i = \frac{2}{N}\hat{J}_i \tag{6.14}$$

$$\hat{H} = \frac{\Lambda}{2}\hat{\mathcal{J}}_z^2 - \hat{\mathcal{J}}_x + \varepsilon\hat{\mathcal{J}}_z. \tag{6.15}$$

where $\Lambda = \tilde{\chi}N/\tilde{\Omega}$ and $\varepsilon = \tilde{\delta}/\tilde{\Omega}$. The dimensionless quantities are $\hbar_{eff} = 2/N$, $\tilde{\omega} = \omega/2\pi\tilde{\Omega}$ and $\tilde{t} = 2\pi\tilde{\Omega}t$. For this system the effective scaling parameter that allows us to go from classical to quantum is the total spin $\hbar_{eff} = 2/N = 1/j$ (ie. the total number of bosonic atoms in the two mode system).

What does the evolution of the undriven Hamiltonian given in Eq. 6.15 look like? This system belongs to the SU(2) group, and the states of the system lie on the surface of the sphere. Let us break down the Hamiltonian terms and what their action is on the sphere. The evolution of the closed system is given by a unitary operation $\psi(t) = \hat{U}\psi(0)$ which will be the exponential operation of the operators. If we just look at $\hat{H} = \frac{\Lambda}{2}\hat{\mathcal{J}}_z^2$, this is just one-axis twisting [71], which, when applied to a CSS leads to a shearing of the state along the $J_z$ direction. The $\hat{H} = \varepsilon\hat{\mathcal{J}}_z$ term is simply a precession about the $J_z$ axis, rotating a state along that axis. The classical orbits that result from the Hamiltonian terms are shown in Fig. 6.1. The classical dynamics comes from a mean field approximation (details in section 6.3.1) for different initial conditions on the phase space of the SU(2) system (see section 2.4.2). The undriven Hamiltonian has been used in the investigation of precision measurements and non-classical state generation [132].

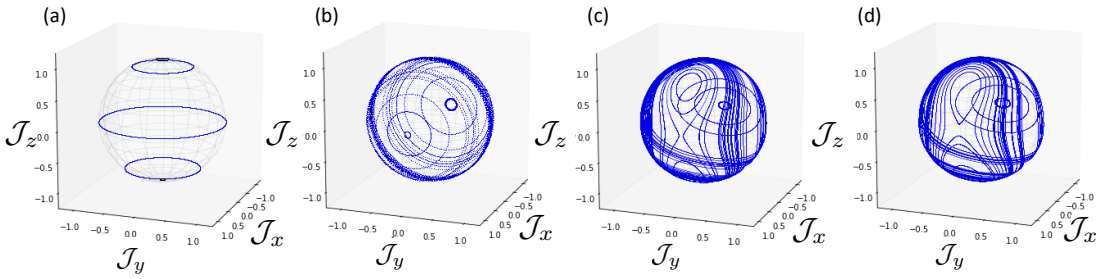


**Figure 6.1:** Classical orbits for different initial conditions for the undriven top. (a) shows the orbits for $\hat{H} = \frac{\Lambda}{2}\hat{\mathcal{J}}_z^2$. (b) shows the orbits for $\hat{H} = \hat{\mathcal{J}}_x$, which gives a simple precession around the $J_x$ axis. (c) shows the orbits for $\hat{H} = \frac{\Lambda}{2}\hat{\mathcal{J}}_z^2 - \hat{\mathcal{J}}_x$ and (d) shows the desymmetrised orbits for $\hat{H} = \frac{\Lambda}{2}\hat{\mathcal{J}}_z^2 - \hat{\mathcal{J}}_x + \varepsilon\hat{\mathcal{J}}_z$.

## 6.2 Quantum Driven Top

Let us now consider the driven version of Eq. 6.15 which is given by

$$\hat{H}_{driven} = \hat{H}_{undriven} - A\sin(\omega_D[t + t_0])\hat{\mathcal{J}}_x, \tag{6.16}$$

where $A$ and $\omega_D$ is the dimensionless strength and frequency of the driving respectively. The total Hamiltonian for the quantum driven top is then given by

$$\hat{H} = \frac{\Lambda}{2}\hat{\mathcal{J}}_z^2 - \Omega_D(t)\hat{\mathcal{J}}_x + \varepsilon\hat{\mathcal{J}}_z, \tag{6.17}$$

where we have the dimensionless term $\Omega_D(t) = 1 + A\sin(\omega_D[t + t_0])$ (we will omit squiggles in further references to dimensionless parameters). The time dependent term $\hat{H} = \Omega_D(t)\hat{\mathcal{J}}_x$ is also a precession about the $J_x$ axis which rotates the state about that axis. The time dependent driving of this term is what makes this system chaotic for certain choices of parameters.

## 6.3 Equations of Motion for Closed System

The equations of motion for the closed system are found using the Heisenberg equations of motion for the observables $\langle\hat{J}_i\rangle$.

$$\frac{\mathrm{d}\langle\hat{J}_i\rangle}{\mathrm{d}t} = \frac{-i}{\hbar}\langle[\hat{J}_i, \hat{H}]\rangle, \tag{6.18}$$

where we have an effective $\hbar_{eff} = 2/N = 1/j$. For the quantum system, we will explicitly refer to the dimensionless angular momentum operators in the form $\hat{\mathcal{J}}_i = \hat{J}_i/j$ from here on and we will refer to the observables in the mean field limit as $\langle\hat{\mathcal{J}}_x\rangle = \mathcal{J}_i$. Substituting in Eq. 6.17 for the Hamiltonian:

$$\begin{aligned}
\frac{\mathrm{d}\hat{J}_x}{\mathrm{d}t} &= -ij\left[\hat{J}_x, \frac{\Lambda}{2}\frac{\hat{J}_z^2}{j^2} - \Omega(t)\frac{\hat{J}_x}{j} + \varepsilon\frac{\hat{J}_z}{j}\right] \\
\frac{\mathrm{d}\hat{J}_y}{\mathrm{d}t} &= -ij\left[\hat{J}_y, \frac{\Lambda}{2}\frac{\hat{J}_z^2}{j^2} - \Omega(t)\frac{\hat{J}_x}{j} + \varepsilon\frac{\hat{J}_z}{j}\right] \\
\frac{\mathrm{d}\hat{J}_z}{\mathrm{d}t} &= -ij\left[\hat{J}_z, \frac{\Lambda}{2}\frac{\hat{J}_z^2}{j^2} - \Omega(t)\frac{\hat{J}_x}{j} + \varepsilon\frac{\hat{J}_z}{j}\right]
\end{aligned} \tag{6.19}$$

which gives the following equations of motion for the expectation values

$$\begin{aligned}
\frac{\mathrm{d}\langle\hat{J}_x\rangle}{\mathrm{d}t} &= -\frac{\Lambda}{2j}(\langle\hat{J}_y\hat{J}_z\rangle + \langle\hat{J}_z\hat{J}_y\rangle) - \varepsilon\langle\hat{J}_y\rangle \\
\frac{\mathrm{d}\langle\hat{J}_y\rangle}{\mathrm{d}t} &= \frac{\Lambda}{2j}(\langle\hat{J}_x\hat{J}_z\rangle + \langle\hat{J}_z\hat{J}_x\rangle) + \Omega(t)\langle\hat{J}_z\rangle + \varepsilon\langle\hat{J}_x\rangle \\
\frac{\mathrm{d}\langle\hat{J}_z\rangle}{\mathrm{d}t} &= -\Omega(t)\langle\hat{J}_y\rangle
\end{aligned} \tag{6.20}$$

### 6.3.1 Coherent Spin States

To initialise our system, we start with the classical state of the system analogously to the choice of the Glauber coherent state for the Duffing oscillator. We initialise with a coherent spin state given in Eq. 2.57 with the three parameters ($\theta$, $\phi$, $j$). The appropriate basis states is the Dicke states described in chapter 2.

### Semiclassical Limit for the Driven Top

We can investigate what happens when the system approaches the classical limit by taking $j \to \infty$ and looking at the mean field expectation values $(\mathcal{J}_x, \mathcal{J}_y, \mathcal{J}_z) = (\langle \hat{\mathcal{J}}_x \rangle, \langle \hat{\mathcal{J}}_y \rangle, \langle \hat{\mathcal{J}}_z \rangle)$. Recall that the commutator is given by $[\hat{\mathcal{J}}_i, \hat{\mathcal{J}}_j] = i\epsilon_{ijk}\hat{\mathcal{J}}_k/j$. In the semiclassical limit we can also make the approximation $\langle \hat{J}_i \hat{J}_j \rangle \approx \langle \hat{J}_i \rangle \langle \hat{J}_j \rangle$ so that the equations of motion become

$$\begin{aligned} \dot{\mathcal{J}}_x &= \frac{\Lambda}{2}(-2\mathcal{J}_y\mathcal{J}_z) - \varepsilon\mathcal{J}_y \\ \dot{\mathcal{J}}_y &= \frac{\Lambda}{2}(2\mathcal{J}_x\mathcal{J}_z) + \Omega(t)\mathcal{J}_z + \varepsilon\mathcal{J}_x \\ \dot{\mathcal{J}}_z &= -\Omega(t)\mathcal{J}_y \end{aligned} \tag{6.21}$$

Without driving ($A = 0$) the system is regular (see Fig. 6.2). However for $A > 0$, regions of chaotic behaviour start to emerge in the phase space (see Fig. 6.3).

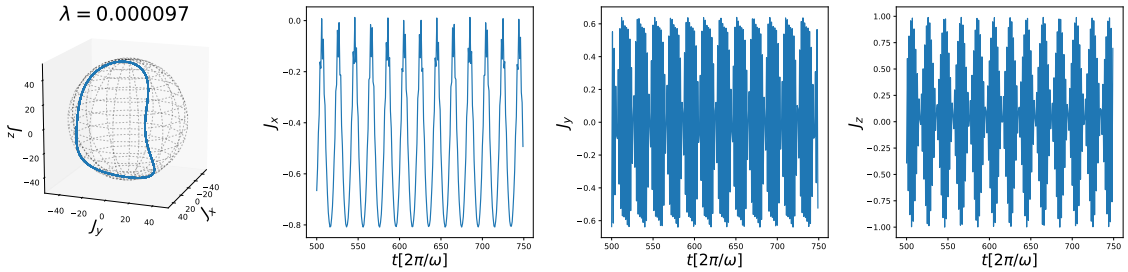


**Figure 6.2:** Poincaré section and time evolution of the physical observables for parameters $\Lambda = 1.5$, $\epsilon = -0.07$, $\omega_D = 1.6$ with driving turned off ($A = 0$). With no driving, the system behaves in a regular fashion shown by the periodic motion and the Lyapunov exponent $\lambda \approx 0$.

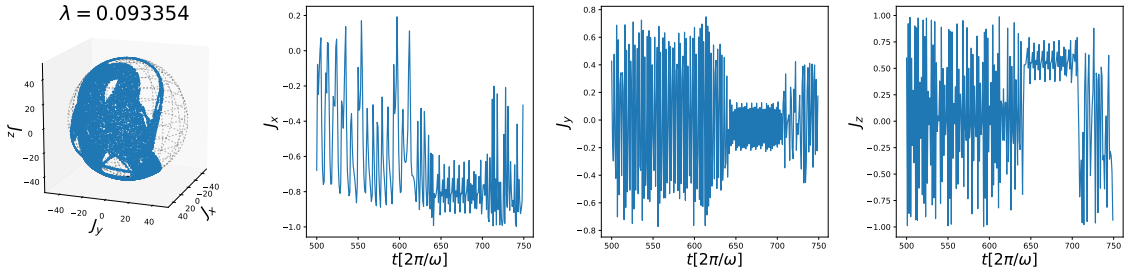


**Figure 6.3:** Poincaré section and time evolution of the physical observables for parameters $\Lambda = 1.5$, $\epsilon = -0.07$, $\omega_D = 1.6$ with driving turned on ($A = 0.07$). For this set of parameters, the dynamics are chaotic with a non zero positive Lyapunov exponent $\lambda = 0.093$.

### Regions of interest in the phase space

By scanning the initial choice of the parameters $(\theta, \phi)$, the emergence of different dynamics becomes apparent. Generally, as the strength of the driving is increased, the presence of chaos in the phase space will increase. For the semiclassical dynamics, we have chosen to look at one set of parameters for the system, ($\Lambda = 1.5$, $\epsilon = -0.07$, $\omega_D = 1.6$) that has also been investigated in [144] for different values of the driving. Scanning through

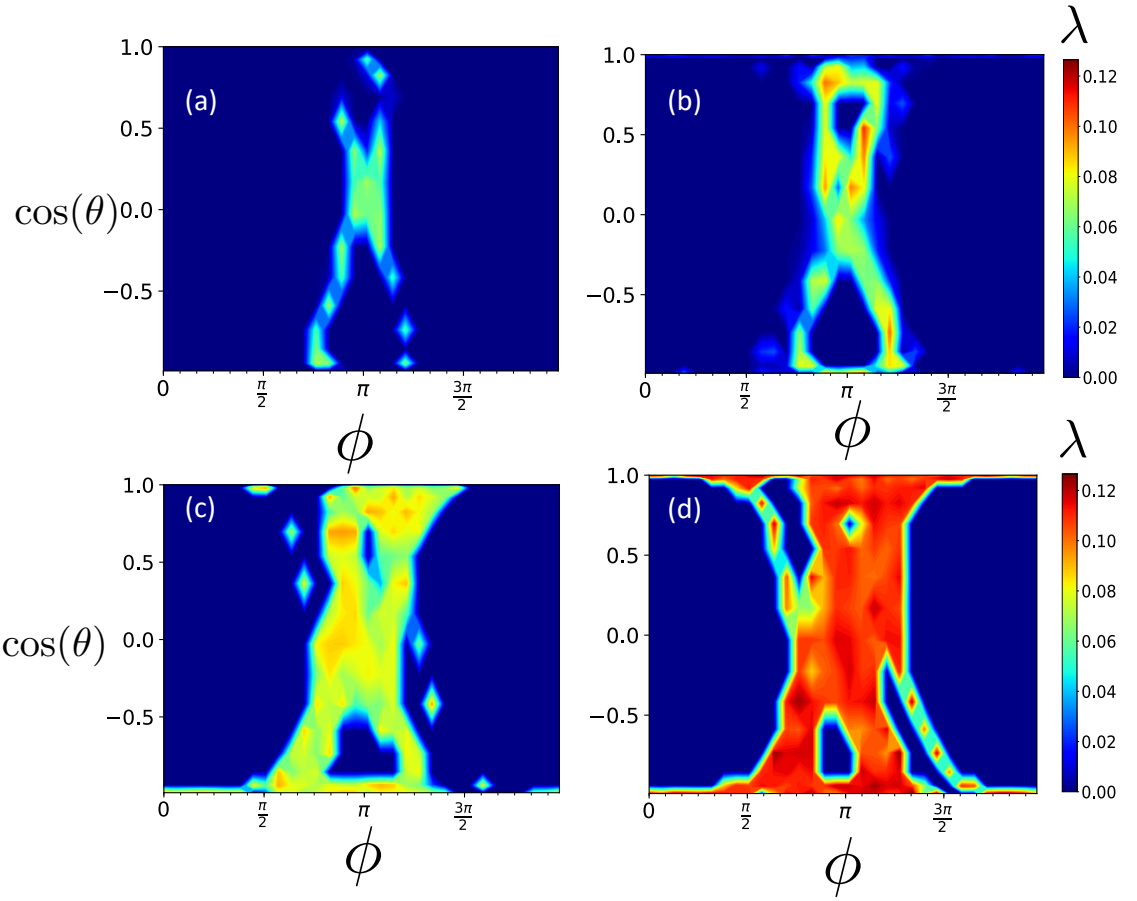


**Figure 6.4:** Lyapunov exponent (values given in the colourbar) for different initial conditions $\phi$ and $\theta$ for parameters $\Lambda = 1.5$, $\epsilon = -0.07$, $\omega_D = 1.6$ for different values of the driving amplitude $A = 0.01$ (a), 0.025 (b), 0.05 (c) and 0.1 (d).

the initial conditions produces a heat map of the Lyapunov exponent that is shown in Fig. 6.4 & 6.5. Fig. 6.4 shows the heat map for increasing driving strengths $A = 0.01$ (a), $A = 0.025$ (b), $A = 0.05$ (c) and $A = 0.1$ (d). These plots show how the sea of chaos gets larger, spreading over the phase space as the driving strength is increased. More initial conditions lead to chaotic dynamics as the driving is increased. This is the behaviour we expect from the kicked top as well when the strength of the delta kicks is increased. Let us look at the Poincaré section and time evolution of the physical observables for the case with no driving ($A = 0$) (Fig. 6.2) and with driving ($A = 0.07$) (Fig. 6.3) for an initial condition that gives chaos when driving is present ($\theta = \pi/2$, $\phi = 2.51$ and $t_0 = 0.9$). These parameters will be used later on as well.

The mixed phase space that we can see from looking at the Lyapunov exponent heat map makes this system somewhat more complicated than the Duffing Oscillator. Just looking at the classical system, we can see that for certain choices of initial condition, the trajectory will tend towards islands of stability or end up in a chaotic sea. This will of course add to the complexity of the quantum system when we introduce noise as a result of the measurement. Does the possibility of tunnelling into one of the many stable islands come into effect due to the noise?

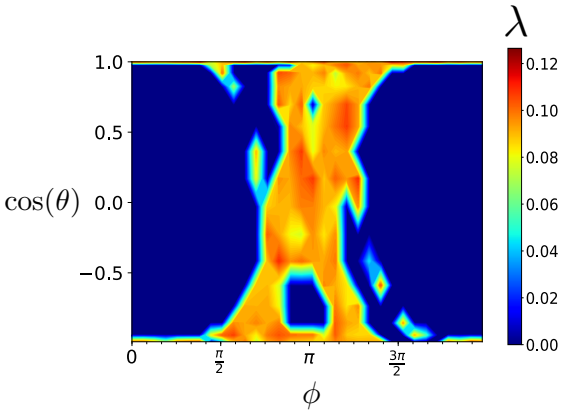


**Figure 6.5:** Lyapunov exponent for different initial conditions $\phi$ and $\theta$ for parameters $\Lambda = 1.5$, $\epsilon = -0.07$, $\omega_D = 1.6$ for the driving amplitude $A = 0.07$ (This is the value we will be using for the quantum simulations as it is the same as that used in [144]).

### 6.3.2 Closed Quantum System

The dynamics of the closed quantum system will mimic that of the classical limit in the very short time as can be seen from Fig. 6.6 where we have plotted the observables $\mathcal{J}_x$, $\mathcal{J}_y$, $\mathcal{J}_z$ for the semiclassical and the closed quantum evolution for the total atom numbers: (a) $N = 200$, (b) $N = 500$ and (c) $N = 1000$. The exact quantum evolution is found by solving the Schrödinger equation (Eq. 2.60) for the state at time $t$ taking the observables to be $\mathcal{J}_i = \langle\psi(t)|\hat{J}_i|\psi(t)\rangle/j$. The two systems follow the same evolution in the short time before the wavepacket spreads in phase space resulting in the loss of spin coherence and behaviour far from the classical behaviour. This separation from the classical dynamics happens over a time called the Ehrenfest time (shown by the red line in the plots). As the size of the system is increased, the separation time will become longer until we reach the classical limit. We can look at this separation time by looking at the expectation values for $\hat{J}_x, \hat{J}_y, \hat{J}_z$.

## 6.4 Driven Top as an Open Quantum System

### 6.4.1 Effect of Dissipation on the Driven Top

Because the classical system does not contain any dissipation, this system is very much not like the system we have studied previously (the Duffing oscillator) and by adding dissipation the system will diverge from the behaviour of the classical system. So how will adding measurement affect the behaviour of this system when it is chaotic? The stronger the measurement the more the measurement back-action will destroy the classical dynamics. The strength of the coupling to the environment will have to be considered carefully when deciding on the optimum balance between the localisation that comes from the measurement and the backaction that drives the system away from the chaotic behaviour that we see in the short time of the closed quantum system.

We will consider a Hermitian coupling to the environment for this system, the $\hat{L} = \sqrt{\gamma}\hat{J}_z$ dephasing is easily achieved in experiments with cold atoms [82, 91]. By monitoring the environment with this Hermitian coupling, we can gain information about

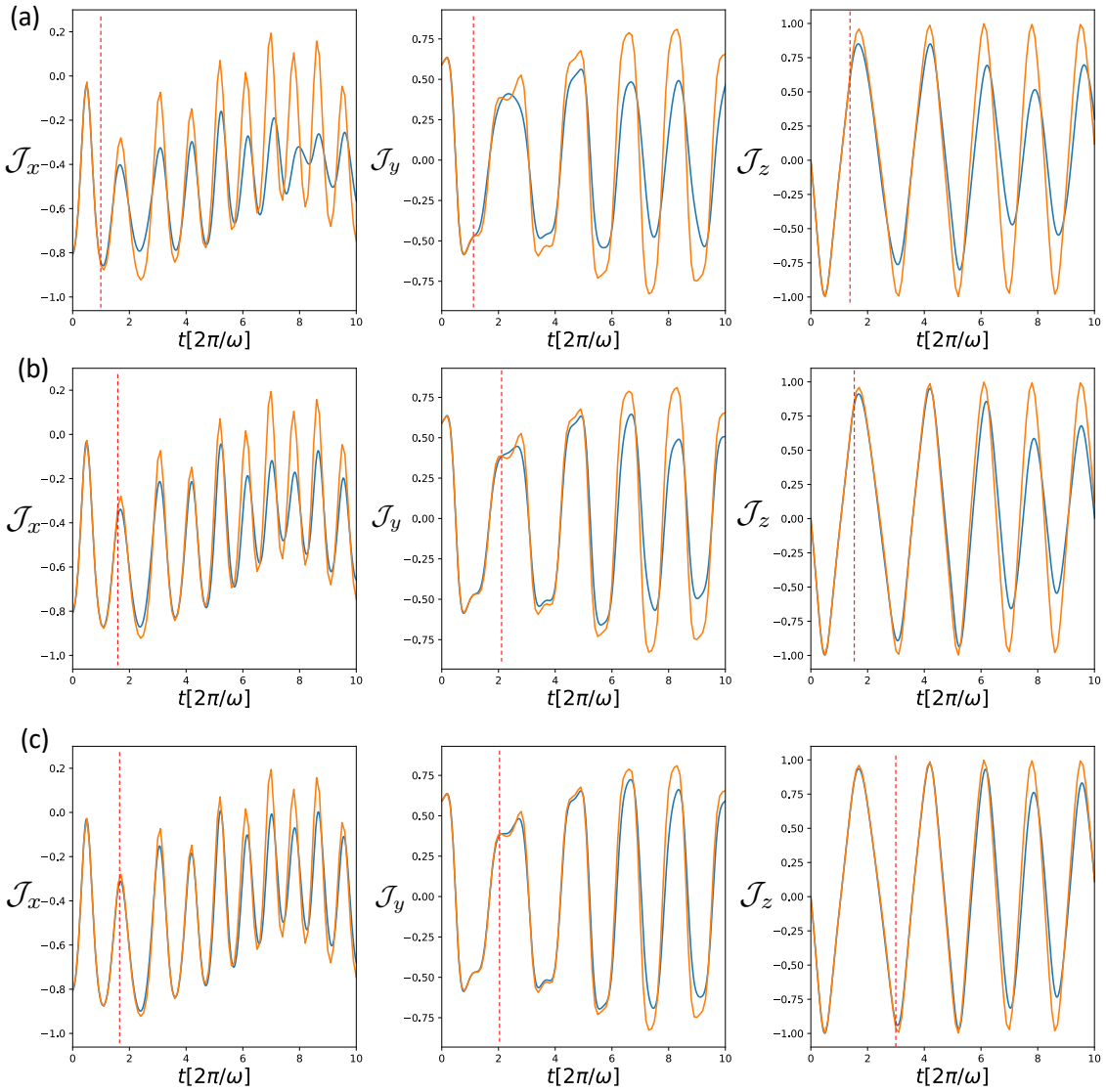


**Figure 6.6:** Time evolution of the physical observables for the closed quantum system (blue) and the semiclassical (orange) for the parameters $\Lambda = 1.5$, $\epsilon = -0.07$, $\omega_D = 1.6$, $\theta_0 = \pi/2$, $\phi_0 = 2.51$, $t_0 = 0.9$ with driving turned on ($A = 0.07$). For this set of parameters, the dynamics are chaotic with a non zero positive Lyapunov exponent $\lambda = 0.093$. This is for (a) $N = 200$, (b) $N = 500$, and (c) $N = 1000$ atoms for the quantum simulation. The red lines give the approximate time at which the two trajectories separate.

the occupation number of the atoms. We want to see if something that is easily achievable will allow us to observe the measurement dependence of chaos and the observation of chaos for this system.

### 6.4.2 $\hat{J}_z$ Dephasing

Consider the master equation (3.20), which describes the unconditional evolution of the system under $\hat{J}_z$ dephasing (no measurement). The equations of motion for $\langle \hat{J}_i \rangle$ are given

by

$$\frac{\mathrm{d}\langle \hat{J}_i \rangle}{\mathrm{d}t} = \mathrm{Tr}[\hat{J}_i \dot{\rho}], \tag{6.22}$$

where the Lindblad operator is given by $\hat{L} = \sqrt{\gamma}\hat{J}_z$ in Eq. 3.20. If we ignore the Hamiltonian evolution, then the dephasing contributes the following terms to the equations of motion

$$\begin{aligned} \frac{\mathrm{d}\langle \hat{J}_x \rangle}{\mathrm{d}t} &= -\frac{\gamma}{2}\langle \hat{J}_x \rangle \\ \frac{\mathrm{d}\langle \hat{J}_y \rangle}{\mathrm{d}t} &= -\frac{\gamma}{2}\langle \hat{J}_y \rangle \\ \frac{\mathrm{d}\langle \hat{J}_z \rangle}{\mathrm{d}t} &= 0, \end{aligned} \tag{6.23}$$

which looks like exponential decay of $\langle \hat{J}_x \rangle$ and $\langle \hat{J}_y \rangle$ while $\langle \hat{J}_z \rangle$ remains constant. This is why it is called a dephasing, its mixing the phase of the state.

**Semiclassical limit for driven top with $\hat{J}_z$ dissipation**

Once again we can obtain the semiclassical limit for the Driven top, but now we have dissipation present in the system. The equations of motion now become

$$\begin{aligned} \dot{\mathcal{J}}_x &= \frac{\Lambda}{2}(-2\mathcal{J}_y\mathcal{J}_z) - \varepsilon\mathcal{J}_y - \frac{\gamma}{2}\mathcal{J}_x \\ \dot{\mathcal{J}}_y &= \frac{\Lambda}{2}(2\mathcal{J}_x\mathcal{J}_z) + \Omega(t)\mathcal{J}_z + \varepsilon\mathcal{J}_x - \frac{\gamma}{2}\mathcal{J}_y \\ \dot{\mathcal{J}}_z &= -\Omega(t)\mathcal{J}_y. \end{aligned} \tag{6.24}$$

For the case of Hermitian coupling, the terms for dephasing appear to be the same for the quantum and the semiclassical case.

## 6.5 Continuous Measurement of a Driven Top

Now that we have opened the driven top to interactions with the environment we can proceed further by considering the continuous measurement of the environment. If we now monitor the environment coupled to the driven top in a continuous way, what will the resulting effect be on the dynamics when the system is chaotic? By considering the monitored system, we will once again produce single trajectories for the conditional system state but will we see the same dependence on the measurement choice that we saw with the Duffing oscillator? To investigate this we once again consider the stochastic evolution of the system conditioned on the continuous measurement (Eq. 3.79). We will once again need to quantify chaos using the Lyapunov exponent. For the driven top, we will need to develop the calculation of the Lyapunov exponent in the new phase space. In this thesis we discuss how we can go about doing that and the challenges that we face in doing so.

### 6.5.1 Homodyne monitoring of a Hermitian output ($\hat{J}_z$ Dephasing): semiclassical approach

Before we look at the quantum system under continuous measurement, let us consider the semiclassical approximation by taking the conditional dynamics to the mean field

limit. By doing so we can take into consideration the interaction with the environment and the continuous measurement in a way that is very easily simulated and will allow us to calculate the Lyapunov exponent for the system easily. In order to obtain the semiclassical equations of motion for the monitored system, we use the same method as in section 6.4.2, taking the evolution of the state under the full nonlinear version of the stochastic Schrödinger equation, given in Stratonovich form (Eq. 3.79). In this case we have a Hermitian coupling $\hat{L}^\dagger = \hat{L}$. The full derivation of the equations of motion for the Hermitian coupling can be found in the appendix (A.1).

$$\begin{aligned}
\mathrm{d}\mathcal{J}_x &= \left[\frac{\Lambda}{2}\left(-2\mathcal{J}_y\mathcal{J}_z\right) - \varepsilon\mathcal{J}_y - \frac{\gamma}{2}(\mathcal{J}_x + \cos(2\phi_{meas})\mathcal{J}_x)\right]\mathrm{d}t + \sqrt{\gamma}\sin(\phi_{meas})\mathcal{J}_y\mathrm{d}W \\
\mathrm{d}\mathcal{J}_y &= \left[\frac{\Lambda}{2}\left(2\mathcal{J}_x\mathcal{J}_z\right) + \Omega(t)\mathcal{J}_z + \varepsilon\mathcal{J}_x - \frac{\gamma}{2}(\mathcal{J}_y + \cos(2\phi_{meas})\mathcal{J}_y)\right]\mathrm{d}t - \sqrt{\gamma}\sin(\phi_{meas})\mathcal{J}_x\mathrm{d}W \\
\mathrm{d}\mathcal{J}_z &= -\Omega(t)\mathcal{J}_y\mathrm{d}t. \qquad (6.25)
\end{aligned}$$

From the equations above we see that the monitoring choice $\phi_{meas} = 0$ will lead to the largest contribution from the dephasing to the dynamics ($\gamma/2(\mathcal{J}_x + \cos(2\phi_{meas})\mathcal{J}_x) = \gamma\mathcal{J}_x$ and similar for $\mathcal{J}_y$), so that as the strength of the measurement increases (ie. as $\gamma$ increases), the dephasing will contribute more to the evolution of the system and the trajectory will depart more from the chaotic trajectory. This can be seen from the numerical simulations of the trajectory, found by solving the stochastic differential equations in XMDS [24]. Let us start with the trajectory given by the semiclassical dynamics and the corresponding Poincaré section on the spherical phase space. Comparison of the evolution for two choices of measurement strength $\gamma = 0.0001$(Fig. 6.7) and $\gamma = 0.1$ (Fig. 6.9) show the significant change to the dynamics and the Lyapunov exponent that results from the increase in the measurement strength, taking the behaviour from chaotic to regular. In contrast, the monitoring choice $\phi_{meas} = \pi/2$ this leads to the cancellation of the dephasing effects ($\gamma/2(\mathcal{J}_x + \cos(2\phi)\mathcal{J}_x) = 0$ and similar for $\mathcal{J}_y$). This choice of measurement for a Hermitian coupling is known as a no-knowledge measurement [138]. In this case, increasing the strength of the measurement will not affect the deterministic evolution at all, instead we get the closed evolution (which is chaotic in the mean field), altered by a stochastic term. We again look at the numerical simulation for two choices of the measurement strength $\gamma = 0.0001$(Fig. 6.8) and $\gamma = 0.1$ (Fig. 6.10). What might be somewhat surprising is that the degree of chaos actually increases beyond that of the closed system when the measurement strength is increased. And this leads to interesting dynamics that seems to fill the entire sphere with points on the Poincaré section; that is, leading to completely random dynamics. This in itself might be useful for other applications, such as generating random quantum states.

Let us now consider the Lyapunov exponent for the monitoring choices in more detail as we change the measurement strength. We show the Lyapunov exponent as a function of the monitoring angle for different measurement strengths for both the undriven top $A = 0$ (Fig. 6.11) and the driven top $A = 0.07$ (Fig. 6.12). As the measurement strength is increased, we see a clear distinction between the measurement angle choices. With the no-knowledge angle $\phi_{meas} = \pi/2$ corresponding to the smallest change as $\gamma$ is increased. What is perhaps more interesting is that for this angle, we also see the emergence of chaos for the undriven top as the measurement strength is increased. These results seem to suggest that the measurement itself acts as a driving force to drive the state of the system towards the chaos. And that the increased stochasticity in the system leads to the

emergence of chaos even when we do not expect it.

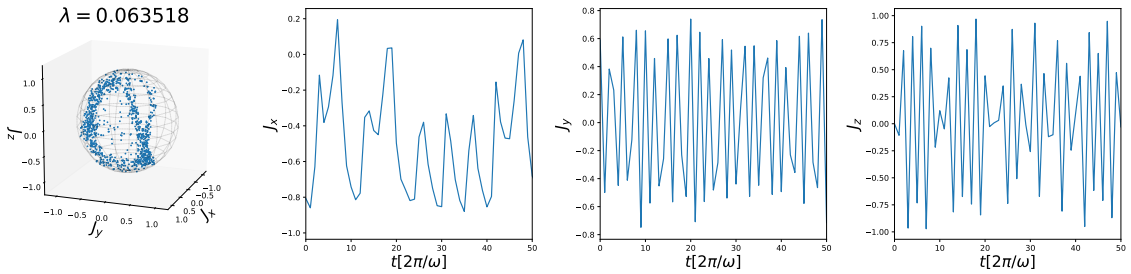


**Figure 6.7:** Semiclassical trajectory under $\hat{L} = \sqrt{\gamma}\hat{J}_z$ dephasing, for parameters $\Lambda = 1.5$, $\epsilon = -0.07$, $\omega_D = 1.6$, and $A = 0.07$. With initial condition $\theta = \pi/2$ and $\phi = 2.51$ and measurement choice $\phi_{meas} = 0$ and $\gamma = 0.0001$.

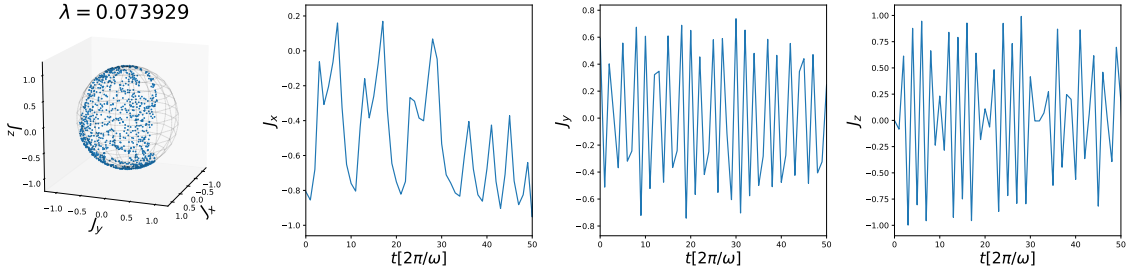


**Figure 6.8:** Semiclassical trajectory under $\hat{L} = \sqrt{\gamma}\hat{J}_z$ dephasing, for parameters $\Lambda = 1.5$, $\epsilon = -0.07$, $\omega_D = 1.6$, and $A = 0.07$. With initial condition $\theta = \pi/2$ and $\phi = 2.51$ and measurement choice $\phi_{meas} = \pi/2$ and $\gamma = 0.0001$.

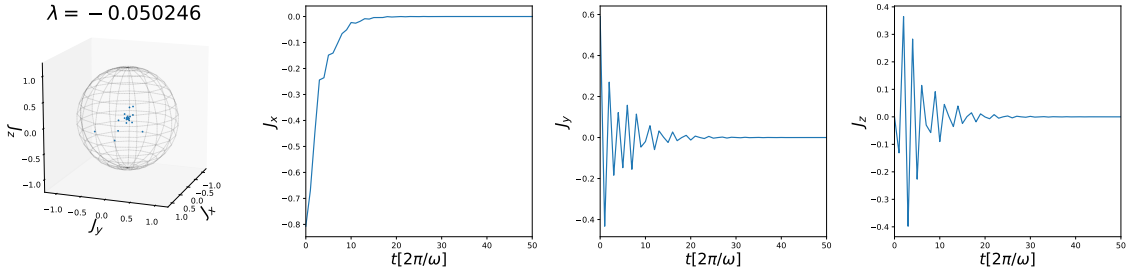


**Figure 6.9:** Semiclassical trajectory under $\hat{L} = \sqrt{\gamma}\hat{J}_z$ dephasing, for parameters $\Lambda = 1.5$, $\epsilon = -0.07$, $\omega_D = 1.6$, and $A = 0.07$. With initial condition $\theta = \pi/2$ and $\phi = 2.51$ and measurement choice $\phi_{meas} = 0$ and $\gamma = 0.1$.

### 6.5.2 Homodyne monitoring of a Hermitian output ($\hat{J}_z$ Dephasing)

Let us consider the full quantum version of the continuously monitored Hermitian output ($\hat{L} = \sqrt{\gamma}\hat{J}_z$). From the previous section we found that for the choice of $\phi_{meas} = \pi/2$ for the measurement angle, we have a no-knowledge measurement [140] which means that no information will be gained about the system as a result of the measurement. If however, we choose a different $\phi_{meas}$, we will have a normal homodyne measurement of the $\hat{J}_z$. So the choice of phase will now correspond to a choice in the effective strength of the

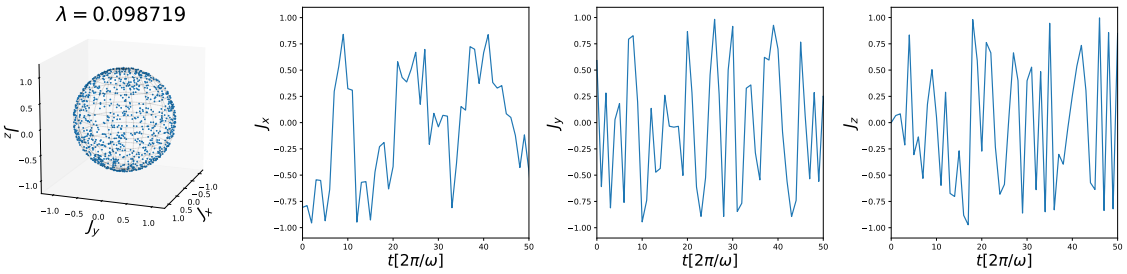


**Figure 6.10:** Semiclassical trajectory under $\hat{L} = \sqrt{\gamma}\hat{J}_z$ dephasing, for parameters $\Lambda = 1.5$, $\epsilon = -0.07$, $\omega_D = 1.6$, and $A = 0.07$. With initial condition $\theta = \pi/2$ and $\phi = 2.51$ and measurement choice $\phi_{meas} = \pi/2$ and $\gamma = 0.1$.

measurement. Recall that the driven top Hamiltonian is given in Eq. 6.17. For the numerical simulation of the driven top, we use the Dicke states $|J, m\rangle$ as our basis states. And we calculate the evolution of the coefficients $C_m$. The SSE will then give us

$$\begin{aligned} \mathrm{d}C_n = \Big[&\langle J,n|\sum_{-\frac{N}{2}}^{\frac{N}{2}} C_m(-i\hat{H})|J,m\rangle - \langle J,n|\sum_{-\frac{N}{2}}^{\frac{N}{2}} C_m \tfrac{1}{2}\gamma\hat{J}_z^2|J,m\rangle \\ &- \langle J,n|\sum_{-\frac{N}{2}}^{\frac{N}{2}} C_m \tfrac{e^{-2i\phi}}{2}\gamma\hat{J}_z^2|J,m\rangle + \langle J,n|\sum_{-\frac{N}{2}}^{\frac{N}{2}} C_m\gamma\langle\hat{J}_z\rangle\hat{J}_z(1-e^{-2i\phi})|J,m\rangle\Big]\mathrm{d}t \\ &+ \langle J,n|\sum_{-\frac{N}{2}}^{\frac{N}{2}} C_m\sqrt{\gamma}\hat{J}_z e^{-i\phi}|J,m\rangle \mathrm{d}W. \end{aligned} \quad (6.26)$$

For the simulations, this simplifies to give

$$\begin{aligned} \mathrm{d}C_n = \Big(&-i(C_n\tfrac{\Lambda}{2}n^2 - \tfrac{1}{2}[C_{n-1}(J^2-(n-1)(n))^{\frac{1}{2}} + C_{n+1}(J^2-(n+1)(n))^{\frac{1}{2}}] + \varepsilon C_n n) \\ &- \gamma\tfrac{C_n}{2}n^2 - \gamma\tfrac{C_n}{2}n^2e^{-2i\phi} + \gamma\langle\hat{J}_z\rangle C_n n(1-e^{-2i\phi})\Big)\mathrm{d}t + \sqrt{\gamma}C_n n e^{-i\phi}\mathrm{d}W. \end{aligned} \quad (6.27)$$

## 6.6 Quantum dynamics for short times

We can now present the results of the simulation of the driven top as a continuously monitored open quantum system. As we mention above, we are unable to quantify chaos without the Lyapunov exponent but we can still observe some interesting dynamical behaviour for the system. Without the quantitative result from the Lyapunov exponents, we rely on the comparisons we can make with the classical dynamics in the short time. From the short time behaviour we can still determine characteristics that differ for different choices of the measurement angle.

We are very much interested in the behaviour of the quantum driven top for high degree of spin where the long time evolution is hard to simulate. What we can instead look at is the dynamics over a short time evolution of up to 100 cycles of the driving. We study the physical observables of the system, given by the expectation values of $(\langle\hat{J}_x\rangle,\langle\hat{J}_y\rangle,\langle\hat{J}_z\rangle)$ and

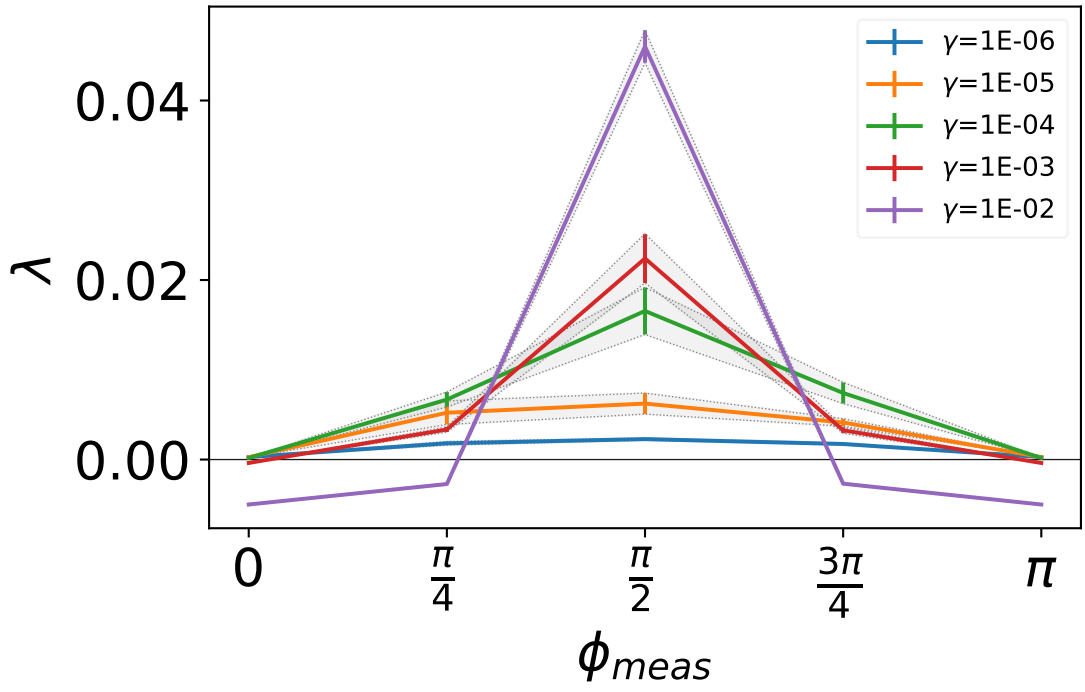


**Figure 6.11:** Plot of $\phi_{meas}$ vs $\lambda$ for the semiclassical system under $\hat{L} = \sqrt{\gamma}\hat{J}_z$ dephasing, for parameters $\Lambda = 1.5$, $\epsilon = -0.07$, $\omega_D = 1.6$ with driving turned off ($A = 0.0$) for different $\gamma$. With initial condition $\theta = \pi/2$ and $\phi = 2.51$.

the associated variances ($Var(\hat{J}_x)$, $Var(\hat{J}_y)$, $Var(\hat{J}_z)$). We present the time evolution of the expectation values and the variances and we also plot the Poincaré section (taking the point every $2\pi/\omega$) and the trajectory on the spherical phase space. We can also look at the spin coherence as the state evolves by looking at the length of the Bloch vector $|\mathbf{J}| = (\langle\hat{J}_x\rangle^2 + \langle\hat{J}_y\rangle^2 + \langle\hat{J}_z\rangle^2)^{1/2}$. All of the above mentioned results are plotted in Fig. 6.13 and Fig. 6.14. For these results we have used the parameters chosen by Tomkovic *et al.* [144] so that we can compare with the results for the closed system dynamics presented in their paper. The choice of $\gamma$ will strongly influence the dynamics of the system. A dephasing that is too strong will dominate the dynamics and result in uninteresting behaviour. If we however choose to set $\gamma = 0$, we will of course obtain the result for the closed quantum system that has already been shown in a previous section. The effect of the choice of $\gamma$ and the measurement strength is itself important to investigate so we consider several values. The results presented are for two orthogonal measurement phases, $\phi_{meas} = 0$ (Fig. 6.13) and $\phi_{meas} = \pi/2$(Fig. 6.14). A direct comparison of the trajectory with the semiclassical counterpart is shown in the bottom plots for both measurement choices. We can immediately see a very large difference between the measurements for this single noise realisation. We see that for $\phi_{meas} = 0$ the trajectory has been strongly driven by the measurement to an island of stability, whereas for $\phi_{meas} = \pi/2$ the trajectory follows the classical dynamics closely and appears to behave in the same chaotic way.

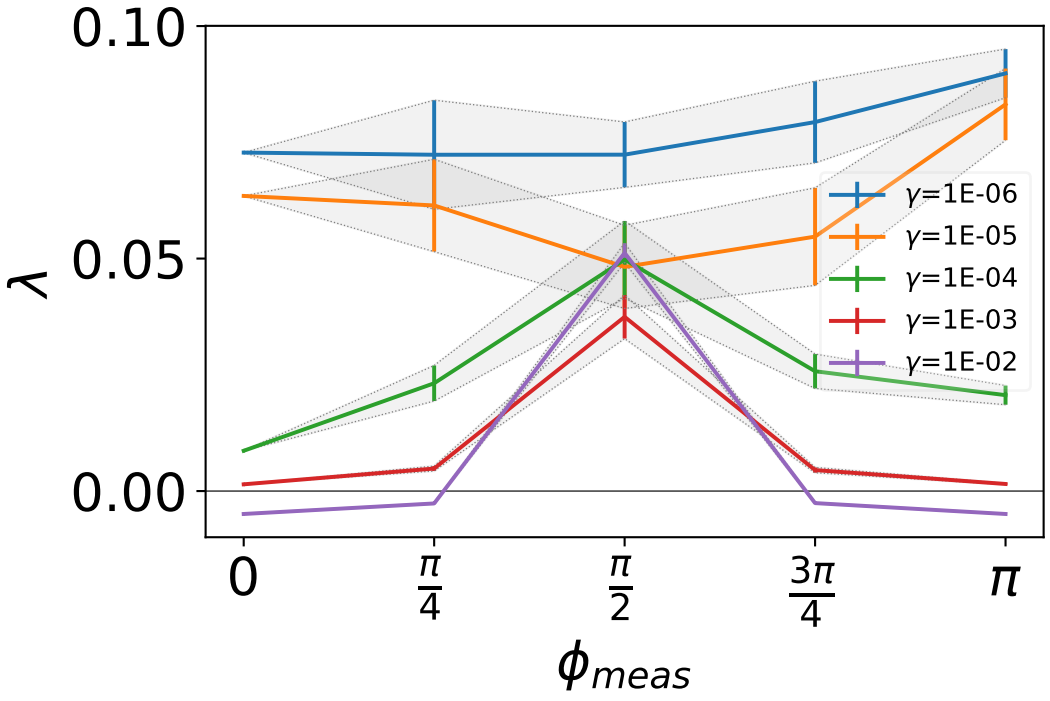


**Figure 6.12:** Plot of $\phi_{meas}$ vs $\lambda$ for the semiclassical system under $\hat{L} = \sqrt{\gamma}\hat{J}_z$ dephasing, for parameters $\Lambda = 1.5$, $\epsilon = -0.07$, $\omega_D = 1.6$ with driving turned on ($A = 0.07$) for different $\gamma$. With initial condition $\theta = \pi/2$ and $\phi = 2.51$.

## 6.7 Breaking time between the classical and quantum

Since the calculation of quantum Lyapunov exponents for the driven top is beyond the current scope of this thesis, we need another way to distinguish between different measurement choices. One possible way to quantify the departure from the classical dynamics is the separation time, which is the time at which the quantum dynamics breaks away from the classical dynamics. The breaking time has been used for both Hamiltonian and dissipative chaotic systems in the past in the investigation of the correspondance between the classical and quantum system when chaos is present in the classical limit [167, 55, 66, 18]. To our knowledge, it has not been used for single quantum trajectories. Here we will investigate whether the separation time could potentially be a useful quantifier for distinguishing how well the quantum trajectories, conditioned by different measurement choices, can track the classical dynamics. In order to validate the results presented here we present the breaking time for the Duffing oscillator in section A.1.2 of the appendix.

For the closed quantum system, the breaking time is defined as the time scale over which the wave function spreads across the available phase space and the quantum corrections become comparable to the classical dynamics. The breaking time is analytically given as [3]

$$\tau_\hbar = \frac{1}{\lambda} \ln\left(\frac{c}{\hbar}\right), \tag{6.28}$$

where $\lambda$ is the Lyapunov exponent of the system and $c$ is a constant that depends on the wave-packet dispersion.

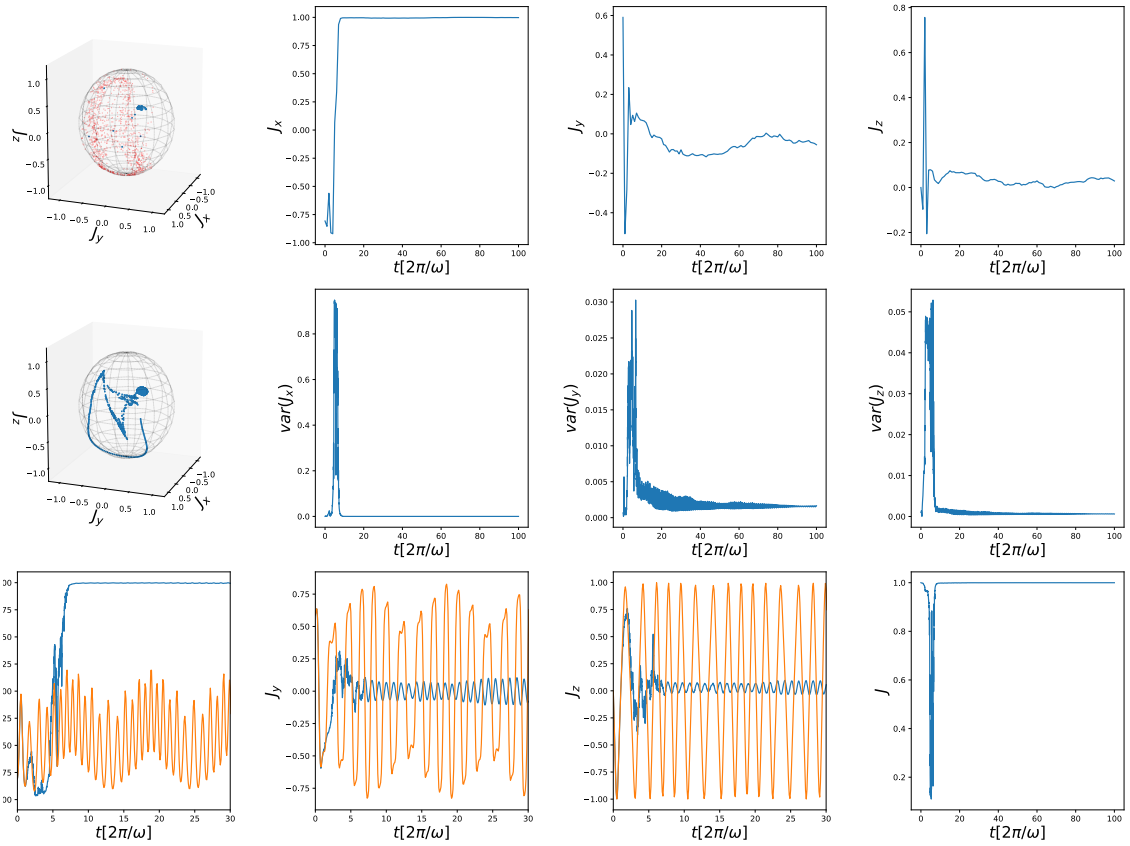


**Figure 6.13:** Short time evolution of the open quantum driven top for parameters $\Lambda = 1.5$, $\varepsilon = -0.07$, $\omega_D = 1.6$, $t_0 = 0.9$, $(\phi_0, \theta_0) = (2.51, \pi/2)$, with driving turned on $(A = 0.07)$, for $N = 1000$ atoms and $\gamma = 10^{-6}$. For this set of parameters, the dynamics are chaotic with a non zero positive Lyapunov exponent $\lambda = 0.093$. This figure shows the results for the measurement phase $\phi_{meas} = 0$.

### 6.7.1 Distance measure

In order to find the time of separation between the classical and quantum trajectories, we require a distance measure between the two $d$. When the distance $d$ reaches a threshold $\epsilon$, the time at which this occurs will be the separation time. Now of course we can choose some arbitrary threshold to reach so we will investigate this for $\varepsilon \pm 5\%$, 10%, 15% and 20%. The distance measure has been previously calculated using the first [55] and second moments of the classical and quantum distribution [18]. In the paper by Carvalho *et al.* [18], the distance measure that was used was the difference between the variance of the classical probability distribution and the variance of the quantum state. Here we do not have the classical probability distribution but are instead considering the classical and quantum trajectories so the distance measure that will be used is the distance between the two systems in phase space, given by the distance in the expectation values:

$$d_t = \sqrt{\Delta J_x(t)^2 + \Delta J_y(t)^2 + \Delta J_z(t)^2}, \tag{6.29}$$

where $\Delta J_x(t) = \langle \hat{J}_x \rangle_{cl}/j - \langle \psi | \hat{J}_x | \psi \rangle / j$ and so on. The distance is calculated at each time step. For an example of what the distance measure looks like for $\phi_{meas} = \pi/2$, see Fig. 6.15.

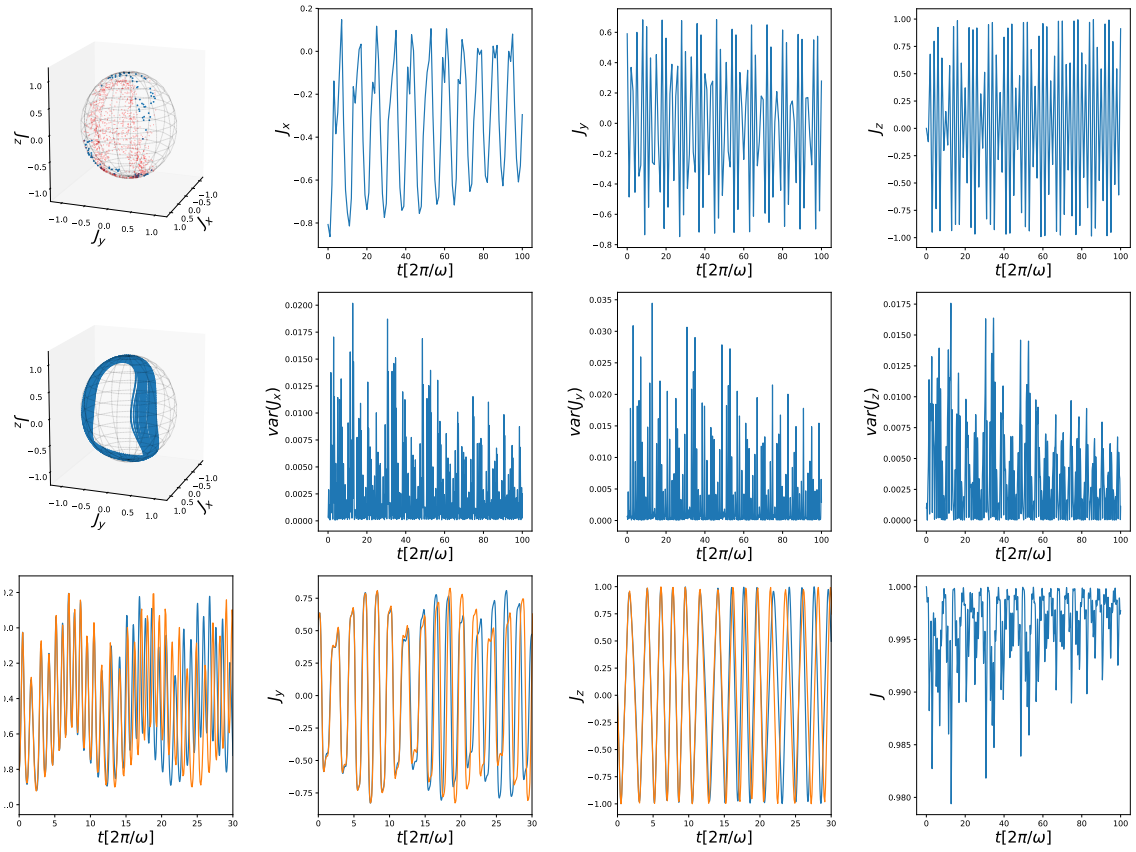


**Figure 6.14:** Short time evolution of the open quantum driven top for parameters $\Lambda = 1.5$, $\varepsilon = -0.07$, $\omega_D = 1.6$ , $t_0 = 0.9$, $(\phi_0, \theta_0) = (2.51, \pi/2)$, with driving turned on $(A = 0.07)$, for $N = 1000$ atoms and $\gamma = 10^{-6}$ . For this set of parameters, the dynamics are chaotic with a non zero positive Lyapunov exponent $\lambda = 0.093$. This figure shows the results for the measurement phase $\phi_{meas} = \pi/2$.

### 6.7.2 Breaking time $\tau_\hbar$

The breaking time is the first point that $d_B > \epsilon$ in the time series. The separation time is averaged over multiple noise realisations for each measurement choice for meaningful comparison. From Fig. 6.15, it is clear that the breaking time occurs for this measurement choice around $\tau_\hbar = 15\Omega/2\pi$. Let us look at the average separation time for five noise realisations for different choices of measurement phase. Fig. 6.16 shows the average separation time for both the driven ($A = 0.07$ shown on left) and undriven ($A = 0$ shown on right) case for $\gamma = 10^{-5}$ (top), $10^{-4}$ (middle), and $10^{-3}$ (bottom) with the following parameters: $\Lambda = 1.5$, $\varepsilon = -0.07$, $\omega_D = 1.6$ , $t_0 = 0.9$, $(\phi_0, \theta_0) = (2.51, \pi/2)$ and $N = 1000$ atoms. The first thing to notice is that there is a definite trend that occurs no matter the leeway on the threshold: the choice $\phi_{meas} = \pi/2$ consistently leads to a separation time that occurs later than any other measurement choice. The orthogonal phase leads to the fastest break down between the classical and quantum, which we would expect given the results for the Lyapunov exponent for the semiclassical system under continuous monitoring. What do these results mean? For the Hermitian coupling to the environment, the measurement phase which corresponds to no gain in knowledge about the system seems to disturb the system the least away from the chaotic dynamics of the classical system. Which seems to hint that the choice of measurement will have some effect on the dynamics of the quantum

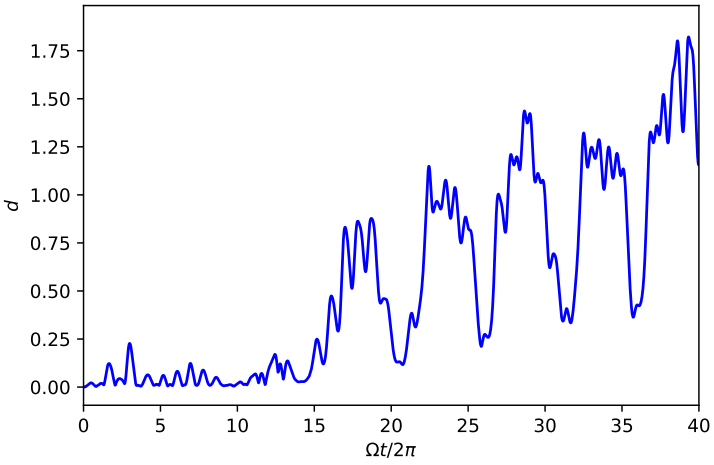


**Figure 6.15:** Distance measure over time for parameters $\Lambda = 1.5$, $\varepsilon = -0.07$, $\Omega = 1.6$ , $t_0 = 0.9$, $(\phi_0, \theta_0) = (2.51, \pi/2)$, with driving turned on ($A = 0.07$), for $N = 1000$ atoms and $\gamma = 10^{-5}$ . This figure shows the results for the measurement phase $\phi_{meas} = \pi/2$.

driven top.

## 6.8 Non-Hermitian coupling to the environment: $\hat{L} = \sqrt{\gamma}\hat{J}_-$

For the Duffing oscillator we considered the non-Hermitian coupling to an environment given by $\hat{L} = \sqrt{\Gamma}\hat{a}$. The analogous non-Hermitian coupling for the driven top is $\hat{L} = \sqrt{\gamma}\hat{J}_-$. A measurement of this form can be engineered in cold atom systems [126]. In this case we do not have the semiclassical dynamics for this coupling but we do have the results for the quantum short time dynamics and we can look at the breaking time in this case. We present the breaking time for non-Hermitian coupling for $\gamma = 10^{-5}$ to $10^{-3}$ with driving turned on ($A = 0.07$) and with driving off ($A = 0.0$) **??**.

## 6.9 Calculating Lyapunov exponents for the driven top

To quantify chaos for the quantum driven top, we once again need to calculate the maximal Lyapunov exponent from the conditional dynamics. In this section, we outline the procedure for achieving this, leaving its numerical implementation a task for future work.

### Distance between two states on the sphere

To calculate the Lyapunov exponent for the quantum Driven top, we need to utilise a similar method to that which was used for the quantum Duffing oscillator. However now our phase space is confined to the surface of the sphere rather than a plane. If we naively follow the method used for the Duffing oscillator and use the metric for $\mathcal{R}(3)$, the distance between two states would be given by:

$$d_t = \sqrt{\Delta J_x(t)^2 + \Delta J_y(t)^2 + \Delta J_z(t)^2}, \tag{6.30}$$

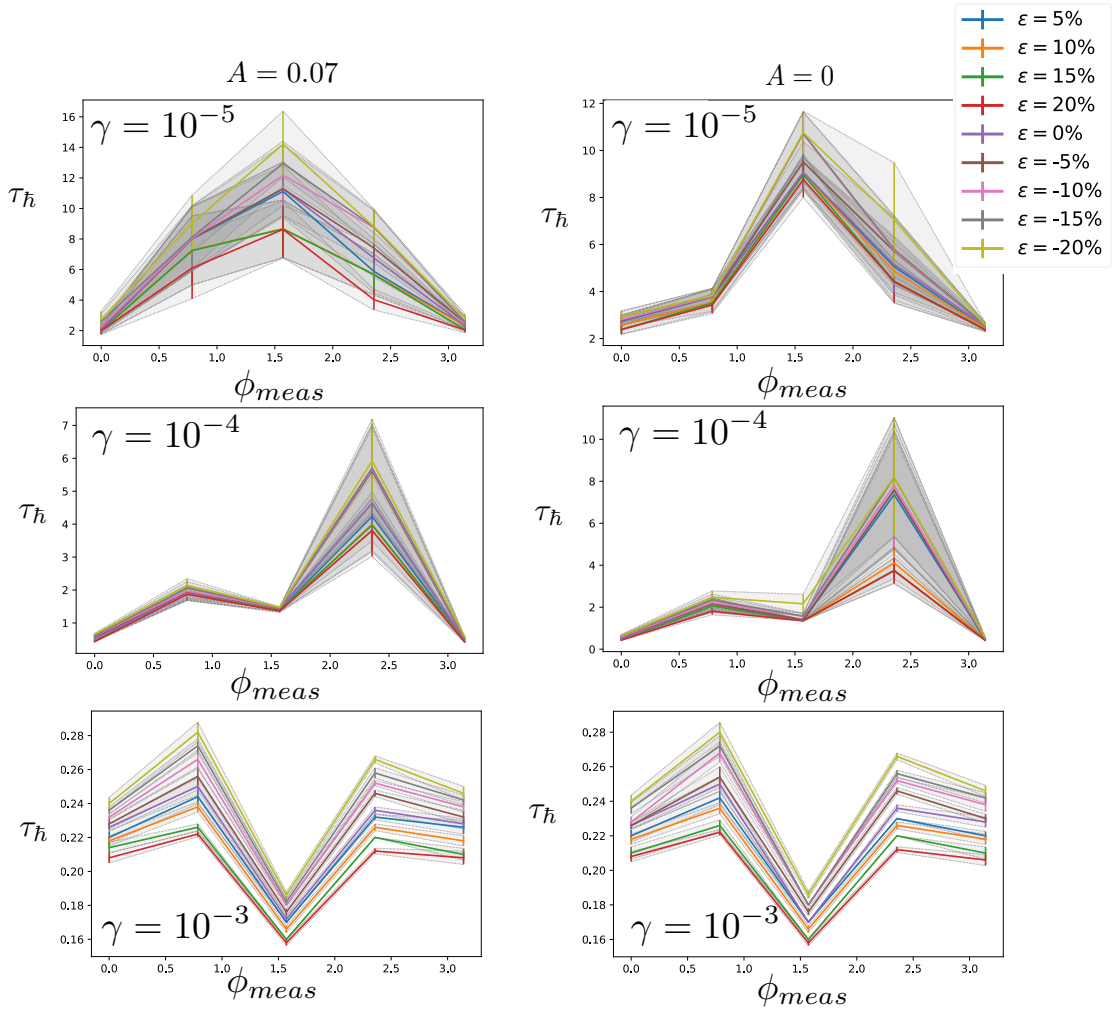


**Figure 6.16:** Average breaking time $\tau_\hbar$ for $\hat{L} = \sqrt{\gamma}\hat{J}_z$ with threshold $\epsilon = 0.25 \pm 5\%, 10\%, 15\%, 20\%$, for parameters $\Lambda = 1.5$, $\varepsilon = -0.07$, $\Omega = 1.6$ , $t_0 = 0.9$, $(\phi_0, \theta_0) = (2.51, \pi/2)$, for $N = 1000$ atoms. The figure shows both the driven ($A = 0.07$ shown on left) and undriven ($A = 0$ shown on right) case for $\gamma = 10^{-5}$ (top), $10^{-4}$ (middle), and $10^{-3}$ (bottom). Each point is averaged over 5 noise realisations and the error bars signify twice the standard error.

where $\Delta J_x(t) = \langle\psi_p(t)|\hat{J}_x|\psi_p(t)\rangle - \langle\psi_f(t)|\hat{J}_x|\psi_f(t)\rangle$ and so on... The problem with using this method is that the distance in $\mathcal{R}(3)$ does not give the distance on the surface of the sphere within which our phase space lies on. We should instead use the metric on the unit 2-sphere which is given by Eq. 2.58. However, as $j \to \infty$, the sphere will be accurately approximated by a flat plane and the distance between the states will be sufficiently infinitesimal to be accurately described by Eq. 6.30. So we can use this for the semiclassical simulations. Then the Lyapunov exponent is given by Eq. 4.3.

### Note on expectation values for quantum system

Because we are now dealing with quantum states that lie on the sphere, the more spread the state is, the more likely we are to see the mean value of the state lying within the sphere which may have consequences on the way we have defined our Lyapunov exponent

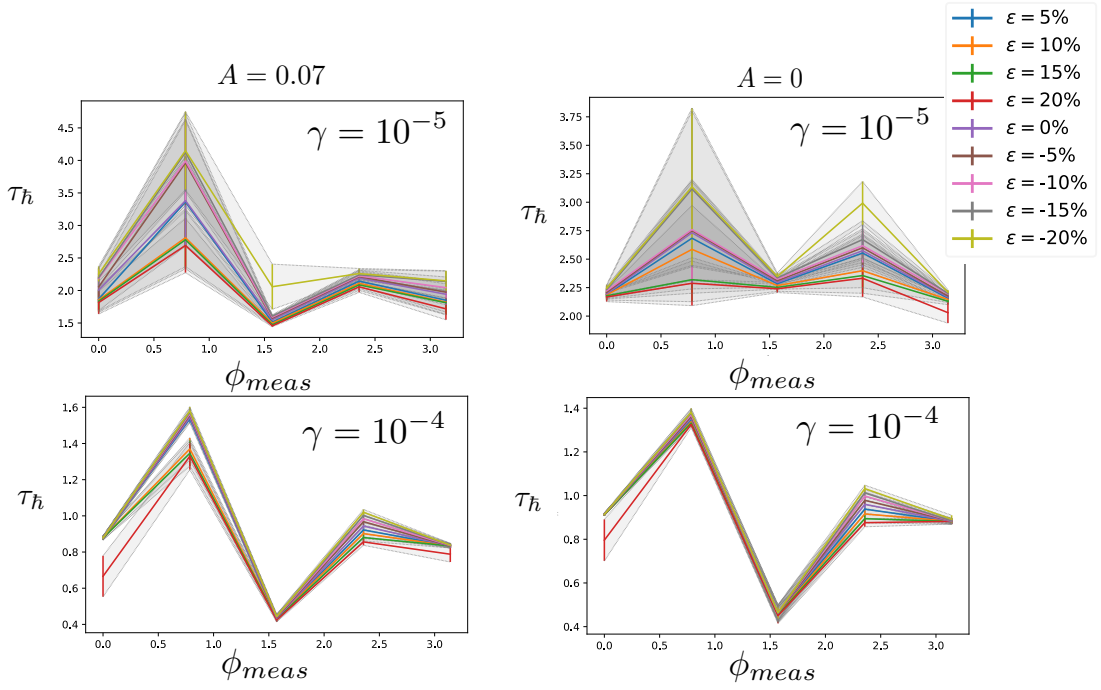


**Figure 6.17:** Average breaking time $\tau_\hbar$ for $\hat{L} = \sqrt{\gamma}\hat{J}_-$ with threshold $\epsilon = 0.25 \pm 5\%, 10\%, 15\%, 20\%$, for parameters $\Lambda = 1.5$, $\varepsilon = -0.07$, $\Omega = 1.6$ , $t_0 = 0.9$, $(\phi_0, \theta_0) = (2.51, \pi/2)$, for $N = 1000$ atoms. The figure shows both the driven ($A = 0.07$ shown on left) and undriven ($A = 0$ shown on right) case for $\gamma = 10^{-5}$ (top), $10^{-4}$ (bottom). Each point is averaged over 5 noise realisations and the error bars signify twice the standard error.

using the expectation values of the state.

### 6.9.1 Rotation of an arbitrary quantum state in SU(2)

The next step in the numerical calculation of the Lyapunov exponent is to reset the perturbed trajectory for the next iteration just as we did with the Duffing oscillator. We perform the reset by replacing the perturbed trajectory with a displaced version of the fiducial trajectory. The trajectory is displaced by the displacement operator. For the SU(2) case where our phase space is now the surface of the sphere, this is given by the rotation of the state on the sphere. In chapter 2 the rotation of a coherent spin state is given by Eq. 2.55. But during the evolution of the system, our state is no longer described as a CSS. This means that we need to apply a rotation on the arbitrary fiducial state at each reset to get the new perturbed state. The rotation of an arbitrary state is given by:

$$e^{-i\delta\hat{\mathbf{n}}\cdot\hat{\mathbf{J}}} = e^{-i\delta(n_x\hat{J}_x + n_y\hat{J}_y + n_z\hat{J}_z)}, \tag{6.31}$$

where $\hat{\mathbf{n}} = n_x\hat{x} + n_y\hat{y} + n_z\hat{z}$ is the normal vector to the plane of rotation and $\delta$ is the angle of rotation. We also need to ensure that the state is rotated in the correct direction (the direction of expansion) so that we end up with the maximal Lyapunov exponent. This is done by considering the geometry of the states on the sphere. Considering the two states

on the sphere, the vector pointing from the origin to each state is given by:

$$\mathbf{v}_f = \langle\psi_f(t)|\hat{J}_x|\psi_f(t)\rangle\hat{x} + \langle\psi_f(t)|\hat{J}_y|\psi_f(t)\rangle\hat{y} + \langle\psi_f(t)|\hat{J}_z|\psi_f(t)\rangle\hat{z}, \tag{6.32}$$

$$\mathbf{v}_p = \langle\psi_p(t)|\hat{J}_x|\psi_p(t)\rangle\hat{x} + \langle\psi_p(t)|\hat{J}_y|\psi_p(t)\rangle\hat{y} + \langle\psi_p(t)|\hat{J}_z|\psi_p(t)\rangle\hat{z}. \tag{6.33}$$

We require that the normal vector to the plane of rotation is orthogonal to both trajectories so that the plane of rotation is the same plane that the two states lie on. The vector orthogonal to both trajectories is given by the cross product:

$$\mathbf{v}_{f\times p} = (\langle\hat{J}_y\rangle_f\langle\hat{J}_z\rangle_p - \langle\hat{J}_z\rangle_f\langle\hat{J}_y\rangle_p)\hat{x} + (\langle\hat{J}_x\rangle_f\langle\hat{J}_z\rangle_p - \langle\hat{J}_z\rangle_f\langle\hat{J}_x\rangle_p)\hat{y} + (\langle\hat{J}_x\rangle_f\langle\hat{J}_y\rangle_p - \langle\hat{J}_y\rangle_f\langle\hat{J}_x\rangle_p)\hat{z}, \tag{6.34}$$

then the normal vector is given simply by $\hat{\mathbf{n}} = \mathbf{v}_{f\times p}/|\mathbf{v}_{f\times p}|$.

### Acting the rotation operator on the arbitrary state

We can use the ordering theorem given in [111] to put the rotation operator into a form that can easily be acted on an arbitrary state. For $\hat{J}_z, \hat{J}_+$ and $\hat{J}_-$, we have

$$[\hat{J}_z, \hat{J}_\pm] = \pm\hat{J}_\pm \quad \text{and} \quad [\hat{J}_+, \hat{J}_-] = 2\hat{J}_z, \tag{6.35}$$

then the operator ordering formula gives

$$e^{(\lambda_+\hat{J}_+ + \lambda_-\hat{J}_- + \lambda_z\hat{J}_z)} = e^{(\Lambda_+\hat{J}_+)}e^{(\ln(\Lambda_z)\hat{J}_z)}e^{(\Lambda_-\hat{J}_-)} \tag{6.36}$$

$$= e^{(\Lambda_-\hat{J}_-)}e^{(-\ln(\Lambda_z)\hat{J}_z)}e^{(\Lambda_+\hat{J}_+)}, \tag{6.37}$$

where

$$\Lambda_z = \left(\cosh(\alpha) - \frac{\lambda_z}{2\alpha}\sinh(\alpha)\right)^{-2} \tag{6.38}$$

$$\Lambda_\pm = \frac{2\lambda_\pm\sinh(\alpha)}{2\alpha\cosh(\alpha) - \lambda_z\sinh(\alpha)} \tag{6.39}$$

$$\alpha^2 = \frac{1}{4}\lambda_z^2 + \lambda_+\lambda_-. \tag{6.40}$$

Rearranging the rotation in Eq. 6.31 to be in the same form, we have:

$$e^{-i\delta\hat{\mathbf{n}}\cdot\hat{\mathbf{J}}} = e^{-i\delta\left[\frac{1}{2}(n_x - in_y)\hat{J}_+ + \frac{1}{2}(n_x + in_y)\hat{J}_- + n_z\hat{J}_z\right]}, \tag{6.41}$$

so that $\lambda_+ = -i\delta(1/2)(n_x - in_y)$, $\lambda_- = -i\delta(1/2)(n_x + in_y)$ and $\lambda_z = -i\delta n_z$. Applying the ordering formula to the rotation, our rotation operator will be in the form given by Eq. A.18 with the coefficients:

$$\Lambda_z = \left(\cos[\tfrac{\delta}{2}] - \frac{n_z\sin[\frac{\delta}{2}]}{\delta}\right)^{-2} \tag{6.42}$$

$$\Lambda_- = \frac{(-in_x + n_y)\delta\sin[\frac{\delta}{2}]}{2\delta\cos[\frac{\delta}{2}] - 2n_z\sin[\frac{\delta}{2}]} \tag{6.43}$$

$$\Lambda_+ = \frac{-(in_x + n_y)\delta\sin[\frac{\delta}{2}]}{2\delta\cos[\frac{\delta}{2}] - 2n_z\sin[\frac{\delta}{2}]}. \tag{6.44}$$

For further details of how this can be acted on the arbitrary state for our simulations, we refer to section A.1 of the appendix.

# 7

# Conclusions and Outlook

This thesis has presented theoretical work on the continuous measurement of open quantum systems whose classical counterpart is chaotic. In the past it has been assumed that the choice of measurement does not have an effect on the emergence of chaos. If we consider the average over noise realisations after all, we obtain the unconditional dynamics given by the Master equation. However it is known that the back-action applied to the quantum system as a result of the measurement can have an effect on the localisation of the wavefunction and control protocols are constructed for quantum systems using the measurement strategy. It is clear in the field of quantum control that measurement can play a role so we should expect it to have an effect on the onset of chaos. Here we quantitatively show that this is in fact true by calculating the Lyapunov exponent in the quantum regime. The aim of this thesis was to shed light on the role that measurement plays in the emergence of chaos from the quantum limit, in order to further our understanding of how chaos comes about from the quantum particles that form the basis of all matter. Given the recent excitement and connection of quantum chaos to much broader fields of research and the rapid increase in quantum technology over past decades, it seems vital that we understand how chaos emerges from quantum systems and study methods of controlling chaos.

## 7.1 Emergence of chaos from a continuously monitored quantum system

In this thesis we have demonstrated the interplay between the quantum interference effects that are induced by the nonlinear dynamics of the quantum Duffing oscillator and the localisation and decoherence given by the choice of continuous measurement. We have quantified through the calculation of the quantum Lyapunov exponent the effect that the continuous measurement has on the quantum Duffing oscillator. When the classical limit is chaotic (dissipation strength $\Gamma = 0.10$), there is a regime in the transition from quantum to classical where the measurement choice influences the emergence of chaos. Depending on the choice of the measurement phase of a homodyne detection scheme,

the dynamics of the system can be regular or chaotic. The rate of the decoherence due to the measurement is what determines this result. Specifically, the measurement phase that is parallel to the interference fringes of the state's Wigner function gives the fastest destruction of these interference fringes and the fastest collapse to a localised state that closely follows the chaotic dynamics of the classical limit. What is perhaps more surprising is that measurement can also induce chaos when the classical system is regular. We show that for a different set of parameters ($\Gamma = 0.05$) where the classical limit is regular, the choice of measurement in the same regime between classical and quantum also leads to a measurement dependence on the quantum Lyapunov exponent, with chaos being present for the quantum and semiclassical case for a certain choice of measurement. In this case the noise from the measurement drives the system to a large spread in position enabling inter-well transitions which are classically forbidden.

## 7.2 Controlling chaos with adaptive measurement techniques

We have developed a quantum control technique that adaptively changes the measurement phase using a real time feedback in order to control the onset of chaos in the quantum regime. This thesis has demonstrated that adaptive measurement can be used to suppress the onset of chaos in the system and as a result create non-classical states that could be used as a resource. This control can also be used to enhance chaos, pushing its onset further into the quantum regime where it might be more experimentally accessible. We have also discussed in detail the feasibility of implementing this control technique in two experimental realisations: an ultracold atoms experiment and a superconducting qubit experiment.

## 7.3 Opening the quantum driven top

So far we have shown the emergence of chaos from a continuously monitored quantum system, using only one toy model, the Duffing oscillator to obtain numerical results. The question is then is there a general effect that could be seen in other chaotic systems or is this system dependent?

This thesis also investigated the effect of continuous measurement on quantum chaos in another quantum system whose classical limit is chaotic: the driven top. This system was chosen for several reasons, the most important being that it is a system that has been experimentally realised in ultracold atomic experiments in the past [19, 144, 94]. Here, we demonstrate both the effect of continuous measurement on this system and the effect that opening this system to the environment can have on the dynamics. However, the classical limit that is often studied is a closed system governed solely by Hamiltonian dynamics. We show that the effect of opening the system can be detrimental to the degree of chaos, unless the measurement is chosen such that it cancels out the decoherence. In this case the system evolves via the Hamiltonian but with the added noise from the measurement. This system is interesting because it is also a many body system where the interaction between atoms plays a role in the evolution of the system. It is also a system that closely resembles the Hamiltonian that is often considered for quantum metrology. It has also been shown that the presence of chaos in precision measurement with this system may be useful for increasing the Fisher information [42] and therefore the amount of information

that can be gained from the precision measurement in sensors.

## 7.4 Future work

**Lyapunov exponent for quantum driven top**

It is clear that the work on the continuous measurement of the driven top is far from done. In chapter 6 we have attempted to ask the same questions that we have asked for the Duffing oscillator. However we are restricted by the inability to calculate the quantum Lyapunov exponents for the SU(2) system. We have detailed a possible method by which it could be done but further investigations are necessary to ensure the validity of the method.

**Imperfect measurement**

Throughout this thesis, we have assumed an ideal measurement of the open quantum system, of course this is not entirely feasible. The practicality of the adaptive measurement for an experimental realisation would require further investigation into the use of the technique with imperfect measurement signal. The technique as it is relies on the information from the measurement signal to inform the next phase choice for the homodyne measurement scheme. It is expected that there will be some robustness in the technique but this would need to be shown by considering the effect that the signal efficiency will have on the Lyapunov exponent as an outcome. This could be done by considering a stochastic master equation and considering a system-filter separation.

**Adaptive control of driven top**

Can we apply the same control technique using adaptive measurement in order to control the onset of chaos in the driven top? This question is beyond the scope of this thesis but it is one that would be very interesting as a further investigation of the system. Using an adaptive measurement technique enabled us to conclusively demonstrate one mechanism by which chaos emerges from the quantum Duffing oscillator. Whether or not the same technique could be used for the driven top is an intriguing and non-trivial question for future work. The use of an adaptive measurement for Duffing oscillator when the classical system is regular is also something that was beyond the scope of this thesis but is something that has been investigated by Sacha Greenfield concurrent to the research presented here and discussed with collaborators [51].

**Measures of chaos**

Here we have shown the quantum Lyapunov exponent as a method to measure the onset of chaos in the quantum Duffing oscillator and proposed a technique to do the same in the theoretical treatment of the driven top. We have also investigated the possibility of using the breaking time [66, 18] between the classical and quantum dynamics for the same purpose, investigating whether it is suitable to distinguish between different measurements, however there are other methods that probe the signatures of chaos in the quantum system which are experimentally being calculated. The Out of Time Order Correlator (OTOC) is one possible technique that is being studied in the field of quantum chaos at the moment [78, 44, 79, 123, 43, 161, 162, 115]. It remains an open question what the OTOC

would look like for a continuously monitored chaotic system. This would be intriguing to study in future works.

### Negativity

For the quantum Duffing oscillator, we discussed the use of the measure of negativity of the Wigner function as a means to distinguish between the different measurements. This enabled us to understand one of the mechanisms by which chaos emerges from the quantum dynamics. The rapid destruction of interference effects leads to the localisation of the state and this results in the onset of chaos. The question of how the Wigner function behaves for the SU(2) system is intriguing as well however it is beyond the scope of this thesis because of the non-triviality of calculating the Wigner function for the SU(2) states. But if we were to calculate it, would we see the same behaviour as the Duffing oscillator? It seems unlikely given that the measurement induces chaos because of the cancellation of the dephasing terms, leading to the chaotic dynamics and random noise dominating. In this case, should we expect a less localised wavefunction?

# References


[1] Yakir Aharonov, David Z. Albert, and Lev Vaidman. "How the result of a measurement of a component of the spin of a spin-1/2 particle can turn out to be 100". In: *Phys. Rev. Lett.* 60 (14 1988), pp. 1351–1354. DOI: 10.1103/PhysRevLett.60.1351. URL: https://link.aps.org/doi/10.1103/PhysRevLett.60.1351.

[2] A. Bäcker, F. Steiner, and P. Stifter. "Spectral statistics in the quantized cardioid billiard". In: *Phys. Rev. E* 52 (3 1995), pp. 2463–2472. DOI: 10.1103/PhysRevE.52.2463. URL: https://link.aps.org/doi/10.1103/PhysRevE.52.2463.

[3] G. P. Berman and G. M. Zaslavsky. "Condition of stochasticity in quantum nonlinear systems". In: *Physica A: Statistical Mechanics and its Applications* 91.3 (1978), pp. 450–460. DOI: https://doi.org/10.1016/0378-4371(78)90190-5. URL: http://www.sciencedirect.com/science/article/pii/0378437178901905.

[4] D. W. Berry and H. M. Wiseman. "Optimal States and Almost Optimal Adaptive Measurements for Quantum Interferometry". In: *Phys. Rev. Lett.* 85 (24 2000), pp. 5098–5101. DOI: 10.1103/PhysRevLett.85.5098. URL: https://link.aps.org/doi/10.1103/PhysRevLett.85.5098.

[5] M. V. Berry and M. Tabor. "Level Clustering in the Regular Spectrum". In: *Proceedings of the Royal Society of London. Series A, Mathematical and Physical Sciences* 356.1686 (1977), pp. 375–394. ISSN: 00804630. URL: http://www.jstor.org/stable/79349.

[6] Tanmoy Bhattacharya, Salman Habib, and Kurt Jacobs. "Continuous Quantum Measurement and the Emergence of Classical Chaos". In: *Phys. Rev. Lett.* 85 (23 2000), pp. 4852–4855. DOI: 10.1103/PhysRevLett.85.4852. URL: http://link.aps.org/doi/10.1103/PhysRevLett.85.4852.

[7] Tanmoy Bhattacharya, Salman Habib, and Kurt Jacobs. "Continuous quantum measurement and the quantum to classical transition". In: *Phys. Rev. A* 67 (4 2003), p. 042103. DOI: 10.1103/PhysRevA.67.042103. URL: http://link.aps.org/doi/10.1103/PhysRevA.67.042103.

[8] M. S. Blok et al. "Manipulating a qubit through the backaction of sequential partial measurements and real-time feedback". In: *Nature Physics* 10 (Feb. 2014), 189 EP –. URL: https://doi.org/10.1038/nphys2881.

[9] O. Bohigas, M. J. Giannoni, and C. Schmit. "Characterization of Chaotic Quantum Spectra and Universality of Level Fluctuation Laws". In: *Phys. Rev. Lett.* 52 (1 1984), pp. 1–4. DOI: 10.1103/PhysRevLett.52.1. URL: https://link.aps.org/doi/10.1103/PhysRevLett.52.1.

[10] Bose. "Plancks Gesetz und Lichtquantenhypothese". In: *Zeitschrift für Physik* 26.1 (1924), pp. 178–181. DOI: 10.1007/BF01327326. URL: https://doi.org/10.1007/BF01327326.

[11] Samuel Boutin et al. "Effect of Higher-Order Nonlinearities on Amplification and Squeezing in Josephson Parametric Amplifiers". In: *Physical Review Applied* 8.5 (2017). ISSN: 2331-7019. DOI: 10.1103/physrevapplied.8.054030. URL: http://dx.doi.org/10.1103/PhysRevApplied.8.054030.

[12] H. P. Breuer and F. Petruccione. *The theory of Open Quantum Systems*. Oxford University Press, Oxford, 2007.

[13] Todd A Brun, Ian C Percival, and Rudiger Schack. "Quantum chaos in open systems: a quantum state diffusion analysis". In: *Journal of Physics A: Mathematical and General* 29.9 (1996), pp. 2077–2090. URL: http://stacks.iop.org/0305-4470/29/2077.

[14] A. O. Caldeira and A. J. Leggett. "Path integral approach to quantum Brownian motion". In: *Physica A: Statistical Mechanics and its Applications* 121.3 (1983), pp. 587–616. DOI: https://doi.org/10.1016/0378-4371(83)90013-4. URL: http://www.sciencedirect.com/science/article/pii/0378437183900134.

[15] P. Campagne-Ibarcq et al. "Observing Quantum State Diffusion by Heterodyne Detection of Fluorescence". In: *Phys. Rev. X* 6 (1 2016), p. 011002. DOI: 10.1103/PhysRevX.6.011002. URL: https://link.aps.org/doi/10.1103/PhysRevX.6.011002.

[16] H. Carmichael. "An Open Systems Approach to Quantum Optics". In: *An Open Systems Approach to Quantum Optics: Lectures Presented at the Université Libre de Bruxelles October 28 to November 4, 1991, Lecture Notes in Physics Monographs, Volume 18. ISBN 978-3-540-56634-2. Springer Berlin Heidelberg, 1993* 18 (1993). DOI: 10.1007/978-3-540-47620-7.

[17] A. R. R. Carvalho and A. Buchleitner. "Web-assisted tunneling in the kicked harmonic oscillator". In: *Phys. Rev. Lett.* 92 (2004), p. 204101.

[18] A. R. R. Carvalho, R. L. de Matos Filho, and L. Davidovich. "Environmental effects in the quantum-classical transition for the delta-kicked harmonic oscillator". In: *Phys. Rev. E* 70.2 (2004), p. 026211. DOI: 10.1103/PhysRevE.70.026211.

[19] S. Chaudhury et al. "Quantum signatures of chaos in a kicked top". In: *Nature* 461.7265 (Oct. 2009), pp. 768–771. URL: http://dx.doi.org/10.1038/nature08396.

[20] Dante R. Chialvo, Robert F. Gilmour Jr, and Jose Jalife. "Low dimensional chaos in cardiac tissue". In: *Nature* 343.6259 (1990), pp. 653–657. DOI: 10.1038/343653a0. URL: https://doi.org/10.1038/343653a0.

[21] Cheng Chin et al. "Feshbach resonances in ultracold gases". In: *Rev. Mod. Phys.* 82 (2 2010), pp. 1225–1286. DOI: 10.1103/RevModPhys.82.1225. URL: https://link.aps.org/doi/10.1103/RevModPhys.82.1225.

[22] P. F. Cohadon, A. Heidmann, and M. Pinard. "Cooling of a Mirror by Radiation Pressure". In: *Phys. Rev. Lett.* 83 (16 1999), pp. 3174–3177. DOI: 10.1103/PhysRevLett.83.3174. URL: https://link.aps.org/doi/10.1103/PhysRevLett.83.3174.

[23] J. Cramer et al. "Repeated quantum error correction on a continuously encoded qubit by real-time feedback". In: *Nature Communications* 7 (May 2016), 11526 EP –. URL: https://doi.org/10.1038/ncomms11526.

[24] Graham R. Dennis, Joseph J. Hope, and Mattias T. Johnsson. "XMDS2: Fast, scalable simulation of coupled stochastic partial differential equations". In: *Computer Physics Communications* 184.1 (2013), pp. 201 –208. ISSN: 0010-4655. DOI: https://doi.org/10.1016/j.cpc.2012.08.016. URL: http://www.sciencedirect.com/science/article/pii/S0010465512002822.

[25] L. Diosi. "Quantum Measurements and Stochastic Processes". In: *Phys. Lett. A* 114 (1986), p. 451.

[26] P. A. M. Dirac. "The quantum theory of the emission and absorption of radiation". In: *Proc. Roy. Soc. London. A* 114 (1927), p. 243.

[27] T. Dittrich and R. Graham. "Continuous Measurements on the Quantum Kicked Rotor". In: *EPL (Europhysics Letters)* 11.7 (1990), p. 589. URL: http://stacks.iop.org/0295-5075/11/i=7/a=002.

[28] T. Dittrich and R. Graham. "Quantum Effects in the Steady State of the Dissipative Standard Map". In: *EPL (Europhysics Letters)* 4.3 (1987), p. 263. URL: http://stacks.iop.org/0295-5075/4/i=3/a=002.

[29] Andrew C. Doherty et al. "Quantum feedback control and classical control theory". In: *Phys. Rev. A* 62 (1 2000), p. 012105. DOI: 10.1103/PhysRevA.62.012105. URL: https://link.aps.org/doi/10.1103/PhysRevA.62.012105.

[30] Georg Duffing. *Erzwungene Schwingungen bei veränderlicher Eigenfrequenz und ihre technische Bedeutung*. 41-42. R, Vieweg & Sohn, 1918.

[31] G. J. Duffy et al. "Experimental investigation of early-time diffusion in the quantum kicked rotor using a Bose-Einstein condensate". In: *Phys. Rev. E* 70 (5 2004), p. 056206. DOI: 10.1103/PhysRevE.70.056206. URL: http://link.aps.org/doi/10.1103/PhysRevE.70.056206.

[32] F. J. Dyson. "The Threefold Way. Algebraic Structure of Symmetry Groups and Ensembles in Quantum Mechanics". In: *Journal of Mathematical Physics* 3 (Nov. 1962), pp. 1199–1215. DOI: 10.1063/1.1703863.

[33] Jessica K. Eastman, Joseph J. Hope, and André R. R. Carvalho. "Tuning quantum measurements to control chaos". In: *Scientific Reports* 7 (2017), p. 44684. ISSN: 2045-2322. DOI: 10.1038/srep44684. URL: http://dx.doi.org/10.1038/srep44684.

[34] A. Eddins et al. "Stroboscopic Qubit Measurement with Squeezed Illumination". In: *Physical Review Letters* 120.4 (2018). ISSN: 1079-7114. DOI: 10.1103/physrevlett.120.040505. URL: http://dx.doi.org/10.1103/PhysRevLett.120.040505.

[35] P. Ehrenfest. "Bemerkung über die angenäherte Gültigkeit der klassischen Mechanik innerhalb der Quantenmechanik". In: *Zeitschrift für Physik* 45.7 (1927), pp. 455–457. DOI: 10.1007/BF01329203. URL: https://doi.org/10.1007/BF01329203.

[36] A Einstein. "Quantentheorie des einatomigen idealen Gases, Sitzungsberichte Kgl". In: *Preuss. Akad. Wiss* 261 (1924).

[37] A. Elben et al. "Rényi Entropies from Random Quenches in Atomic Hubbard and Spin Models". In: *Phys. Rev. Lett.* 120 (5 2018), p. 050406. DOI: 10.1103/PhysRevLett.120.050406. URL: https://link.aps.org/doi/10.1103/PhysRevLett.120.050406.

[38] A. Erturk and D.J. Inman. "Broadband piezoelectric power generation on high-energy orbits of the bistable Duffing oscillator with electromechanical coupling". In: *Journal of Sound and Vibration* 330.10 (2011). Dynamics of Vibro-Impact Systems, pp. 2339 –2353. ISSN: 0022-460X. DOI: http://dx.doi.org/10.1016/j.jsv.2010.11.018. URL: http://www.sciencedirect.com/science/article/pii/S0022460X10007807.

[39] P. J. Everitt et al. "Observation of a modulational instability in Bose-Einstein condensates". In: *Phys. Rev. A* 96 (4 2017), p. 041601. DOI: 10.1103/PhysRevA.96.041601. URL: https://link.aps.org/doi/10.1103/PhysRevA.96.041601.

[40] Bianca Borem Ferreira, Marcelo Amorim Savi, and Aline Souza de Paula. "Chaos control applied to cardiac rhythms represented by ECG signals". In: *Physica Scripta* 89.10 (2014), p. 105203. URL: http://stacks.iop.org/1402-4896/89/i=10/a=105203.

[41] R. P Feynman and F. L Vernon. "The theory of a general quantum system interacting with a linear dissipative system". In: *Annals of Physics* 24 (1963), pp. 118–173. DOI: https://doi.org/10.1016/0003-4916(63)90068-X. URL: http://www.sciencedirect.com/science/article/pii/000349166390068X.

[42] Lukas J. Fiderer and Daniel Braun. "Quantum metrology with quantum-chaotic sensors". In: *Nature Communications* 9.1 (2018), p. 1351. DOI: 10.1038/s41467-018-03623-z. URL: https://doi.org/10.1038/s41467-018-03623-z.

[43] Ignacio García-Mata et al. "Chaos Signatures in the Short and Long Time Behavior of the Out-of-Time Ordered Correlator". In: *Phys. Rev. Lett.* 121 (21 2018), p. 210601. DOI: 10.1103/PhysRevLett.121.210601. URL: https://link.aps.org/doi/10.1103/PhysRevLett.121.210601.

[44] Martin Gärttner et al. "Measuring out-of-time-order correlations and multiple quantum spectra in a trapped-ion quantum magnet". In: *Nature Physics* 13.8 (2017), pp. 781–786. ISSN: 1745-2481. DOI: 10.1038/nphys4119. URL: http://dx.doi.org/10.1038/NPHYS4119.

[45] G. Gauthier et al. "Direct imaging of a digital-micromirror device for configurable microscopic optical potentials". In: *Optica* 3.10 (2016), pp. 1136–1143. DOI: 10.1364/OPTICA.3.001136. URL: http://www.osapublishing.org/optica/abstract.cfm?URI=optica-3-10-1136.

[46] Shohini Ghose et al. "Chaos, entanglement, and decoherence in the quantum kicked top". In: *Phys. Rev. A* 78 (4 2008), p. 042318. DOI: 10.1103/PhysRevA.78.042318. URL: http://link.aps.org/doi/10.1103/PhysRevA.78.042318.

[47] Shohini Ghose et al. "Recovering classical dynamics from coupled quantum systems through continuous measurement". In: *Phys. Rev. A* 67 (5 2003), p. 052102. DOI: 10.1103/PhysRevA.67.052102. URL: http://link.aps.org/doi/10.1103/PhysRevA.67.052102.

[48] Shohini Ghose et al. "Transition to classical chaos in a coupled quantum system through continuous measurement". In: *Phys. Rev. A* 69 (5 2004), p. 052116. DOI: 10.1103/PhysRevA.69.052116. URL: http://link.aps.org/doi/10.1103/PhysRevA.69.052116.

[49] Vittorio Giovannetti, Seth Lloyd, and Lorenzo Maccone. "Quantum Metrology". In: *Phys. Rev. Lett.* 96 (1 2006), p. 010401. DOI: 10.1103/PhysRevLett.96.010401. URL: https://link.aps.org/doi/10.1103/PhysRevLett.96.010401.

[50] Roy J. Glauber. "Coherent and Incoherent States of the Radiation Field". In: *Phys. Rev.* 131 (6 1963), pp. 2766–2788. DOI: 10.1103/PhysRev.131.2766. URL: https://link.aps.org/doi/10.1103/PhysRev.131.2766.

[51] S. Greenfield. "Adaptive measurement semiclassical Duffing oscillator". This is unpublished research.

[52] Arne L. Grimsmo. "Time-Delayed Quantum Feedback Control". In: *Phys. Rev. Lett.* 115 (6 2015), p. 060402. DOI: 10.1103/PhysRevLett.115.060402. URL: https://link.aps.org/doi/10.1103/PhysRevLett.115.060402.

[53] F. Haake, M. Kuś, and R. Scharf. "Classical and quantum chaos for a kicked top". In: *Zeitschrift für Physik B Condensed Matter* 65.3 (1987), pp. 381–395. DOI: 10.1007/BF01303727. URL: http://dx.doi.org/10.1007/BF01303727.

[54] Salman Habib, Kurt Jacobs, and Kosuke Shizume. "Emergence of Chaos in Quantum Systems Far from the Classical Limit". In: *Physical Review Letters* 96.1, 010403 (2006), p. 010403. DOI: 10.1103/PhysRevLett.96.010403. URL: http://link.aps.org/abstract/PRL/v96/e010403.

[55] Salman Habib, Kosuke Shizume, and Wojciech Hubert Zurek. "Decoherence, Chaos, and the Correspondence Principle". In: *Phys. Rev. Lett.* 80 (20 1998), pp. 4361–4365. DOI: 10.1103/PhysRevLett.80.4361. URL: http://link.aps.org/doi/10.1103/PhysRevLett.80.4361.

[56] Ryan Hamerly and Hideo Mabuchi. "Coherent controllers for optical-feedback cooling of quantum oscillators". In: *Phys. Rev. A* 87 (1 2013), p. 013815. DOI: 10.1103/PhysRevA.87.013815. URL: https://link.aps.org/doi/10.1103/PhysRevA.87.013815.

[57] Klemens Hammerer, Anders S. Sørensen, and Eugene S. Polzik. "Quantum interface between light and atomic ensembles". In: *Rev. Mod. Phys.* 82 (2 2010), pp. 1041–1093. DOI: 10.1103/RevModPhys.82.1041. URL: https://link.aps.org/doi/10.1103/RevModPhys.82.1041.

[58] Ramon van Handel, John K Stockton, and Hideo Mabuchi. "Modelling and feedback control design for quantum state preparation". In: *Journal of Optics B: Quantum and Semiclassical Optics* 7.10 (2005), S179. URL: http://stacks.iop.org/1464-4266/7/i=10/a=001.

[59] Serge Haroche and Jean-Michel Raimond. *Exploring the Quantum: Atoms, Cavities, and Photons (Oxford Graduate Texts)*. 1st ed. Oxford University Press, USA, Oct. 2006. ISBN: 0198509146. URL: http://www.amazon.com/exec/obidos/redirect?tag=citeulike07-20\&path=ASIN/0198509146.

[60] Aram W. Harrow and Ashley Montanaro. "Quantum computational supremacy". In: *Nature* 549 (Sept. 2017), 203 EP –. URL: https://doi.org/10.1038/nature23458.

[61] B. L. Higgins et al. "Entanglement-free Heisenberg-limited phase estimation". In: *Nature* 450 (Nov. 2007), 393 EP –. URL: http://dx.doi.org/10.1038/nature06257.

[62] Masashi Hirose and Paola Cappellaro. "Coherent feedback control of a single qubit in diamond". In: *Nature* 532 (Apr. 2016), 77 EP –. URL: https://doi.org/10.1038/nature17404.

[63] O. Hosten et al. "Quantum phase magnification". In: *Science* 352.6293 (2016), pp. 1552–1555. ISSN: 0036-8075. DOI: 10.1126/science.aaf3397. eprint: http://science.sciencemag.org/content/352/6293/1552.full.pdf. URL: http://science.sciencemag.org/content/352/6293/1552.

[64] M R Hush et al. "Controlling spontaneous-emission noise in measurement-based feedback cooling of a BoseÄìEinstein condensate". In: *New Journal of Physics* 15.11 (2013), p. 113060. URL: http://stacks.iop.org/1367-2630/15/i=11/a=113060.

[65] Kocirc;di HUSIMI. "Some Formal Properties of the Density Matrix". In: *Proceedings of the Physico-Mathematical Society of Japan. 3rd Series* 22.4 (1940), pp. 264–314. DOI: 10.11429/ppmsj1919.22.4_264.

[66] A. Iomin and G. M. Zaslavsky. "Breaking time for the quantum chaotic attractor". In: *Phys. Rev. E* 67 (2 2003), p. 027203. DOI: 10.1103/PhysRevE.67.027203. URL: https://link.aps.org/doi/10.1103/PhysRevE.67.027203.

[67] Holger Kantz and Thomas Schreiber. *Nonlinear Time Series Analysis*. Cambridge: Cambridge University Press, 2003. ISBN: 9780521529020. DOI: DOI:10.1017/CBO9780511755798. URL: https://www.cambridge.org/core/books/nonlinear-time-series-analysis/519783E4E8A2C3DCD4641E42765309C7.

[68] Arie Kapulkin and Arjendu K. Pattanayak. "Nonmonotonicity in the Quantum-Classical Transition: Chaos Induced by Quantum Effects". In: *Physical Review Letters* 101.7, 074101 (2008), p. 074101. DOI: 10.1103/PhysRevLett.101.074101. URL: http://link.aps.org/abstract/PRL/v101/e074101.

[69] Anatole Kenfack and Karol Życzkowski. "Negativity of the Wigner function as an indicator of non-classicality". In: *Journal of Optics B: Quantum and Semiclassical Optics* 6.10 (2004), p. 396. URL: http://stacks.iop.org/1464-4266/6/i=10/a=003.

[70] R. A. Kidd, M. K. Olsen, and J. F. Corney. "Quantum chaos in a Bose-Hubbard dimer with modulated tunneling". In: *Phys. Rev. A* 100 (1 2019), p. 013625. DOI: 10.1103/PhysRevA.100.013625. URL: https://link.aps.org/doi/10.1103/PhysRevA.100.013625.

[71] Masahiro Kitagawa and Masahito Ueda. "Squeezed spin states". In: *Phys. Rev. A* 47 (6 1993), pp. 5138–5143. DOI: 10.1103/PhysRevA.47.5138. URL: https://link.aps.org/doi/10.1103/PhysRevA.47.5138.

[72] B.G. Klappauf et al. "Quantum chaos with cesium atoms: pushing the boundaries". In: *Physica D: Nonlinear Phenomena* 131.1â4 (1999). Classical Chaos and its Quantum Manifestations, pp. 78 –89. ISSN: 0167-2789. DOI: http://dx.doi.org/10.1016/S0167-2789(98)00221-8. URL: http://www.sciencedirect.com/science/article/pii/S0167278998002218.

[73] A. Kolovsky and A. Buchleitner. "Quantum Chaos in the Bose-Hubbard model". In: *Europhys. Lett.* 68 (2004), p. 632.

[74] K Kraus. "General state changes in quantum theory". In: *Annals of Physics* 64.2 (1971), pp. 311–335. DOI: https://doi.org/10.1016/0003-4916(71)90108-4. URL: http://www.sciencedirect.com/science/article/pii/0003491671901084.

[75] Aravind Kumar, Shaikh Faruque Ali, and A. Arockiarajan. "Enhanced Energy Harvesting from Nonlinear Oscillators via Chaos Control". In: *IFAC-PapersOnLine* 49.1 (2016), pp. 35–40. ISSN: 2405-8963. DOI: http://dx.doi.org/10.1016/j.ifacol.2016.03.025. URL: http://www.sciencedirect.com/science/article/pii/S2405896316300258.

[76] F. C. M. Lau and C. K. Tse. *Chaos-Based Digital Communication Systems*. Springer, Berlin, Heidelberg, 2003.

[77] U. Leonhardt, P.L. Knight, and A. Miller. *Measuring the Quantum State of Light*. Cambridge Studies in Modern Optics. Cambridge University Press, 1997. ISBN: 9780521497305. URL: https://books.google.co.uk/books?id=wmsJy1A_cyIC.

[78] R. J. Lewis-Swan et al. "Unifying scrambling, thermalization and entanglement through measurement of fidelity out-of-time-order correlators in the Dicke model". In: *Nature Communications* 10.1 (2019), p. 1581. DOI: 10.1038/s41467-019-09436-y. URL: https://doi.org/10.1038/s41467-019-09436-y.

[79] Jun Li et al. "Measuring Out-of-Time-Order Correlators on a Nuclear Magnetic Resonance Quantum Simulator". In: *Physical Review X* 7.3 (2017). ISSN: 2160-3308. DOI: 10.1103/physrevx.7.031011. URL: http://dx.doi.org/10.1103/PhysRevX.7.031011.

[80] Sheng-Kai Liao et al. "Satellite-to-ground quantum key distribution". In: *Nature* 549 (Aug. 2017), 43 EP –. URL: https://doi.org/10.1038/nature23655.

[81] G. Lindblad. "On the generators of quantum dynamical semigroups". In: *Comm. Math. Phys.* 48.2 (1976), pp. 119–130. URL: https://projecteuclid.org:443/euclid.cmp/1103899849.

[82] D. Linnemann et al. "Quantum-Enhanced Sensing Based on Time Reversal of Nonlinear Dynamics". In: *Physical Review Letters* 117.1 (2016). ISSN: 1079-7114. DOI: 10.1103/physrevlett.117.013001. URL: http://dx.doi.org/10.1103/PhysRevLett.117.013001.

[83] M. Lombardi and A. Matzkin. "Entanglement and chaos in the kicked top". In: *Phys. Rev. E* 83 (1 2011), p. 016207. DOI: 10.1103/PhysRevE.83.016207. URL: http://link.aps.org/doi/10.1103/PhysRevE.83.016207.

[84] Edward N. Lorenz. "Deterministic Nonperiodic Flow". In: *Journal of the Atmospheric Sciences* 20.2 (1963), pp. 130–141. DOI: 10.1175/1520-0469(1963)020<0130:DNF>2.0.CO;2. URL: https://doi.org/10.1175/1520-0469(1963)020<0130:DNF>2.0.CO;2.

[85] Juan Maldacena, Stephen H. Shenker, and Douglas Stanford. "A bound on chaos". In: *Journal of High Energy Physics* 2016.8 (2016), p. 106. ISSN: 1029-8479. DOI: 10.1007/JHEP08(2016)106. URL: https://doi.org/10.1007/JHEP08(2016)106.

[86] V. E. Manucharyan et al. "Microwave bifurcation of a Josephson junction: Embedding-circuit requirements". In: *Physical Review B* 76.1 (2007). ISSN: 1550-235X. DOI: 10.1103/physrevb.76.014524. URL: http://dx.doi.org/10.1103/PhysRevB.76.014524.

[87] G. D. McDonald et al. "Bright Solitonic Matter-Wave Interferometer". In: *Phys. Rev. Lett.* 113 (1 2014), p. 013002. DOI: 10.1103/PhysRevLett.113.013002. URL: https://link.aps.org/doi/10.1103/PhysRevLett.113.013002.

[88] E. J. Meier et al. "Exploring quantum signatures of chaos on a Floquet synthetic lattice". In: *ArXiv e-prints* (May 2017). arXiv: 1705.06714 [cond-mat.quant-gas].

[89] G. J. Milburn et al. "Quantum dynamics of an atomic Bose-Einstein condensate in a double-well potential". In: *Phys. Rev. A* 55 (6 1997), pp. 4318–4324. DOI: 10.1103/PhysRevA.55.4318. URL: https://link.aps.org/doi/10.1103/PhysRevA.55.4318.

[90] Vincent Mourik et al. "Exploring quantum chaos with a single nuclear spin". In: *Phys. Rev. E* 98 (4 2018), p. 042206. DOI: 10.1103/PhysRevE.98.042206. URL: https://link.aps.org/doi/10.1103/PhysRevE.98.042206.

[91] J. T. Muhonen et al. "Coherent control via weak measurements in $^{31}$P single-atom electron and nuclear spin qubits". In: *ArXiv e-prints* (Feb. 2017). arXiv: 1702.07991 [quant-ph].

[92] Manuel H. Muñoz-Arias et al. *Simulating nonlinear dynamics of collective spins via quantum measurement and feedback*. 2019. arXiv: 1907.12606 [quant-ph].

[93] K. W. Murch et al. "Observing single quantum trajectories of a superconducting quantum bit". In: *Nature* 502 (Oct. 2013), 211 EP –. URL: https://doi.org/10.1038/nature12539.

[94] C. Neill et al. "Ergodic dynamics and thermalization in an isolated quantum system". In: *Nat Phys* 12.11 (Nov. 2016), pp. 1037–1041. URL: http://dx.doi.org/10.1038/nphys3830.

[95] And Lorenzo Maccone. "Using Entanglement Against Noise in Quantum Metrology". In: *Phys. Rev. Lett.* 113 (25 2014), p. 250801. DOI: 10.1103/PhysRevLett.113.250801. URL: https://link.aps.org/doi/10.1103/PhysRevLett.113.250801.

[96] Michael A. Nielsen and Isaac L. Chuang. *Quantum Computation and Quantum Information: 10th Anniversary Edition*. 10th. New York, NY, USA: Cambridge University Press, 2011. ISBN: 1107002176, 9781107002173.

[97] Samuel P. Nolan, Stuart S. Szigeti, and Simon A. Haine. "Optimal and Robust Quantum Metrology Using Interaction-Based Readouts". In: *Phys. Rev. Lett.* 119 (19 2017), p. 193601. DOI: 10.1103/PhysRevLett.119.193601. URL: https://link.aps.org/doi/10.1103/PhysRevLett.119.193601.

[98] V. I. Oseledets. "A multiplicative ergodic theorem. Lyapunov characteristic numbers for dynamical systems". In: *Trans. Moscow Math. Soc.* 19 (1968), pp. 197–231.

[99] Yukihiro Ota and Ichiro Ohba. "Crossover from classical to quantum behavior of the Duffing oscillator through a pseudo-Lyapunov-exponent". In: *Phys. Rev. E* 71 (1 2005), p. 015201. DOI: 10.1103/PhysRevE.71.015201. URL: http://link.aps.org/doi/10.1103/PhysRevE.71.015201.

[100] E. Ott, T. M. Antonsen, and J. D. Hanson. "Effect of Noise on Time-Dependent Quantum Chaos". In: *Phys. Rev. Lett.* 53 (23 1984), pp. 2187–2190. DOI: 10.1103/PhysRevLett.53.2187. URL: http://link.aps.org/doi/10.1103/PhysRevLett.53.2187.

[101] Edward Ott, Celso Grebogi, and James A. Yorke. "Controlling chaos". In: *Phys. Rev. Lett.* 64.11 (1990).

[102] Arjendu K. Pattanayak and William C. Schieve. "Gaussian wave-packet dynamics: Semiquantal and semiclassical phase-space formalism". In: *Phys. Rev. E* 50 (5 1994), pp. 3601–3615. DOI: 10.1103/PhysRevE.50.3601. URL: https://link.aps.org/doi/10.1103/PhysRevE.50.3601.

[103] Arjendu K. Pattanayak, Bala Sundaram, and Benjamin D. Greenbaum. "Parameter Scaling in the Decoherent Quantum-Classical Transition for Chaotic Systems". In: *Phys. Rev. Lett.* 90 (1 2003), p. 014103. DOI: 10.1103/PhysRevLett.90.014103. URL: http://link.aps.org/doi/10.1103/PhysRevLett.90.014103.

[104] B. Peaudecerf et al. "Adaptive Quantum Nondemolition Measurement of a Photon Number". In: *Phys. Rev. Lett.* 112 (8 2014), p. 080401. DOI: 10.1103/PhysRevLett.112.080401. URL: http://link.aps.org/doi/10.1103/PhysRevLett.112.080401.

[105] Ian Percival. *Quantum State Diffusion*. Jan. 1999.

[106] Luca Pezzè et al. "Quantum metrology with nonclassical states of atomic ensembles". In: *Rev. Mod. Phys.* 90 (3 2018), p. 035005. DOI: 10.1103/RevModPhys.90.035005. URL: https://link.aps.org/doi/10.1103/RevModPhys.90.035005.

[107] B. Pokharel et al. "Dynamical complexity in the quantum to classical transition". In: *ArXiv e-prints* (Apr. 2016). arXiv: 1604.02743 [quant-ph].

[108] Bibek Pokharel et al. "Chaos and dynamical complexity in the quantum to classical transition". In: *Scientific Reports* 8.1 (2018). ISSN: 2045-2322. DOI: 10.1038/s41598-018-20507-w. URL: http://dx.doi.org/10.1038/s41598-018-20507-w.

[109] K. Pyragas. "Continuous control of chaos by self-controlling feedback". In: *Physics Letters A* 170.6 (1992), pp. 421–428. DOI: https://doi.org/10.1016/0375-9601(92)90745-8. URL: http://www.sciencedirect.com/science/article/pii/0375960192907458.

[110] J M Radcliffe. "Some properties of coherent spin states". In: *Journal of Physics A: General Physics* 4.3 (1971), pp. 313–323. DOI: 10.1088/0305-4470/4/3/009. URL: https://doi.org/10.1088%2F0305-4470%2F4%2F3%2F009.

[111] Paul M Radmore and Stephen M Barnett. *Methods in theoretical quantum optics*. Cambridge University Press, 1997.

[112] M. G. Raizen et al. "An experimental realization of the quantum -kicked rotor". In: *Quantum and Semiclassical Optics: Journal of the European Optical Society Part B* 8 (1996), pp. 687–692.

[113] Jason F. Ralph, Kurt Jacobs, and Mark J. Everitt. "Observing quantum chaos with noisy measurements and highly mixed states". In: *Physical Review A* 95.1 (2017). ISSN: 2469-9934. DOI: 10.1103/physreva.95.012135. URL: http://dx.doi.org/10.1103/PhysRevA.95.012135.

[114] T C Ralph, A P Lund, and H M Wiseman. "Adaptive phase measurements in linear optical quantum computation". In: *Journal of Optics B: Quantum and Semiclassical Optics* 7.10 (2005), S245. URL: http://stacks.iop.org/1464-4266/7/i=10/a=007.

[115] Josef Rammensee, Juan Diego Urbina, and Klaus Richter. "Many-Body Quantum Interference and the Saturation of Out-of-Time-Order Correlators". In: *Phys. Rev. Lett.* 121 (12 2018), p. 124101. DOI: 10.1103/PhysRevLett.121.124101. URL: https://link.aps.org/doi/10.1103/PhysRevLett.121.124101.

[116] Alexander K. Ratcliffe et al. "Scaling Trapped Ion Quantum Computers Using Fast Gates and Microtraps". In: *Phys. Rev. Lett.* 120 (22 2018), p. 220501. DOI: 10.1103/PhysRevLett.120.220501. URL: https://link.aps.org/doi/10.1103/PhysRevLett.120.220501.

[117] M Rigo and N Gisin. "Unravellings of the master equation and the emergence of a classical world". In: *Quantum and Semiclassical Optics: Journal of the European Optical Society Part B* 8.1 (1996), p. 255.

[118] M Rigo, F Mota-Furtado, and P F O'Mahony. "Continuous stochastic Schrödinger equations and localization". In: *Journal of Physics A: Mathematical and General* 30.21 (1997), p. 7557.

[119] N. Roch et al. "Observation of Measurement-Induced Entanglement and Quantum Trajectories of Remote Superconducting Qubits". In: *Phys. Rev. Lett.* 112 (17 2014), p. 170501. DOI: 10.1103/PhysRevLett.112.170501. URL: https://link.aps.org/doi/10.1103/PhysRevLett.112.170501.

[120] Filipe J. Romeiras et al. "Controlling chaotic dynamical systems". In: *Physica D* 58 (1992), pp. 165–192.

[121] Andreas. Rößler. "Runge–Kutta Methods for the Strong Approximation of Solutions of Stochastic Differential Equations". In: *SIAM Journal on Numerical Analysis* 48.3 (2010), pp. 922–952. DOI: 10.1137/09076636X. URL: https://doi.org/10.1137/09076636X.

[122] Otto E. Rössler. "Chaos and Chemistry". In: *Nonlinear Phenomena in Chemical Dynamics*. Ed. by Christian Vidal and Adolphe Pacault. Berlin, Heidelberg: Springer Berlin Heidelberg, 1981, pp. 79–87. ISBN: 978-3-642-81778-6.

[123] Efim B. Rozenbaum, Sriram Ganeshan, and Victor Galitski. "Lyapunov Exponent and Out-of-Time-Ordered Correlator's Growth Rate in a Chaotic System". In: *Physical Review Letters* 118.8 (2017). ISSN: 1079-7114. DOI: 10.1103/physrevlett.118.086801. URL: http://dx.doi.org/10.1103/PhysRevLett.118.086801.

[124] M. F. Santos et al. "Quantum Computing with Incoherent Resources and Quantum Jumps". In: *Phys. Rev. Lett.* 108 (17 2012), p. 170501. DOI: 10.1103/PhysRevLett.108.170501. URL: https://link.aps.org/doi/10.1103/PhysRevLett.108.170501.

[125] R Schack, T A Brun, and I C Percival. "Quantum state diffusion, localization and computation". In: *Journal of Physics A: Mathematical and General* 28.18 (1995), p. 5401. URL: http://stacks.iop.org/0305-4470/28/i=18/a=028.

[126] Athreya Shankar et al. "Continuous Real-Time Tracking of a Quantum Phase Below the Standard Quantum Limit". In: *Physical Review Letters* 122.23 (2019). ISSN: 1079-7114. DOI: 10.1103/physrevlett.122.233602. URL: http://dx.doi.org/10.1103/PhysRevLett.122.233602.

[127] Stephen H. Shenker and Douglas Stanford. "Black holes and the butterfly effect". In: *Journal of High Energy Physics* 2014.3 (2014), p. 67. DOI: 10.1007/JHEP03(2014)067. URL: https://doi.org/10.1007/JHEP03(2014)067.

[128] Lukas M. Sieberer et al. "Digital quantum simulation, Trotter errors, and quantum chaos of the kicked top". In: *npj Quantum Information* 5.1 (2019), p. 78. DOI: 10.1038/s41534-019-0192-5. URL: https://doi.org/10.1038/s41534-019-0192-5.

[129] James E. Skinner et al. "Application of chaos theory to biology and medicine". In: *Integrative Physiological and Behavioral Science* 27.1 (1992), pp. 39–53. DOI: 10.1007/BF02691091. URL: https://doi.org/10.1007/BF02691091.

[130] G. Spagnolli et al. "Crossing Over from Attractive to Repulsive Interactions in a Tunneling Bosonic Josephson Junction". In: *Phys. Rev. Lett.* 118 (23 2017), p. 230403. DOI: 10.1103/PhysRevLett.118.230403. URL: https://link.aps.org/doi/10.1103/PhysRevLett.118.230403.

[131] T.P. Spiller and J.F. Ralph. "The emergence of chaos in an open quantum system". In: *Physics Letters A* 194.4 (1994), pp. 235 –240. ISSN: 0375-9601. DOI: 10.1016/0375-9601(94)91244-0. URL: http://www.sciencedirect.com/science/article/pii/0375960194912440.

[132] Helmut Strobel et al. "Fisher information and entanglement of non-Gaussian spin states". In: *Science* 345.6195 (2014), pp. 424–427. ISSN: 0036-8075. DOI: 10.1126/science.1250147. eprint: http://science.sciencemag.org/content/345/6195/424.full.pdf. URL: http://science.sciencemag.org/content/345/6195/424.

[133] S.H. Strogatz. *Nonlinear Dynamics and Chaos: With Applications to Physics, Biology, Chemistry, and Engineering*. Studies in Nonlinearity. Avalon Publishing, 2014. ISBN: 9780813349114. URL: https://books.google.co.uk/books?id=jeFVDgAAQBAJ.

[134] Gerald Jay Sussman and Jack Wisdom. "Chaotic Evolution of the Solar System". In: *Science* 257.5066 (1992), pp. 56–62. ISSN: 0036-8075. DOI: 10.1126/science.257.5066.56. eprint: https://science.sciencemag.org/content/257/5066/56.full.pdf. URL: https://science.sciencemag.org/content/257/5066/56.

[135] Brian Swingle et al. "Measuring the scrambling of quantum information". In: *Physical Review A* 94.4 (2016). ISSN: 2469-9934. DOI: 10.1103/physreva.94.040302. URL: http://dx.doi.org/10.1103/PhysRevA.94.040302.

[136] S. S. Szigeti et al. "Continuous measurement feedback control of a Bose-Einstein condensate using phase-contrast imaging". In: *Phys. Rev. A* 80 (1 2009), p. 013614. DOI: 10.1103/PhysRevA.80.013614. URL: https://link.aps.org/doi/10.1103/PhysRevA.80.013614.

[137] S. S. Szigeti et al. "Feedback control of an interacting Bose-Einstein condensate using phase-contrast imaging". In: *Phys. Rev. A* 82 (4 2010), p. 043632. DOI: 10.1103/PhysRevA.82.043632. URL: https://link.aps.org/doi/10.1103/PhysRevA.82.043632.

[138] S. S. Szigeti et al. "Robustness of system-filter separation for the feedback control of a quantum harmonic oscillator undergoing continuous position measurement". In: *Phys. Rev. A* 87 (1 2013), p. 013626. DOI: 10.1103/PhysRevA.87.013626. URL: http://link.aps.org/doi/10.1103/PhysRevA.87.013626.

[139] Stuart S. Szigeti, Robert J. Lewis-Swan, and Simon A. Haine. "Pumped-Up SU(1,1) Interferometry". In: *Phys. Rev. Lett.* 118 (15 2017), p. 150401. DOI: 10.1103/PhysRevLett.118.150401. URL: https://link.aps.org/doi/10.1103/PhysRevLett.118.150401.

[140] Stuart S. Szigeti et al. "Ignorance Is Bliss: General and Robust Cancellation of Decoherence via No-Knowledge Quantum Feedback". In: *Phys. Rev. Lett.* 113 (2 2014), p. 020407. DOI: 10.1103/PhysRevLett.113.020407. URL: https://link.aps.org/doi/10.1103/PhysRevLett.113.020407.

[141] Stuart S. Szigeti et al. "Squeezed-light-enhanced atom interferometry below the standard quantum limit". In: *Phys. Rev. A* 90 (6 2014), p. 063630. DOI: 10.1103/PhysRevA.90.063630. URL: https://link.aps.org/doi/10.1103/PhysRevA.90.063630.

[142] P. Szlachetka and K. Grygiel. "Chaos in Optical Systems". In: *Modern Nonlinear Optics*. John Wiley Sons, Ltd, 2002, pp. 353–427. ISBN: 9780471231486. DOI: 10.1002/0471231487.ch4. eprint: https://onlinelibrary.wiley.com/doi/pdf/10.1002/0471231487.ch4. URL: https://onlinelibrary.wiley.com/doi/abs/10.1002/0471231487.ch4.

[143] Matthew S. Taubman et al. "Intensity feedback effects on quantum-limited noise". In: *Journal of the Optical Society of America B* 12.10 (1995), pp. 1792–1800. DOI: 10.1364/JOSAB.12.001792. URL: http://josab.osa.org/abstract.cfm?URI=josab-12-10-1792.

[144] J. Tomkovič et al. "Experimental observation of the Poincaré-Birkhoff scenario in a driven many-body quantum system". In: *Physical Review A* 95.1 (2017). ISSN: 2469-9934. DOI: 10.1103/physreva.95.011602. URL: http://dx.doi.org/10.1103/PhysRevA.95.011602.

[145] J. Tomkovič. "A driven two-component BEC: Chaos in a Macroscopic Quantum System". PhD thesis. Ruperto-Carola-University of Heidelberg, 2013.

[146] Max Trostel et al. "Characterizing Complex Dynamics in the Classical and Semi-Classical Duffing Oscillator Using Ordinal Patterns Analysis". In: *Entropy* 20.2 (2018), p. 40. ISSN: 1099-4300. DOI: 10.3390/e20010040. URL: http://dx.doi.org/10.3390/e20010040.

[147] Frank Verstraete, Michael M. Wolf, and J. Ignacio Cirac. "Quantum computation and quantum-state engineering driven by dissipation". In: *Nature Physics* 5 (July 2009), 633 EP –. URL: https://doi.org/10.1038/nphys1342.

[148] Guanglei Wang, Ying-Cheng Lai, and Celso Grebogi. "Transient chaos - a resolution of breakdown of quantum-classical correspondence in optomechanics". In: *Scientific Reports* 6 (Oct. 2016), 35381 EP –. URL: http://dx.doi.org/10.1038/srep35381.

[149] G Wendin. "Quantum information processing with superconducting circuits: a review". In: 80.10 (2017), p. 106001. DOI: 10.1088/1361-6633/aa7e1a. URL: http://dx.doi.org/10.1088/1361-6633/aa7e1a.

[150] P. B. Wigley et al. "Non-destructive shadowgraph imaging of ultra-cold atoms". In: *Opt. Lett.* 41.20 (2016), pp. 4795–4798. DOI: 10.1364/OL.41.004795. URL: http://ol.osa.org/abstract.cfm?URI=ol-41-20-4795.

[151] EP Wigner. "On a quasiprobability distribution in quantum mechanics". In: *Phys. Rev* 40 (1932), p. 749.

[152] Eugene P. Wigner. "On the Distribution of the Roots of Certain Symmetric Matrices". In: *Annals of Mathematics* 67.2 (1958), pp. 325–327. ISSN: 0003486X. URL: http://www.jstor.org/stable/1970008.

[153] H. M. Wiseman. "Adaptive Phase Measurements of Optical Modes: Going Beyond the Marginal $Q$ Distribution". In: *Phys. Rev. Lett.* 75.25 (1995), pp. 4587–4590.

[154] H. M. Wiseman. "Quantum theory of continuous feedback". In: *Phys. Rev. A* 49 (3 1994), pp. 2133–2150. DOI: 10.1103/PhysRevA.49.2133. URL: https://link.aps.org/doi/10.1103/PhysRevA.49.2133.

[155] H M Wiseman. "Quantum trajectories and quantum measurement theory". In: *Quantum and Semiclassical Optics: Journal of the European Optical Society Part B* 8.1 (1996), p. 205. URL: http://stacks.iop.org/1355-5111/8/i=1/a=015.

[156] H. M. Wiseman and L. Diósi. "Complete parameterization, and invariance, of diffusive quantum trajectories for Markovian open systems". In: *Chemical Physics* 268.1-3 (2001), pp. 91 –104.

[157] H. M. Wiseman and G. J. Milburn. "Quantum theory of field-quadrature measurements". In: *Phys. Rev. A* 47.1 (1993), pp. 642–662. DOI: 10.1103/PhysRevA.47.642.

[158] Howard M. Wiseman and Gerard J. Milburn. *Quantum Measurement and Control*. Cambridge University Press, 2010.

[159] Alan Wolf et al. "Determining Lyapunov exponents from a time series". In: *Physica D: Nonlinear Phenomena* 16.3 (1985), pp. 285 –317.

[160] Q. Xie and W. Hai. "Quantum entanglement and chaos in kicked two-component Bose-Einstein condensates". In: *The European Physical Journal D* 33.2 (2005), pp. 265–272. ISSN: 1434-6079. DOI: 10.1140/epjd/e2005-00054-4. URL: http://dx.doi.org/10.1140/epjd/e2005-00054-4.

[161] Bin Yan, Lukasz Cincio, and Wojciech H. Zurek. *Information Scrambling and Loschmidt Echo*. 2019. arXiv: 1903.02651 [quant-ph].

[162] Nicole Yunger Halpern, Brian Swingle, and Justin Dressel. "Quasiprobability behind the out-of-time-ordered correlator". In: *Physical Review A* 97.4 (2018). ISSN: 2469-9934. DOI: 10.1103/physreva.97.042105. URL: http://dx.doi.org/10.1103/PhysRevA.97.042105.

[163] I. I. Yusipov et al. "Quantum Lyapunov exponents beyond continuous measurements". In: *Chaos: An Interdisciplinary Journal of Nonlinear Science* 29.6 (2019), p. 063130. DOI: 10.1063/1.5094324. eprint: https://doi.org/10.1063/1.5094324. URL: https://doi.org/10.1063/1.5094324.

[164] Jing Zhang et al. "Quantum feedback: Theory, experiments, and applications". In: *Physics Reports* 679 (2017), pp. 1–60. DOI: https://doi.org/10.1016/j.physrep.2017.02.003. URL: http://www.sciencedirect.com/science/article/pii/S0370157317300479.

[165] Sisi Zhou et al. "Achieving the Heisenberg limit in quantum metrology using quantum error correction". In: *Nature Communications* 9.1 (2018), p. 78. DOI: 10.1038/s41467-017-02510-3. URL: https://doi.org/10.1038/s41467-017-02510-3.

[166] Wojciech Hubert Zurek and Juan Pablo Paz. "Decoherence, chaos, and the second law". In: *Phys. Rev. Lett.* 72 (16 1994), pp. 2508–2511. DOI: 10.1103/PhysRevLett.72.2508. URL: http://link.aps.org/doi/10.1103/PhysRevLett.72.2508.

[167] Wojciech Hubert Zurek and Juan Pablo Paz. "Quantum chaos: a decoherent definition". In: *Physica D: Nonlinear Phenomena* 83.1 (1995). Quantum Complexity in Mesoscopic Systems, pp. 300 –308. ISSN: 0167-2789. DOI: https://doi.org/10.1016/0167-2789(94)00271-Q. URL: http://www.sciencedirect.com/science/article/pii/016727899400271Q.

[168] Wojciech Hubert Zurek and Juan Pablo Paz. *Why We Don't Need Quantum Planetary Dynamics: Decoherence and the Correspondence Principle for Chaotic Systems*. 1996. arXiv: quant-ph/9612037 [quant-ph].

# A

# Appendix

## A.1 Appendix for Chapter 6

### A.1.1 Derivation of the equations of motion for a Hermitian coupling operator

We begin with the SSE in Stratonovich form given in Eq. 3.79. In stratonovich form, the equations of motion obey regular calculus. For a general operator $\hat{G}$, the equations of motion for the expectation values for a continuously monitored system is given by

$$\mathrm{d}\langle\hat{G}\rangle = \langle\psi|\hat{G}\mathrm{d}|\psi\rangle + \mathrm{d}\langle\psi|\hat{G}|\psi\rangle. \tag{A.1}$$

Let's break this down into each term from the SSE: We have the Hamiltonian term first

$$\mathrm{d}\langle\hat{G}\rangle_{\hat{H}term} = \frac{i}{\hbar}\langle[\hat{H}, G]\rangle, \tag{A.2}$$

where we have assumed we are dealing with a hermitian Hamiltonian. Now for the next $\mathrm{d}t$ term.

$$\begin{aligned}\mathrm{d}\langle\hat{G}\rangle_{\hat{L}term} = &\langle\psi|\hat{G}\left(-\frac{\hat{L}^\dagger\hat{L}}{2} + \frac{\langle\hat{L}^\dagger\hat{L}\rangle}{2} + \langle\hat{L}^\dagger\rangle\hat{L} - \langle\hat{L}^\dagger\rangle\langle\hat{L}\rangle\right)|\psi\rangle\mathrm{d}t \\ &+ \langle\psi|\left(-\frac{\hat{L}^\dagger\hat{L}}{2} + \frac{\langle\hat{L}^\dagger\hat{L}\rangle}{2} + \langle\hat{L}\rangle\hat{L}^\dagger - \langle\hat{L}^\dagger\rangle\langle\hat{L}\rangle\right)\hat{G}|\psi\rangle\mathrm{d}t\end{aligned} \tag{A.3}$$

$$= \left(\langle\hat{G}\hat{L}\rangle\langle\hat{L}^\dagger\rangle + \langle\hat{L}^\dagger\hat{G}\rangle\langle\hat{L}\rangle - \frac{\langle\hat{G}\hat{L}^\dagger\hat{L}\rangle}{2} - \frac{\langle\hat{L}^\dagger\hat{L}\hat{G}\rangle}{2} + \langle\hat{G}\rangle\langle\hat{L}^\dagger\hat{L}\rangle - 2\langle\hat{G}\rangle\langle\hat{L}^\dagger\rangle\langle\hat{L}\rangle\right)\mathrm{d}t. \tag{A.4}$$

Now we make the assumption that we are dealing with a hermitian coupling operator $\hat{L} = \hat{L}^\dagger$.

$$\mathrm{d}\langle\hat{G}\rangle_{\hat{L}term} = \left(\langle\hat{G}\hat{L}\rangle\langle\hat{L}\rangle + \langle\hat{L}\hat{G}\rangle\langle\hat{L}\rangle - \frac{\langle\hat{G}\hat{L}^2\rangle}{2} - \frac{\langle\hat{L}^2\hat{G}\rangle}{2} + \langle\hat{G}\rangle\langle\hat{L}^2\rangle - 2\langle\hat{G}\rangle\langle\hat{L}\rangle\langle\hat{L}\rangle\right)\mathrm{d}t. \tag{A.5}$$

Next we use the fact that $\langle\hat{G}\hat{L}^2\rangle = \langle\hat{L}\hat{G}\hat{L}\rangle + \langle[\hat{G},\hat{L}]\hat{L}\rangle$ and $\langle\hat{L}^2\hat{G}\rangle = \langle\hat{L}\hat{G}\hat{L}\rangle - \langle\hat{L}[\hat{G},\hat{L}]\rangle$.

$$\mathrm{d}\langle\hat{G}\rangle_{\hat{L}term} = \left(\langle\hat{G}\hat{L}\rangle\langle\hat{L}\rangle + \langle\hat{L}\hat{G}\rangle\langle\hat{L}\rangle - \langle\hat{L}\hat{G}\hat{L}\rangle + \frac{1}{2}(\langle[\hat{G},\hat{L}]\hat{L}\rangle - \langle\hat{L}[\hat{G},\hat{L}]\rangle) + \langle\hat{G}\rangle\langle\hat{L}^2\rangle - 2\langle\hat{G}\rangle\langle\hat{L}\rangle\langle\hat{L}\rangle\right)\mathrm{d}t. \tag{A.6}$$

In the meanfield limit the only surviving term will be

$$\mathrm{d}\langle\hat{G}\rangle_{\hat{L}term} = \frac{1}{2}(\langle[\hat{G},\hat{L}]\hat{L}\rangle - \langle\hat{L}[\hat{G},\hat{L}]\rangle)\mathrm{d}t. \tag{A.7}$$

Now for the $u$ terms:

$$\begin{aligned}\mathrm{d}\langle\hat{G}\rangle_{uterm} = & -\frac{u}{2}\langle\psi|\hat{G}\left(\hat{L}^2 - 2\hat{L}\langle\hat{L}\rangle - \langle\hat{L}^2\rangle + 2\langle\hat{L}\rangle^2\right)|\psi\rangle\mathrm{d}t \\ & -\frac{u^*}{2}\langle\psi|\left(\hat{L}^{\dagger 2} - 2\hat{L}^\dagger\langle\hat{L}^\dagger\rangle - \langle\hat{L}^{\dagger 2}\rangle + 2\langle\hat{L}^\dagger\rangle^2\right)\hat{G}|\psi\rangle\mathrm{d}t \end{aligned} \tag{A.8}$$

$$\begin{aligned} = & -\frac{u}{2}\left(\langle\hat{G}\hat{L}^2\rangle - 2\langle\hat{G}\hat{L}\rangle\langle\hat{L}\rangle + 2\langle\hat{G}\rangle\langle\hat{L}\rangle^2 - \langle\hat{G}\rangle\langle\hat{L}^2\rangle\right)\mathrm{d}t \\ & -\frac{u^*}{2}\left(\langle\hat{L}^{\dagger 2}\hat{G}\rangle - 2\langle\hat{L}^\dagger\hat{G}\rangle\langle\hat{L}^\dagger\rangle + 2\langle\hat{G}\rangle\langle\hat{L}^\dagger\rangle^2 - \langle\hat{G}\rangle\langle\hat{L}^{\dagger 2}\rangle\right)\mathrm{d}t. \end{aligned} \tag{A.9}$$

For hermitian coupling $\hat{L} = \hat{L}^\dagger$:

$$\begin{aligned}\mathrm{d}\langle\hat{G}\rangle_{uterm} = & -\frac{u}{2}\left(\langle\hat{G}\hat{L}^2\rangle - 2\langle\hat{G}\hat{L}\rangle\langle\hat{L}\rangle + 2\langle\hat{G}\rangle\langle\hat{L}\rangle^2 - \langle\hat{G}\rangle\langle\hat{L}^2\rangle\right)\mathrm{d}t \\ & -\frac{u^*}{2}\left(\langle\hat{L}^2\hat{G}\rangle - 2\langle\hat{L}\hat{G}\rangle\langle\hat{L}\rangle + 2\langle\hat{G}\rangle\langle\hat{L}\rangle^2 - \langle\hat{G}\rangle\langle\hat{L}^2\rangle\right)\mathrm{d}t, \end{aligned} \tag{A.10}$$

and using our definition of $u = \exp(-2i\phi)$:

$$\begin{aligned}\mathrm{d}\langle\hat{G}\rangle_{uterm} = & -\frac{1}{2}\big(\cos(2\phi)\left[\langle\hat{G}\hat{L}^2\rangle + \langle\hat{L}^2\hat{G}\rangle - 2\langle\hat{G}\hat{L}\rangle\langle\hat{L}\rangle - 2\langle\hat{L}\hat{G}\rangle\langle\hat{L}\rangle + 4\langle\hat{G}\rangle\langle\hat{L}\rangle^2 - 2\langle\hat{G}\rangle\langle\hat{L}^2\rangle\right] \\ & + \sin(2\phi)\left[-i(\langle\hat{G}\hat{L}^2\rangle - \langle\hat{L}^2\hat{G}\rangle) + 2i(\langle\hat{G}\hat{L}\rangle\langle\hat{L}\rangle - \langle\hat{L}\hat{G}\rangle\langle\hat{L}\rangle)\right]\big)\mathrm{d}t \end{aligned} \tag{A.11}$$

$$\begin{aligned} = & -\frac{1}{2}\big(\cos(2\phi)\left[2\langle\hat{L}\hat{G}\hat{L}\rangle + (\langle[\hat{G},\hat{L}]\hat{L}\rangle - \langle\hat{L}[\hat{G},\hat{L}]\rangle) - 2\langle\hat{G}\hat{L}\rangle\langle\hat{L}\rangle - 2\langle\hat{L}\hat{G}\rangle\langle\hat{L}\rangle + 4\langle\hat{G}\rangle\langle\hat{L}\rangle^2 - 2\langle\hat{G}\rangle\langle\hat{L}^2\rangle\right] \\ & + \sin(2\phi)\left[-i(\langle[\hat{G},\hat{L}]\hat{L}\rangle + \langle\hat{L}[\hat{G},\hat{L}]\rangle) + 2i(\langle\hat{L}\rangle\langle[\hat{G},\hat{L}]\rangle)\right]\big)\mathrm{d}t. \end{aligned} \tag{A.12}$$

For the meanfield approximation, we are left with

$$\mathrm{d}\langle\hat{G}\rangle_{uterm} = -\frac{1}{2}\cos(2\phi)\left(\langle[\hat{G},\hat{L}]\hat{L}\rangle - \langle\hat{L}[\hat{G},\hat{L}]\rangle\right)\mathrm{d}t. \tag{A.13}$$

And finally the noise terms

$$\begin{aligned} \mathrm{d}\langle\hat{G}\rangle_{noiseterm} &= \langle\psi|\hat{G}(\hat{L}-\langle\hat{L}\rangle)|\psi\rangle\mathrm{d}\xi + \langle(|\hat{L}^\dagger-\langle\hat{L}^\dagger\rangle)\hat{G}|\psi\rangle\mathrm{d}\xi^* \\ &= \left(\langle\hat{G}\hat{L}\rangle - \langle\hat{G}\rangle\langle\hat{L}\rangle\right)\mathrm{d}\xi + \left(\langle\hat{L}^\dagger\hat{G}\rangle - \langle\hat{G}\rangle\langle\hat{L}^\dagger\rangle\right)\mathrm{d}\xi^*. \end{aligned} \tag{A.14}$$

For hermitian coupling and using our definition $\mathrm{d}\xi = \exp(-i\phi)\mathrm{d}W$:

$$\begin{aligned} \mathrm{d}\langle\hat{G}\rangle_{noiseterm} &= \cos(\phi)\left(\langle\hat{G}\hat{L}\rangle + \langle\hat{L}\hat{G}\rangle - 2\langle\hat{G}\rangle\langle\hat{L}\rangle\right)\mathrm{d}W + \sin(\phi)\left(-i(\langle\hat{G}\hat{L}\rangle - \langle\hat{L}\hat{G}\rangle)\right)\mathrm{d}W \\ &= -\sin(\phi)\left(i\langle[\hat{G},\hat{L}]\rangle\right)\mathrm{d}W. \end{aligned} \tag{A.15}$$

So the equation of motion for a general operator $\hat{G}$ is given by:

$$\begin{aligned} \mathrm{d}\langle\hat{G}\rangle = \frac{i}{\hbar}\langle[\hat{H},G]\rangle + \frac{1}{2}(\langle[\hat{G},\hat{L}]\hat{L}\rangle - \langle\hat{L}[\hat{G},\hat{L}]\rangle)\mathrm{d}t - \frac{1}{2}\cos(2\phi)\left(\langle[\hat{G},\hat{L}]\hat{L}\rangle - \langle\hat{L}[\hat{G},\hat{L}]\rangle\right)\mathrm{d}t \\ - \sin(\phi)\left(i\langle[\hat{G},\hat{L}]\rangle\right)\mathrm{d}W. \end{aligned} \tag{A.16}$$

### A.1.2 Validating the separation time using results from the Duffing oscillator

To be sure that we can use the separation time as a measure to distinguish between the different measurement choices, we need to do the same for the Duffing oscillator as well, a system for which we have quantum Lyapunov exponents that also quantify the difference. So let us look at the Duffing oscillator for two orthogonal measurement choices $\phi = \pi/2$ and $\phi = 0$. We will use the same technique that we have used for the Driven top, looking at the time that the quantum trajectory in phase space departs from the classical counterpart.

$$d_t = \sqrt{\Delta Q(t)^2 + \Delta P(t)^2}. \tag{A.17}$$

Fig. A.1 shows the average separation time for different measurement choices for the Duffing oscillator. First we notice that the difference in the separation time is not so large for this system. But we also see that the result for $\phi = 0$ and $\phi = \pi/2$ follow the trend of the quantum Lyapunov exponents in this case. So perhaps this warrants that the separation time could be a useful tool for distinguishing the effect that the measurement has on the chaotic dynamics?

### A.1.3 Deriving the rotation of an arbitrary state for SU(2)

Recall from the main text, that the arbitrary rotation of a state in SU(2) is given by

$$e^{(\lambda_+\hat{J}_+ + \lambda_-\hat{J}_- + \lambda_z\hat{J}_z)} = e^{(\Lambda_+\hat{J}_+)}e^{(\ln(\Lambda_z)\hat{J}_z)}e^{(\Lambda_-\hat{J}_-)} \tag{A.18}$$

$$= e^{(\Lambda_-\hat{J}_-)}e^{(-\ln(\Lambda_z)\hat{J}_z)}e^{(\Lambda_+\hat{J}_+)}, \tag{A.19}$$

Now lets apply the operators to the state in parts to simplify it and use the series expansion of an exponential:

$$e^{(\Lambda_-\hat{J}_-)}|m\rangle = \sum_{k=0}^{\infty}\frac{(\Lambda_-)^k}{k!}\hat{J}_-^k|m\rangle. \tag{A.20}$$

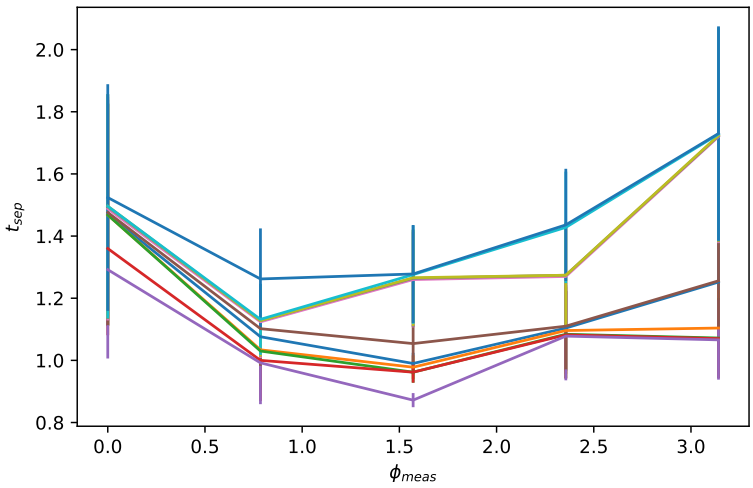


**Figure A.1:** Average breaking time $\tau_\hbar$ for the quantum Duffing oscillator with threshold $\epsilon = 2 \pm 5\%, 10\%, 15\%, 20\%$. Each point is averaged over 5 noise realisations and the error bars signify twice the standard error.

What is $\hat{J}_-^k|m\rangle$?

$$\hat{J}_-|m\rangle = \left(J^2 - m(m-1)\right)^{1/2}|m-1\rangle \tag{A.21}$$

$$\hat{J}_-\hat{J}_-|m\rangle = \left(J^2 - (m-1)(m-2)\right)^{1/2}\left(J^2 - m(m-1)\right)^{1/2}|m-2\rangle \tag{A.22}$$

$$\vdots \tag{A.23}$$

$$\begin{aligned}\hat{J}_-^k|m\rangle &= \left(J^2 - (m-(k-1))(m-k)\right)^{1/2} \ldots \left(J^2 - m(m-1)\right)^{1/2}|m-k\rangle \\ &= \prod_{i=1}^{k}\left(J^2 - (m-(i-1))(m-i)\right)^{1/2}|m-k\rangle.\end{aligned} \tag{A.24}$$

The action of the exponential operator on the arbitrary state is then given by:

$$e^{(\Lambda_-\hat{J}_-)}|m\rangle = \sum_{k=0}^{\infty}\frac{(\Lambda_-)^k}{k}\prod_{i=1}^{k}\left(J^2 - (m-(i-1))(m-i)\right)^{1/2}|m-k\rangle. \tag{A.25}$$

Moving onto the next operation on the state:

$$e^{(\ln(\Lambda_z)\hat{J}_z)}e^{(\Lambda_-\hat{J}_-)}|m\rangle, \tag{A.26}$$

this is easier since we are dealing with the eigenstates of the $\hat{J}_z$ operator, $\exp(\hat{J}_z)|m\rangle = \exp(m)|m\rangle$.

$$= \sum_{k=0}^{\infty}\frac{(\Lambda_-)^k}{k!}\prod_{i=1}^{k}\left(J^2 - (m-(i-1))(m-i)\right)^{1/2}e^{(\ln(\Lambda_z)\hat{J}_z)}|m-k\rangle, \tag{A.27}$$

$$= \sum_{k=0}^{\infty}\frac{(\Lambda_-)^k}{k!}\prod_{i=1}^{k}\left(J^2 - (m-(i-1))(m-i)\right)^{1/2}e^{(\ln(\Lambda_z)(m-k))}|m-k\rangle. \tag{A.28}$$

Now, finally we include the final operation:

$$e^{(\Lambda_+ \hat{J}_+)} e^{(\ln(\Lambda_z)\hat{J}_z)} e^{(\Lambda_- \hat{J}_-)} |m\rangle, \tag{A.29}$$

$$= \sum_{k=0}^{\infty} \frac{(\Lambda_-)^k}{k!} \prod_{i=1}^{k} \left(J^2 - (m-(i-1))(m-i)\right)^{1/2} e^{(\ln(\Lambda_z)(m-k))} \cdot \sum_{q=0}^{\infty} \frac{(\Lambda_+)^q}{q!} \hat{J}_+^q |m-k\rangle. \tag{A.30}$$

What is $\hat{J}_+^q |m-k\rangle$?

$$\hat{J}_+ |m-k\rangle = \left(J^2 - (m-k)(m-k+1)\right)^{1/2} |m-k+1\rangle \tag{A.31}$$

$$\hat{J}_+ \hat{J}_+ |m-k\rangle = \left(J^2 - (m-k+1)(m-k+2)\right)^{1/2} \left(J^2 - (m-k)(m-k+1)\right)^{1/2} |m-k+2\rangle \tag{A.32}$$

$$\vdots \tag{A.33}$$

$$\begin{aligned} \hat{J}_+^q |m-k\rangle = & \left(J^2 - (m-k+(q-1))(m-k+q)\right)^{1/2} \\ & \ldots \left(J^2 - (m-k)(m-k+1)\right)^{1/2} |m-k+q\rangle \end{aligned} \tag{A.34}$$

$$= \prod_{p=1}^{q} \left(J^2 - (m-k+(p-1))(m-k+p)\right)^{1/2} |m-k+q\rangle. \tag{A.35}$$

Therefore we have

$$= \sum_{k=0}^{\infty} \frac{(\Lambda_-)^k}{k!} \prod_{i=1}^{k} \left[\left(J^2 - (m-(i-1))(m-i)\right)^{1/2}\right] e^{(\ln(\Lambda_z)(m-k))} \cdot \sum_{q=0}^{\infty} \frac{(\Lambda_+)^q}{q!} \prod_{p=1}^{q} \left[\left(J^2 - (m-k+(p-1))(m-k+p)\right)^{1/2}\right] |m-k+q\rangle. \tag{A.36}$$

So the entire thing is now

$$\begin{aligned} & e^{-in\phi} \sum_m c_m \left[\ldots\right] \langle n|m-k+q\rangle \\ = \; & e^{-in\phi} \sum_m c_m \left[\ldots\right] \delta_{n,m-k+q} \\ = \; & e^{-in\phi} c_{m\to n+k-q} \left[\ldots\right], \end{aligned} \tag{A.37}$$

where [...] is Eq.A.36 above. Now, what are the limits on this equation for the code? The sums will not be infinite since we are dealing with a truncated basis. We can't go below $c_0$ so we must have $q \leq n$ We must have $n+k-q < N$, so $k < N-n+q$. For the simulations we then have

$$\langle n|\psi_{PB}\rangle = e^{-in\phi}\sum_{q=0}^{q\leq n}\frac{(\Lambda_+)^q}{q!}\prod_{p=1}^{q}\left[\left(J^2-(n-q+(p-1))(n-q+p)\right)^{1/2}\right]e^{(\ln(\Lambda_z)(n-j))}$$
$$\cdot\sum_{k=0}^{k<N-n+q}\frac{(\Lambda_-)^k}{k!}\prod_{i=1}^{k}\left[\left(J^2-((n+k-q)-(i-1))(n+k-q-i)\right)^{1/2}\right]c_{n+k-q} \quad \text{(A.38)}$$